Titre: Title:	Boron Nitride Nanotubes: Understanding Dispersibility and Functionalization to Improve Dispersion into Elastomers
Auteur: Author:	Cristina Sofia Torres Castillo
Date:	2022
Type:	Mémoire ou thèse / Dissertation or Thesis
Référence: Citation:	Torres Castillo, C. S. (2022). Boron Nitride Nanotubes: Understanding Dispersibility and Functionalization to Improve Dispersion into Elastomers [Thèse de doctorat, Polytechnique Montréal]. PolyPublie. https://publications.polymtl.ca/10743/

POLYTECHNIQUE MONTRÉAL

affiliée à l'Université de Montréal

Boron Nitride Nanotubes: Understanding Dispersibility and Functionalization to Improve Dispersion into Elastomers

CRISTINA SOFIA TORRES CASTILLO

Département de génie chimique

Thèse présentée en vue de l'obtention du diplôme de *Philosophiæ Doctor*

Génie chimique

Octobre 2022

POLYTECHNIQUE MONTRÉAL

affiliée à l'Université de Montréal

Cette thèse intitulée :

Boron Nitride Nanotubes: Understanding Dispersibility and Functionalization to Improve Dispersion into Elastomers

présentée par **Cristina Sofia TORRES CASTILLO**

en vue de l'obtention du diplôme de *Philosophiæ Doctor*

a été dûment acceptée par le jury d'examen constitué de :

Fabio CICOIRA, président
Jason Robert TAVARES, membre et directeur de recherche
Julian SELF, membre
Éric DAVID, membre externe

DEDICATION

To my beloved family, for always being there for me.

To my cousin Martha Ruth.

ACKNOWLEDGEMENTS

First of all, I would like to thank my supervisor Prof. Jason R. Tavares for giving the opportunity of undertaking this research project. He made me challenge myself in different situations and do things that I didn't know I was capable of doing. He made me growth not only in the professional aspect but also in the personal one. Thank you for your guidance and encouragement.

I would like to thank the members of the Chemical Engineering Department, for helping me in one way or another. To Prof. Basil Favis, for believing in me at the beginning of this journey. Special thanks go to Gino Robin and Martine Lamarche, for helping me ordering new materials and have provided me with lab equipment. To Matthieu Gautier and Claire Cerclé, for the trainings received and discussions about some analyses/experiments. To Alexandre Bréard, for always answering my administrative questions with a smile. To Mariia Kopach, for giving me a warm welcome at the very beginning of my PhD.

I would like to thank the Natural Sciences and Engineering Research Council of Canada (NSERC) and Prima Québec for their financial support. I also thank the Mexican National Council for Science and Technology (CONACyT), for the scholarship provided (number: 739894). I would also like to thank Dr. Jeremy Mehlem, Dr. Xavier Cauchy, and Dr. Richard Dolbec, for the supply of the main materials used in this project and for their valuable comments/discussions during our monthly meetings.

I would like to thank Prof. Fabio Cicoria, Prof. Eric David and Prof. Julian Self for accepting being part of the jury and for reviewing this thesis. I would like to thank the members of the PhotoSEL team: Evelyne, Wendell, Hamed, Alessio, Simon, David, Sergio, Charles, Mélanie, Martin, Somayeh, and Adya, for their support. I appreciated the interesting discussions that we had during the group meetings and the good times spent inside and outside the lab. Thanks to Dr. Martin Lennox, for his words of encouragement at the beginning of the pandemic. Special thanks go to Mr. Wendell Raphael, for helping me with the translation to French of the abstract and to Dr. Shahir Karami, for his support during my graduate studies. Thanks are given to my interns: Paul-Henri Verger, Alekhya V. Veerubhotla, Shing Chi Ho and Arianne Poissant, for their valuable contributions to this project. Special thanks are directed to my friends: Hela, Mina, Ivan, Angela, Fernanda, Laura, Mohammad, and Zack, for their friendship and good moments. To my friends

from McGill university: Prisca, Gaby, Oscar, Brenda, Emmanuel, and Alejandra, in whom I found a second family. Thanks to Mr. Gerardo Juarez and Mrs. Jacqueline Perez, for letting me stay in their house when I just arrived in Montreal, and to Ms. Xiomara Sanchez, for offering me a home in difficult times.

Finally, I would like to express my infinite gratitude to my parents, Amada and Javier, and to my brothers, Javier and Rodrigo, for their unconditional support. Very special thanks go to my lovely mom, Amada, who was always there for me and gave me advice no matter what, and to my big brother Javier, for made me focus on what was important and for his constant encouragement. Without their unconditional support, simply, I would not be here today.

RÉSUMÉ

Les nanotubes de nitrure de bore (BNNT) sont des nanofeuilles laminées composées d'atomes de B et de N alternés dans un réseau en nid d'abeille. Ils alimentent l'intérêt des scientifiques depuis plusieurs décennies en raison de leurs propriétés extraordinaires : ils possèdent des propriétés mécaniques compétitives ainsi qu'une grande stabilité chimique et thermique. De façon similaires que les nanotubes de carbone (CNT), les BNNT possèdent une conductivité thermique élevée, mais diffèrent par leur comportement électrique : ce sont des isolants électriques. Ils sont donc de parfaits candidats pour la fabrication de composites polymères nécessitant une conductivité thermique et une isolation électrique élevées, comme dans les dispositifs électroniques. Néanmoins, la principale limitation lors de l'incorporation des BNNT (et en général des nanoparticules) dans des polymères ou des milieux liquides est leur tendance à s'agglomérer en raison de leur énergie de surface élevée. L'incompatibilité entre les nanotubes et le milieu liquide peut également poser un problème.

Des traitements de surface sont généralement effectués aux nanoparticules afin d'améliorer leur compatibilité avec les polymères. Ces traitements peuvent être divisés en approches covalentes et non covalentes. Ces dernières impliquent souvent l'utilisation d'un surfactant ou d'un polymère pour envelopper la surface des nanotubes sans endommager leur structure chimique. Bien que ces techniques préservent les propriétés intrinsèques des nanotubes, elles souffrent d'une déstabilisation à des températures aussi basses que 70 °C. En revanche, les approches covalentes sont privilégiées pour les applications à haute température. Elles impliquent la fixation de nouvelles espèces chimiques sur les BNNT, modifiant la chimie de leur surface et parfois leurs propriétés. Selon l'application finale, une fonctionnalisation ou l'autre est préférée.

Les BNNT possèdent un caractère polaire léger, dû à leurs liaisons ioniques partielles B-N. Pour réussir leur incorporation dans des polymères non polaires, des traitements physiques ou chimiques sont souvent nécessaires. Le caoutchouc styrène-butadiène (SBR), un polymère non polaire, possède des propriétés intéressantes qui le rendent attrayant pour les applications nécessitant une grande déformabilité, comme dans l'industrie du pneu. Cependant, ce matériau d'intérêt présente un inconvénient majeur: sa faible conductivité thermique.

Dans cette thèse, nous avons étudié trois aspects de la manipulation, de la modification de surface et du traitement des BNNTs :

1) L'évaluation de leur dispersibilité dans des milieux liquides, afin de déterminer leur affinité chimique avec une variété de solvants organiques ;

2) Leur fonctionnalisation chimique vers des surfaces hydrophiles en utilisant une approche abordable en phase gazeuse, fonctionnant dans des conditions ambiantes ;

3) L'utilisation d'un mélange binaire basé sur les paramètres de solubilité pour améliorer leur compatibilité/dispersion avec des polymères non polaires, tels que le SBR.

Dans la première partie, nous avons caractérisé la dispersibilité des BNNT dans des solvants organiques par des paramètres de solubilité. Leurs paramètres de cohésion étaient : $\{\delta_d ; \delta_p ; \delta_h\} = \{16,8 ; 10,7 ; 14,7\}$ avec un paramètre de solubilité totale $\delta_t = 24,7$ $MPa^{1/2}$. La pureté et la densité du matériau ainsi que les propriétés physiques des solvants ont été prises en compte afin de compenser les différences de densité et de viscosité lors du calcul des temps de sédimentation. Ces coordonnées sont différentes de celles rapportées par de précédents auteurs et pourraient orienter les chercheurs par erreur. Les résultats montrent que les BNNTs possèdent une surface légèrement polaire, en accord avec la nature chimique des liaisons B-N.

Dans la deuxième partie, nous avons ajouté des fonctionnalités d'oxygène sur les BNNT par une technique en phase gazeuse, soit le déposition chimique en phase vapeur photo-initié (PICVD), en utilisant un flux de déchets (syngas) comme réactifs. Une augmentation de l'oxygène atomique de 7,8% à 37,1% a été observée après le traitement. Ce niveau d'oxydation est plus élevé que ceux rapportés dans la littérature utilisant des traitements plasma. La consommation d'énergie de la source lumineuse (lampe UVC fonctionnant à 30 W) était de 0,03 kWh, ce qui se traduit par un coût de 0,002 CAD, tandis que le coût des gaz d'alimentation (CO, H_2 et Ar) était de 0,055 CAD pour 1 h de traitement. Ce procédé extrêmement peu coûteux fait du PICVD, utilisant du syngas, une approche prometteuse pour la modification de surface à grande échelle.

Dans la troisième partie, nous avons fabriqué des nanocomposites SBR/BNNT présentant des propriétés thermiques et viscoélastiques améliorées grâce à une technique simplifiée de moulage dans un solvant. Un mélange binaire de toluène/acétate d'éthyle (80:20 vol) a été choisi comme milieu de dispersion, en tenant compte des paramètres de solubilité des deux matériaux. Cette

méthode ne nécessite pas de modification de surface, comme cela a été requis dans d'autres travaux. Les nanocomposites résultants ont montré jusqu'à 35% d'amélioration de la conductivité thermique et une augmentation de 235% du module de stockage dans le balayage de fréquence, lorsqu'une charge de BNNT de 10% en poids a été utilisée.

ABSTRACT

Boron nitride nanotubes (BNNTs) are rolled nanosheets composed of alternating B and N atoms in a honeycomb network. They have attracted scientific attention in the last decades due to their extraordinary properties: they possess competitive mechanical properties, as well as high chemical and thermal stabilities. Similar to carbon nanotubes (CNTs), they possess a high thermal conductivity, but differ in their electrical behavior: BNNTs are electrical insulators. Thus, BNNTs are perfect candidates for fabrication of polymeric composites requiring high thermal conductivity and electrical insulation, such as in electronic devices. Nevertheless, the main limitation when incorporating BNNTs (and in general, nanoparticles) into polymers or liquid media is their tendency to agglomerate due to their high surface energy. The incompatibility of the nanotubes and the liquid media may be an issue as well.

Surface treatments of nanoparticles are often performed to improve their compatibility with polymers. These treatments can be divided into covalent and non-covalent approaches. Non-covalent techniques often involve the use of a surfactant or polymer to wrap the surface of the nanotubes, with no damage to their chemical structure. Although these techniques preserve the intrinsic properties of the nanotubes, they suffer from destabilization at temperatures as low as 70 °C. On the other hand, covalent approaches are preferred for applications at high temperatures. They involve the attachment of new chemical species on the BNNTs, modifying its surface chemistry, and sometimes, its properties. Depending on the final application, one functionalization or the other is preferred.

BNNTs posses a mild polar character, due to their partial ionic B-N bonds. For their successful incorporation into non-polar polymers, physical or chemicals treatments are often required. Styrene-butadiene rubber (SBR), a non-polar polymer, possesses interesting properties which makes it attractive for applications requiring high deformability, such as in the tire industry. However, one drawback it its low thermal conductivity.

In this thesis, we investigated three aspects for the handling, surface modification, and processing of BNNTs:

1) Assessment of their dispersibility in liquid media, to determine their chemical affinity with a variety of organic solvents;

2) Chemical functionalization towards hydrophilic surfaces using an affordable gas-phase approach, operating at ambient conditions;

3) Use of a binary mixture based on solubility parameters to improve their compatibility/dispersion with non-polar polymers, such as SBR.

In the first part, we characterized the dispersibility of BNNTs in organic solvents through solubility parameters. Their cohesion parameters were: $\{\delta_d; \delta_p; \delta_h\} = \{16.8; 10.7; 14.7\}$ with a total solubility parameter, $\delta_t = 24.7$ $MPa^{1/2}$. Purity of the material and density, as well as physical properties of the solvents were considered, to compensate for differences in density and viscosity when calculating sedimentation times. These coordinates are different from that reported by previous authors, and could mistakenly orient researchers. The outcome shows that the BNNTs posses a mildly polar surface, in agreement with the chemical nature of B-N bonds.

In the second part, we incorporated oxygen functionalities on the BNNTs through a gas-phase technique, namely photo-initiated chemical vapor deposition (PICVD), using a waste stream (syngas) as reactants. An increase in the atomic oxygen from 7.8% to 37.1% was observed after the treatment. This level of oxidation is higher than the ones reported in the literature using plasma treatments. The energy consumption of the light source (UVC lamp operating at 30 W) was 0.03 kWh, translating into a cost of $0.002 CAD, while the cost of the fed gases (CO, H_2, and Ar) was $0.055 6 CAD for 1 h treatment. This extremely low-cost process makes syngas PICVD a promising approach for surface modification at a large scale.

In the third part, we fabricated SBR/BNNT nanocomposites with improved thermal and viscoelastic properties though a simplified solvent casting technique. A binary mixture of toluene/ethyl acetate (80:20 vol) was chosen as the dispersing medium, taking into account solubility parameters of both materials. This method does not require surface modification, as was required in other works. The resulting nanocomposites showed up to 35% of improvement in thermal conductivity and a 235% increase in storage modulus in the frequency sweep, when a BNNT loading of 10 wt% was used.

TABLE OF CONTENTS

DEDICATION iii

ACKNOWLEDGEMENTS iv

RÉSUMÉ vi

ABSTRACT ix

TABLE OF CONTENTS xi

LIST OF TABLES xv

LIST OF FIGURES xvii

LIST OF SYMBOLS AND ABBREVIATIONS xxi

LIST OF APPENDICES xxv

CHAPTER 1 INTRODUCTION 1

CHAPTER 2 LITERATURE REVIEW 4

2.1 Boron nitride nanotubes 4

2.1.2 Methods of synthesis 10

2.1.3 Applications 11

2.2 Thermally conductive polymer-BN nanocomposites 11

2.3 Characterization of rubber compounds for tire applications 15

2.4 Surface modification of BNNTs 16

2.5 Photo initiated chemical vapor deposition 21

2.6 Solubility parameters 23

2.6.1 Characterization of polymers 25

2.6.2 Characterization of nanoparticles 25

CHAPTER 3 OBJECTIVES AND ORGANIZATION OF THE ARTICLES 27

3.1 Objectives 27

3.1.1 General objective 27

3.1.2 Specific objectives 27

3.2 Organization of the articles 28

CHAPTER 4 ARTICLE 1 : CHEMICAL AFFINITY AND DISPERSIBILITY OF BORON NITRIDE NANOTUBES 30

4.1 Introduction 31

4.2 Theory 33

4.3 Experimental part 36

4.3.1 Materials and methods 36

4.3.2 Microscopy 37

4.3.3 Sedimentation tests 38

4.4 Results and discussion 38

4.4.1 Ultrasonication and dispersion 38

4.4.2 Time-dependent dispersion state 41

4.4.3 Dispersion end state 41

4.4.4 HSP analysis 43

4.5 Conclusions 51

CHAPTER 5 ARTICLE 2 : COVALENT FUNCTIONALIZATION OF BORON NITRIDE NANOTUBES THROUGH PHOTO-INITIATED CHEMICAL VAPOUR DEPOSITION 53

5.1 Introduction 54

5.2 Materials and methods 59

5.2.1 Materials 59

5.2.2 Methods 59

5.3 Results and discussion 61

5.3.1 Fourier-transform infrared spectroscopy 65
5.3.2 Contact angle measurements and surface energy 66
5.3.3 Dispersion tests 68
5.4 Conclusions 70
CHAPTER 6 ARTICLE 3 : THERMALLY CONDUCTIVE STYRENE-BUTADIENE RUBBER/BORON NITRIDE NANOTUBES COMPOSITES 72
6.1 Introduction 73
6.2 Materials and Methods 76
6.2.1 Materials 76
6.2.2 Methods 77
6.3 Results and Discussion 79
6.3.1 Hansen Solubility Parameters of Styrene Butadiene Rubber 79
6.3.2 Fabrication Styrene-Butadiene Rubber/Boron Nitride Nanotubes Composites 83
6.4 Conclusions 91
CHAPTER 7 GENERAL DISCUSSION 93
7.1 Studying dispersibility of BNNT in organic solvents 93
7.2 Covalent functionalization of BNNTs 94
7.3 Improving dispersion of BNNT into SBR 102
7.4 Experimental considerations 103
CHAPTER 8 CONCLUSIONS AND RECOMMENDATIONS 105
8.1 Summary and conclusions 105
8.2 Original contributions 106
8.3 Recommendations 107
REFERENCES 109

APPENDICES..... 133

LIST OF TABLES

Table 2.1 Summary of some thermally conductive polymer/BN nanocomposites. 12

Table 2.2 Summary of some surface treatments of BNNTs. 17

Table 2.3 Comparative table of CVD techniques [93], [94]. 21

Table 4.1 HSP, sedimentation time, dispersion state, Ra, and RED of the solvents used in sedimentation tests. Solvents are classified based on their dispersion states at the end of the sedimentation period (Figure B.4). 39

Table 5.1 Comparison of some covalent functionalization approaches of boron nitride nanotubes (BNNTs) in the liquid phase. 55

Table 5.2 Comparison of some covalent functionalization approaches of boron nitride nanotubes (BNNTs) in the gas phase. 57

Table 5.3 Atomic composition of untreated and treated boron nitride nanotubes (BNNTs). 62

Table 5.4 Static contact angle and surface energy of BNNT films. 67

Table 5.5 Water ARCA and SE for untreated and treated BNNT. 68

Table 6.1 Summary of polymer/BN nanocomposites with improved thermal conductivity (TC). 74

Table 6.2 Nomenclature of composites prepared. 78

Table 6.3 HSPs, scores, and Ra and RED numbers of the solvents used for the dissolution of SBR. 79

Table 6.4 Calculated HSPs and Red numbers of binary mixtures of toluene/ethyl acetate. 83

Table 7.1 Effect of PICVD parameters on wettability of silicon wafers. 95

Table 7.2 Influence of CO cylinder age on PICVD treatments 97

Table B.1 Purity, supplier and physical properties of the solvents used in the sedimentation tests. 136

Table B.2 HSP, sedimentation time and dispersion state of the solvents used in sedimentation tests. 139

LIST OF FIGURES

Figure 2.1 Structural model of single-walled BNNTs. Boron atoms are in blue, nitrogen atoms in gray, taken from Torres-Castillo et al. (2020) [25]. 5

Figure 2.2 Schematics displaying the anisotropy of thermal conductivity in micrometer-sized a) BN particles and b) BNNTs. BN particles have high thermal conductivity in the (002) crystal plane with poor thermal conductivity along the [002] direction, taken from Zhi et al. (2009) [21]. 7

Figure 2.3 Super hydrophobicity of a BNNT film. The cross-sectional view of the sample shows the vertically aligned BNNTs, taken from Boinovich et al. (2011) [38]. 9

Figure 2.4 Scheme of the induction plasma process for the mass production of BNNTs, taken from Kim et al. (2014) [33]. 11

Figure 2.5 Graphical representation of the Hansen. Good solvents (white points) are inside the sphere while bad solvents (black points) are outside, taken from Ma et al. (2013) [112]. 25

Figure 4.1 Structure of single-walled BNNTs. Boron atoms are in blue, nitrogen atoms in grey. 32

Figure 4.2 Representative TEM images of BNNTs dispersed in ethanol. (A and B) BNNTs have a diameter of approximately 5 nm. The inset in (A) shows they are double walled. (C and D) BNNT length is on the order of a few μm, and some BN hollow cages remain in the material. 37

Figure 4.3 Dispersibility of BNNTs at tsed in A) ethanol, B) methanol, and C) acetic acid. 42

Figure 4.4 Hansen space of BNNTs. The green circles correspond to the good solvents, the blue triangles to intermediate ones and the red squares to poor ones. The black diamond represents the centre of the sphere. Full symbols correspond to solvents inside the sphere while empty symbols to solvents outside. 45

Figure 4.5 2D projections to help with the visualization of the data presented in fig 4. A) δd vs δp, B) δd vs δh, C) δp vs δh and D) dispersion state vs δt. Good, intermediate and bad solvents are represented by green, blue and red circles, respectively. 46

Figure 4.6 Hansen space of BNNTs obtained in this work (blue sphere) and the results obtained by Tiano et al. [44] (black sphere). The green circles, blue triangles and red squares correspond to good, intermediate and poor solvents determined in this work. 49

Figure 4.7 Hansen space of BNNTs obtained in this work considering total dispersibility (blue sphere), partial dispersibility (gray sphere) and Tiano's results (black sphere). 50

Figure 5.1 Schematic of the PICVD reactor. 60

Figure 5.2 (A) Untreated and (B) treated boron nitride nanotubes (BNNT) films (rectangles of ~ 2 cm x 1 cm). 61

Figure 5.3 (A) B1s, (C) N1s, (E) O1s, and (G) C1s high-resolution spectra for untreated boron nitride nanotubes (BNNTs), and (B) B1s, (D) N1s, (F) O1s, (H) C1s, and (I) Fe2p2 high-resolution spectra for treated BNNTs. 64

Figure 5.4 FTIR spectra of (A) untreated and (B) treated BNNTs. The inset shows a zoom in the 2800 – 3800 cm-1 range. 65

Figure 5.5 Water contact angle of (A) untreated and (B) treated BNNTs. 66

Figure 5.6 Dispersions of untreated BNNTs in (A) water, (B) methanol, and (C) acetic acid after having elapsed their respective sedimentation time, tsed. 70

Figure 5.7 Dispersions of t-BNNTs in water, methanol and acetic acid taken (A) immediately after sonication, (B) 48 h, and (C) 120 h after sonication. 70

Figure 6.1 Methodology followed for the fabrication of SBR/BNNTs nanocomposites. 78

Figure 6.2 Hansen space for SBR (gray sphere) and BNNTs (blue sphere). Good solvents for SBR are represented with green dots, intermediate solvents with blue dots and bad solvents with red dots. 81

Figure 6.3 SBR composites obtained by solvent casting containing 0 wt% (a), 1 wt% (b), 5 wt% (c), and 10 wt% (d) of BNNTs. 84

Figure 6.4 Variation of storage modulus (G') (a), loss modulus (G'') (b), and complex viscosity (η*) (c) of SBR/BNNTs composites as a function of strain. Standard deviation was calculated

considering three different samples for each composite. The exception to this is the composite at 10 wt% of BNNTs, where only one measurement was performed..... 86

Figure 6.5 Variation of storage modulus (G') (a), loss modulus (G'') (b), and tan δ (c) of SBR/BNNTs as a function of angular frequency. Standard deviation was calculated considering three different samples for each composite. The exception to this is the composite at 10 wt% of BNNTs, where only one measurement was performed..... 87

Figure 6.6 TEM images of SBR/BNNTs nanocomposites at 1 wt%. Some arrows are pointing out to individual nanotubes and others pointing out to BNNTs aggregates. 88

Figure 6.7. Thermal conductivity of the SBR/BNNTs nanocomposites. Standard deviation was calculated considering three different samples for each composite. The exception to this is the composite at 10 wt% of BNNTs, where only one measurement was performed..... 89

Figure 7.1 PICVD reaction system indicating position of the sample. 98

Figure 7.2 Irradiance of the UVC lamp at p = 45 cm and h = 10.5 cm. 99

Figure 7.3 Irradiance of the UVC lamp at p = 45 cm and h = 3.5 cm. 100

Figure 7.4 Proposed reaction configurations to optimize the light delivered to the PICVD system, a) three UVC lamps around the quartz tube, and b) one lamp at the entrance. 101

Figure B.1 Pictures of the dispersions taken immediately after sonication. Solvents from left to right are: (A) DMF, benzyl alcohol, acetic acid, toluene, methanol, ethanol, propylene carbonate, cyclohexane, THF, ethyl acetate, tert-butanol, ethyl benzoate and (B) MEK, d-limonene, acetonitrile, DMSO, chloroform, heptane, 1,2-dioxane, dichloromethane, 2-propanol, DMAc, acetone, formamide, ethylene glycol and water. 141

Figure B.2 BNNTs dispersions in ethylene glycol and benzyl alcohol applying high energy during sonication. 141

Figure B.3 Evolution of the dispersion state over time in A) propylene carbonate, B) ethyl benzoate and C) DMSO. Pictures of the vials were taken at 0, 1, 2, 4, 6, 8, 24, 48, 72, 96, 120 and 150 h after sonication. 142

Figure B.4 Pictures of the vials taken after a relative sedimentation time (RST) of 1.0295 x 1011 s2/m2. Solvents from left to right are: (A,B) N,N’-dimethylformamide, benzyl alcohol, acetic acid, toluene, methanol, ethanol, propylene carbonate, cyclohexane, tetrahydrofuran, ethyl acetate, tert-butanol, ethyl benzoate, methyl ethyl ketone and (C,D) d-limonene, acetonitrile, dimethyl sulfoxide, chloroform, heptane, 1,4-dioxane, dichloromethane, 2-propanol, N,N’-dimethylacetamide, acetone, formamide, ethylene glycol and water. 143

LIST OF SYMBOLS AND ABBREVIATIONS

a-BN plates	Aligned Boron Nitride Plates
APTES	Aminopropyl-triethoxysilane
ARCA	Advancing and Receding Contact Angles
ATR	Attenuated Total Reflectance
BE	Binding Energy
BN	Boron Nitride
BNNSs	Boron Nitride Nanosheets
BNNTs	Boron Nitride Nanotubes
BOCVD	Boron Oxide Chemical Vapor Deposition
CA	Contact Angle
CAH	Contact Angle Hysteresis
CNTs	Carbon Nanotubes
CNCs	Cellulose Nanocrystals
CVD	Chemical Vapor Deposition
DCM	Dichloromethane
DMA	Dynamic Mechanical Analysis
DMAc	*N,N'*-Dimethylacetamide
DMF	Dimethyl Formamide
DMSO	Dimethyl Sulfoxide
ESC	Environmental stress cracking
EG	Ethylene glycol
EtOH	Ethanol

f-BNNTs	Functionalized Boron Nitride Nanotubes
f-CNTs	Functionalized Carbon Nanotubes
f-hBN	Functionalized hexagonal Boron Nitride
FTIR	Fourier-transform infrared
HABS	Hydrogen-Assisted BNNT Synthesis
h-BN	hexagonal Boron Nitride
HDPE	High-density Polyethylene
HSP	Hansen Solubility Parameters
IPA	2-propanol
IPDI	Isophorone Diisocyanate
m-BNNTs	Modified Boron Nitride Nanotubes
MEK	Methyl Ethyl Ketone
MeOH	Methanol
MTPS	Modified Transient Plane Source
MWCNTs	Multiwalled Carbon Nanotubes
NMP	N-methyl-2-pyrrolidone
PC	Polycarbonate
PDMS	Poly(dimethylsiloxane)
PECVD	Plasma-enhanced Chemical Vapor Deposition
PE-PLD	Plasma-enhanced Pulsed-laser Deposition
PET	Polyethylene terephthalate
PEVA	Poly(ethylene vinyl alcohol)
Phr	Parts per hundred of rubber

PICVD	Photo-initiated Chemical Vapor Deposition
PMMA	Poly(methyl methacrylate)
PmPV	Poly[m-phenylenevinylene-co-(2,5-dioctoxy-p-phenylenevinylene)]
PS	Polystyrene
PS-DVB	Polystyrene-divinylbenzene
PVA	Polyvinyl Alcohol
PVB	Poly(vinyl butyral)
PVC	Pressurized Vapor Condenser
PVF	Polyvinyl formal
PVP	Polyvinylpyrrolidone
RED	Relative Energy Difference
RGO	Reduced Graphene Oxide
RH	Relative Humidity
RST	Relative Sedimentation Time
SBR	Styrene Butadiene Rubber
SE	Surface Energy
Syngas	Synthesis gas
TACVD	Thermally Activated Chemical Vapor Deposition
t-BNNTs	Treated Boron Nitride Nanotubes
TEM	Transmission Electron Microscopy
THF	Tetrahydrofuran
TPU	Thermoplastic polyurethane
UV	Ultraviolet

XSBR	Carboxylated Styrene Butadiene Rubber
XPS	XPS X-ray Photoelectron Spectroscopy

LIST OF APPENDICES

Appendix A METHODS OF SYNTHESIS OF BNNT 133

Appendix B ARTICLE 1 SUPPLEMENTARY INFORMATION 136

Appendix C ARTICLE 2 SUPPLEMENTARY INFORMATION 146

Appendix D ARTICLE 3 SUPPLEMENTARY INFORMATION 149

Appendix E LIST OF CONTRIBUTIONS 150

CHAPTER 1 INTRODUCTION

Polymers, macromolecules composed of many repeating units, have a wide range of applications, going from every-day products such as plastic bags to engineering materials used in the automotive or aerospace industries. Styrene-butadiene rubber (SBR), a synthetic rubber, possesses high impact strength and tensile strength, good resilience , as well as good abrasion resistance [1], [2], properties that makes it suitable for applications requiring high deformability, such as in passenger tires [1], [2], [3]. However, SBR possess low mechanical properties [4], [5] and as for most polymers, low thermal conductivity [5]. The need for tires with improved thermal conductivity is crucial to improve heat dissipation.

Tires are the elements of a vehicle that allows its movement forward, being the only parts that are in contact with the road [6]. They are designed to withstand hundreds of times their weight (up to 300 times) and to work properly in cold and hot environments (-50 ^{o}C to 80 ^{o}C) [7]. Their performance can be evaluated considering three main properties: rolling resistance, wear resistance and wet grip [8], [9], known as the "magic triangle". Rolling resistance, defined as the force that is opposed to the natural movement of the tire, leads to a heat buildup in the tire [10]. Dissipation of this heat is crucial to extend the durability of the tire.

Different fillers such as carbon black [11], [12] silica [4], clays [13], and carbon-based nanomaterials [5], [14], have been used to improve the thermal conductivity and mechanical properties of SBR, which is one of the main components of tires. However, new materials are constantly sought to keep improving the performance of the tires.

Boron nitride nanotubes, analogous structures to carbon nanotubes, are composed by alternating B and N atoms in a hexagonal network. BNNTs possess competitive mechanical properties such as a Young's modulus of 1.2 TPa [15], and a tensile strength of up to 33 GPa [16]. They also possess very high chemical and thermal stability, with decomposition temperatures above 800 °C [15], [17], making them ideal candidates for high temperature applications [17]. Their constant bandgap of 5.5 eV [18], [19], independent of tube chirality and diameter, provides them with electrical insulation. In addition, they possess a high thermal conductivity, with experimental values of ~ 350 /mK for nanotubes with diameters of 30-40 nm [20], [21]. Because of all these extraordinary properties, they are ideal candidates for fabrication of thermally conductive electrically insulating materials [21].

For a successful incorporation of nanoparticles into polymers, physical or chemical treatments are often needed. Covalent and non-covalent approaches are performed to reach this objective. While covalent approaches involve the creation of new chemical bonds on the surface of nanoparticles, they alter their original surface chemistry, modifying its intrinsic properties. On the other hand, non-covalent approaches preserve the intrinsic properties of the particles but suffer from being reversible and unstable at high temperatures. Both types of modifications can be performed in the liquid or gas phase. Liquid approaches are usually carried out in multiple steps, making the process potentially longer or complex. In addition, the removal of any impurity/undesired product is often required. Most of the time, liquid-phase approaches use toxic organic solvents and chemicals, making the process harmful to the environment. Gas-phase methodologies have emerged as an alternative to the former processes. They are usually performed in one step, which reduces the treatment time. The use of gaseous reactants eliminates the need of removal of undesired species. However, most of these techniques are carried out employing high energy or sophisticated equipment, making the process expensive.

The main objective of this work is to identify and validate a method to incorporate BNNTs into elastomer formulations, to improve thermal conductivity.

This thesis is composed of seven chapters, comprising three articles that have been published in peer-review journals.

- Chapter 2 provides an extensive literature review on five main themes: 1) behavior and properties of BNNTs, 2) thermally conductive polymer/BNNTs composites, 3) surface modification of BNNTs, 4) photo-initiated chemical deposition, and 5) solubility parameters.
- Chapter 3 summarizes the key gaps in knowledge in the field, and presents the specific objectives of the work, along with the organization of the articles.
- Chapters 4, 5 and 6 contain the three articles presenting the analysis and discussion of the main results of this work.
- Chapter 7 presents the general discussion in relationship to the results obtained throughout this work, as well as secondary results of interest.

- Chapter 8 exposes the conclusions and recommendations of this work, summarizing the main findings and original contributions.

CHAPTER 2 LITERATURE REVIEW

To meet the general objective, it is necessary to understand some concepts. This literature review is focused on five main themes: 1) behavior and properties of BNNTs, 2) thermally conductive polymer/BNNTs composites, 3) surface modification of BNNTs, 4) photo-initiated chemical deposition, and 5) solubility parameters.

2.1 Boron nitride nanotubes

First synthesized in 1995 by Chopra et al. [22], boron nitride nanotubes (BNNTs) have been extensively studied in the last two decades. They are counterparts of carbon nanotubes (CNTs) where C atoms are replaced by alternating B and N atoms in a honeycomb network [23], [19], [18], [15] (Figure 2.1). BNNTs have been gaining interest in the scientific community due to their outstanding properties and potential applications in polymer matrices to improve mechanical performance and thermal conductivity, in electronics for heat dissipation or in hydrogen storage devices.

Due to their similar structures, a comparison between BNNTs and CNTs is inevitable. Both possess similar stiffness (∼1.2 TPa) [15] and thermal conductivity of ~ 350 W/m K at diameters of ~ 35 nm [15] [18]. However, what makes them different is their electrical properties: BNNTs are electrical insulators, having a stable bandgap of 5-6 eV, [18], [15], [24] in comparison with the semiconducting/conductive behavior of CNTs. Another difference is the polarity. BNNTs possess local dipole moments, due to their partial ionic B-N bonds [15], [18], while CNTs, composed only by C atoms, are considered as non-polar materials. Regarding the thermal stability, BNNTs have been shown to be stable up to ~ 800 °C in air [17], [15] in comparison with the degradation temperature of 500 °C for CNTs. Another difference between the two nanotubes is their physical appearance: pure BNNTs present a white color while CNTs are black [18].

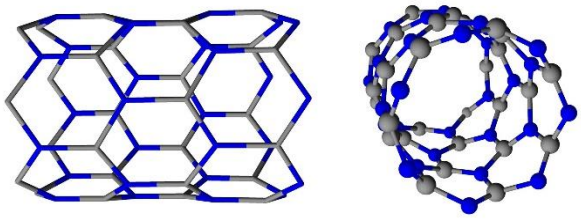

Figure 2.1 Structural model of single-walled BNNTs. Boron atoms are in blue, nitrogen atoms in gray, taken from Torres-Castillo et al. (2020) [25].

2.1.1.1 Electromagnetic properties

Although BNNTs are structurally similar to CNTs, they present different electronic behavior. BNNTs are classified as insulating materials due to a constant band gap of ~ 5.5 eV [18], [19], in comparison with a semiconducting behavior of the former. A dielectric constant of 5.90 has been calculated for BNNTs through theoretical studies, independent of radius, diameter, and chirality. However, it is possible to tune the electronic structure of BNNTs, by applying electric or magnetic fields or by doping them with other elements such as carbon or fluorine [18]. Even though BNNTs are electrical insulators, they exhibit very high thermal conductivities. This is attributed to the way that the thermal transfer takes place (via phonons instead of electrons) [23]. Because of that, they can be used in applications for heat dissipation, being thermally conductive materials while being electrical insulators.

Magnetic properties of BNNTs have been studied mainly theoretically [18]. Spontaneous magnetization can be induced through doping with carbon, although other approaches exist. For instance, a strong magnetic field can be induced with a chemisorption treatment using fluorine, being adsorbed on B atoms. The magnetic moment depends in a great extent on the atom that is used for doping the nanotube [15].

A piezoelectric behavior is observed in BNNTs due to their intrinsic partially ionic B-N bond [26], which differentiates from their counterpart CNTs. In BNNTs, an axial deformation of up to 1% has been obtained as a response of an electric field applied with a strength of 10 V nm^{-1} [15].

2.1.1.2 Optical properties

The optical behavior of BNNTs depends on the number of walls that form the nanostructure. In the case of multi-walled nanotubes, only one absorption peak is observed at 213.8 nm (5.8 eV) [27], [28] whereas for single-walled BNNTs, two absorption peaks can be seen at 278.6 and 225.4 nm (4.45 and 5.5 eV, respectively) [29], [28]. When BNNTs are subjected to light excitation (photoluminescence) or beams of electrons (cathodoluminescence) they emit violet or ultraviolet light [27], [28].

2.1.1.3 Thermal conductivity

Theoretical studies have reported a thermal conductivity in the range of 3000 - 6000 W/mK [18], [30] for BNNTs, while experimental data show values as high as 2400 W/mK for a 28-μm-thick BNNT films [31]. Thermal conductivity varies depending on the diameter, with a significant decrement when the diameter is increased. This is the reason why thermal conductivity is higher in nanotubes with a few walls, in comparison with the multiple layers in bulky materials [18].

Thermal conductivity in one-dimensional BN nanostructures (nanotubes) can be explained considering small hexagonal BN (h-BN) crystals as a starting point to obtain BNNTs. High thermal transfer in traditional two-dimensional h-BN powder is carried out in the (002) plane, while a poor thermal conductivity is present along the [002] direction, as can be seen in Figure 2.2a. The thermal transfer inside the (002) plane is much higher than the one observed along the [002] direction (Figure 2.2b). Based on that, one-dimensional BNNTs composed only of rolled (002) planes possess a high thermal conductivity along their axis direction, with experimental values of 200-300 W/mK for nanotubes of ~ 35 nm in diameter [20], [21]. This property decreases with the increase in nanotube diameter. On the other hand, thermal conductivity values in the transverse direction are around one order of magnitude lower, in the range of 20-30 W/mK [20] .

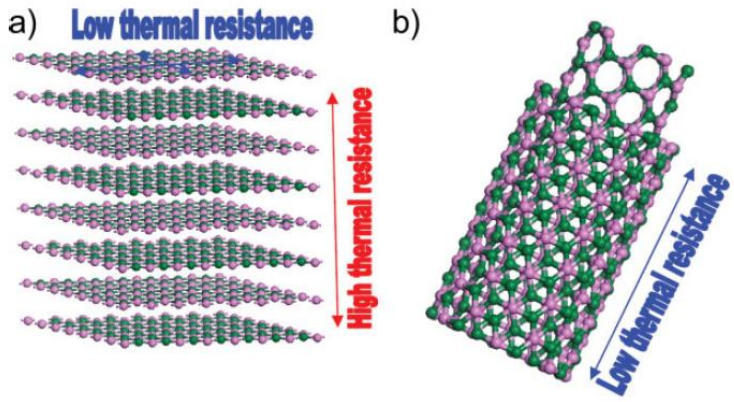

Figure 2.2 Schematics displaying the anisotropy of thermal conductivity in micrometer-sized a) BN particles and b) BNNTs. BN particles have high thermal conductivity in the (002) crystal plane with poor thermal conductivity along the [002] direction, taken from Zhi et al. (2009) [21].

Thermal conductivity values of BNNTs in the form of bucky paper have also been reported. Jakubinek et al. [32] prepared BNNTs sheets composed of 100% randomly oriented BNNTs. The in-plane thermal conductivity of purified BNNT sheets measured at 300 °K was ~ 1.5 Wm/K while the thermal conductivity of the BNNT network in those sheets was in the range of 9.4-11.7 W/mK. The BNNTs used were synthesized by the hydrogen-catalyzed induction thermal plasma process [33]. This method is briefly described in section 2.1.2 Methods of synthesis and is the one employed to produce BNNTs used in the present research work.

2.1.1.4 Chemical and thermal stability

The high chemical stability of BNNTs comes from the very stable B-N bonds [23]. A binding energy of 7-8 eV has been reported for a hexagonal B-N bond [34]. Thus, to carry out a covalent functionalization, an energy of 7-8 eV would be needed to break the B-N bonds. Depending on the method chosen for the chemical functionalization, electrons/ions or radicals should provide that energy to break the B-N bonds. In plasma technology, electrons should provide that energy and in the case of photoinitiated chemical vapor deposition, radicals, which are formed from the photo dissociation of reactants. In addition, it is possible to weaken the B-N bond through the intentional formation of defects. This can be done for example, by the creation of nitrogen vacancies (V_N) or by doping with other elements [34]. BNNTs have been doped with C, Eu and F [35]. In the case of

C-doping [36], B-C-N structures were formed after the treatment, which are a hybrid of hexagonal BN and graphite. These hybrids materials are considered semiconductors, where the chemical structure determines the band gap. The C-doping reduced the bandgap of pristine BNNTs from ~ 5.5 eV to 3.89 eV for the hybrid material, making it a semiconductor. Other kinds of defects comprise the presence of B-N-H bonds in the honeycomb network, instead of B-N, generated during synthesis [33].

Regarding their thermal stability, BNNTs are characterized to present high resistance to oxidative environments. They are resistant to at least temperatures of 800 ºC in air. The thermal degradation depends on the crystalline nanostructure and defects present in the sample. High crystallinity and low defect nanotubes lead to a higher thermal stability [18]. In fact, they have reached thermal stabilities up to 1100 ºC in air [15].

2.1.1.5 Wetting properties and solubility

The wetting properties of pristine BNNTs have been studied in several works. It has been reported that BNNTs possess a super hydrophobic surface [37] [38] [39], based on water contact angle measurements performed on bucky papers. Figure 2.3 shows the superhydrophobic nature of BNNTs films, due to the vertical alignment of the nanotubes. However, if we look at the chemical composition, we can see that the difference in electronegativity between B and N atoms leads to a partial ionic bond in the BNNT structure, providing them with a partial polarity.-In order to explain the discrepancies between the hydrophobicity or hydrophilicity of these nanomaterials, we need to pay attention at the type of BNNTs used, either in solid form (bucky paper) or in liquid state (i.e. dispersions). When BNNTs films are used for contact angle measurements, the results are influenced by surface properties such as roughness, alignment of the nanotubes, curvature, packing density or chemical heterogeneities [37], [38], [39], [33]. The more vertically aligned nanotubes in the film, the more voids it will contain, and thus, the more hydrophobic the surface [38], [39]. The synthesis method used have also an impact on the final surface properties of BNNTs [40], [33], by conferring chemical heterogeneities.

Yum et al. [41] calculated the wetting properties of individual BNNTs applying the Wilhelmy method. The estimated total surface energy (γ_s) was 26.7 mN/m, with a dispersive component (γ_s^d) of 22.5 mN/m and a polar component (γ_s^p) equal to 4.3 mN/m. In another work, Wu et al. [42] determined the wettability and surface energy of BNNSs. The water contact angle was 61.9 ° and the surface energy (γ_s) 50.54 mJ/m^2, with dispersive (γ_s^d) and polar components (γ_s^p) of 38.82 mJ/m^2 and 11.72 mJ/m^2, respectively. In the liquid phase, Mutz et al. [43] estimated the Hildebrand solubility parameter (δ_t) of BNNTs through static light scattering and refractometry. Based on their results, only dispersive interactions were considered, excluding polar and hydrogen-bonding ones. In another work, Tiano et al. [44] determined the solubility parameters of as-synthesized BNNTs through dispersion tests. In their work, the parameters indicated a mild polar surface. Amorphous boron was present in their work, and physical properties of the solvents and nanotubes were not considered.

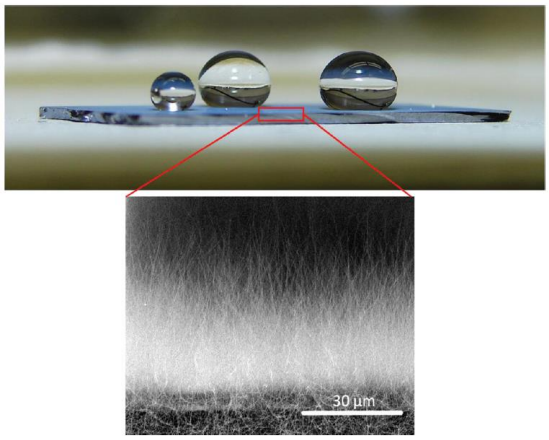

Figure 2.3 Super hydrophobicity of a BNNT film. The cross-sectional view of the sample shows the vertically aligned BNNTs, taken from Boinovich et al. (2011) [38].

Relative humidity plays an important role on contact angle measurements. As reported by Holysz et al. [45], high humidity contents would lead to adsorption of water by the substrate, which in turn, would affect the wettability properties.

As we could see, depending on the purity, nature and morphology of the BNNTs, different wettability and surface properties are obtained. Thus, when reporting contact angle results, surface

energy or solubility parameters, the synthesis method and the morphology of the BNNTs must be stated. These parameters play a significant role on determining those properties.

2.1.2 Methods of synthesis

BNNTs were first synthesized in 1995, by arc discharge [22]. After that, several methods such as substitution reaction [46], laser ablation [47], ball milling [48], chemical vapor deposition [49], [50], [51], [15], [52] plasma-enhance pulsed-laser deposition (PE-PLD) [53], or pressurized vapor condenser (PVC) [54] have been employed for their synthesis. A detailed description of these methods can be found in Appendix A.

Although different approaches exist, the main limitation of these methods is the low quality (large diameter nanotubes and low crystallinity) of BNNTs obtained, and in most cases, the low yield, with production rates of only 1g/h. Just a few works have been able to produce the high quality (small diameter few-walled nanotubes) and gram level-BNNTs [52], [50], [54], [33], [55]. One of this is the hydrogen-assisted BNNT synthesis (HABS) process nanotubes [33], developed in 2013 by the National Research Council Canada. The success for obtaining high purity material relies on the use of a non-metal catalyst (H_2), and an extremely high cooling rate during the growth of the nanotubes. In brief, hexagonal boron nitride (h-BN) powder as well as N_2 and H_2 gases are fed into a thermal plasma reactor (Figure 2.4). At high temperatures, the materials vaporize easily allowing their separation into individual species (B, N and H). Then, a high cooling rate at the inlet of the reactor is applied, to generate nano-droplets of boron. The subsequent growth of BNNTs is achieved due to the presence of reactive nitrogen intermediates under high temperature. The use of H_2 in the reactive gases is crucial because it allows the formation of B-N-H species and impedes the nitridation of individual nitrogen. The as-obtained BNNTs possess a beige color attributed to some amorphous boron impurities. For its removal, the material is heated at 425 ˚C in an air environment for not less than 72 h, to oxidize the boron to B_2O_3 [33]. A subsequent purification step at higher temperature (between 300 – 900 ˚C) using chlorine is performed, for further removal unoxidized boron, amorphous BN, $B_wN_xO_yH_z$ species, and for dehydrogenation of $B_xN_yH_z$ by products [56].

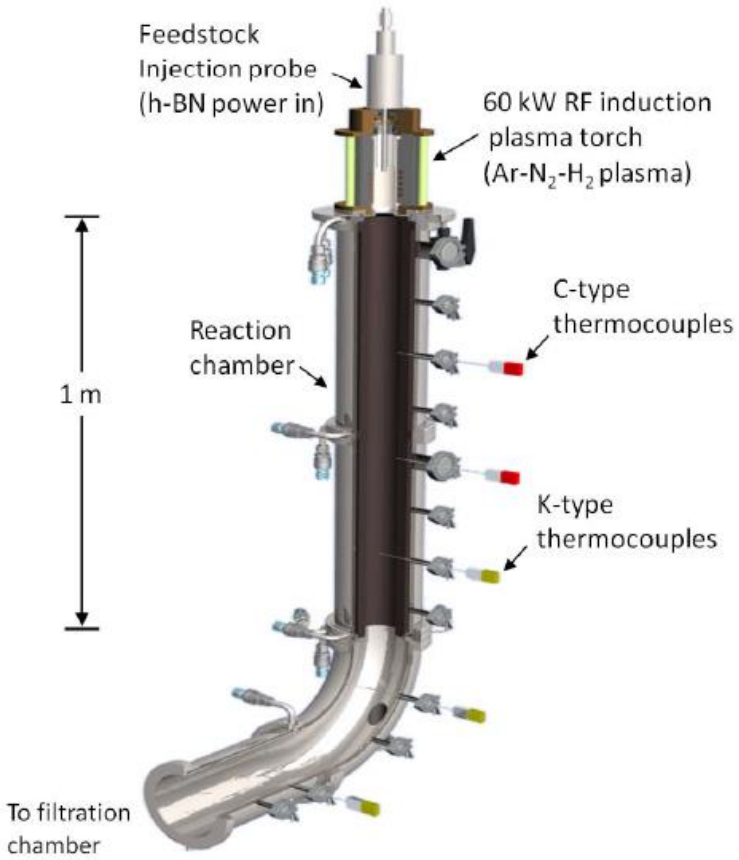

Figure 2.4 Scheme of the induction plasma process for the mass production of BNNTs, taken from Kim et al. (2014) [33].

2.1.3 Applications

Due to the extraordinary mechanical properties, BNNTs find potential applications as a reinforcing agents in polymers [57], [28], [23], [58], [59] and in ceramic materials [15], [60] and due to their high surface area, they are good candidates for hydrogen storage devices [18], [61]. In addition, because of their unique combination of thermal conductivity and electrical insulation, BNNTs can be used for heat dissipation in electronic packaging [21], [62], [63], [64]. They could also be used in tires for heat dissipation.

2.2 Thermally conductive polymer-BN nanocomposites

Due to their high thermal conductivity, BNNTs have been used to improve the heat dissipation in polymers. They are ideal candidates for fabrication of lightweight thermally conductive materials

with electrical isolation. This section covers the literature review comprising polymer/BNNTs nanocomposites with improved thermal conductivity. Table 2.1 shows a summary of some thermally conductive polymer/BN nanocomposites. ([1]a-BNNT stands for aligned BNNTs, m-BNNTs for modified BNNTs (non-covalent functionalization) and f-BNNTs for covalently functionalized BNNTs. X-SBR stands for carboxylated SBR).

Table 2.1 Summary of some thermally conductive polymer/BN nanocomposites.

Matrix	**BN nanostructure**	**Fabrication of the composites**	**BN %**	**TC of polymer (W/mK)**	**Max. TC of composite (W/mK)**	**Ref.**
PVA	a-BNNTs[1]	Electrospinning and hot-pressing	10 wt%	0.11	0.54	[20]
PS PMMA PEVA PVB	a-BNNTs[1]	Filtration and hot-pressing	35 wt% 24 wt% 37 wt% 18 wt%	0.18 0.15 0.17 0.24	3.61 3.16 2.5 1.81	[21]
PVF PVA	1) m-BNNTs[1] 2) m-BNNTs[1]	Solvent casting	1) 10 wt% 2) 3 wt%	1) 0.18 2) ~ 0.11	1) 0.45 2) ~ 0.30	[65]
PVP	a-BNNTs[1]	Electrospinning	30 wt%	0.27	~ 0.57	[66]
TPU	BNNTs	Solvent casting	1 wt%	-	14.5	[55]

TPU	1) BNNTs 2) m-BNNTs	Filtration	1) 42 wt% 2) 49 wt%	-	1) 2.9 2) 3.0	[67]
PC	a-BN plates[1]	Hot-pressing process	18.5 vol%	~ 0.225	3.09	[64]
Epoxy	f-BNNTs[1]	-	10 wt%	~ 0.25	~ 1.63	[68]
Epoxy	f-BNNTs[1]	Sonication and stirring	30 wt%	0.2	2.77	[62]
Epoxy	BNNTs	Impregnation	30 wt%	~ 0.2	2.9	[32]
Epoxy	m-BNNTs-BNNSs[1]	Mixing, evaporation and curing	2 wt%	0.19	0.47	[30]
Polymer-derived ceramic	BNNTs	Polymer derived ceramic processing	35.4 vol%	~ 0.196	4.123	[60]
SBR	BN nanoplatelets	Stirring, coagulation, mixing	1.5 wt%	0.2	0.26	[69]
SBR	1) h-BN 2) BNNSs 3) f-BNNSs[1]	Slurry compounding	10.5 vol %	0.16	1) 0.28 2) 0.43 3) 0.57	[70]

SBR	a,m-BNNSs[1]	Stirring, evaporation, two-roll mill mixing, compression	27.5 vol%	0.192	1.50	[42]
XSBR	1) hBN 2) f-hBN	Latex compounding	90 phr	0.09	1) ~ 0.45 2) 0.54	[71]
XSBR	1) BNNS 2) f-BNNS	Latex compounding, shear mixing	90 phr	0.09	1) 0.57 2) 0.66	[72]

Despite the very high values estimated and measured for BNNTs, modest increases are obtained when used in polymeric matrices. This can be attributed to the interfacial thermal resistance between the nanotubes [73], [74] and between the nanotubes and the polymer [30], [66], [63]. To reduce this interfacial resistance, physical and chemical treatments have been conducted. Fu et al. [73] reduced the interfacial thermal resistance between nanotubes by introducing "brigdes" with silver nanoparticles. A significant increase in thermal conductivity was observed in the composites. In another work, Zhang et al. [75], performed a simulation work of C doping of BNNTs to chemically activate their surface. Then, NH_2 functionalization was carried out. The doped functionalized epoxy/BNNTs (BNNT-A-EP) composites showed improved properties, with a thermal conductivity of 2.52 W/mK, 23.5 % and 77.5% higher than their undoped functionalized composite (BNNT-B-EP) and the undoped composite (BNNT-EP).

Another way to improve the thermal conductivity of the composites is by the alignment of the nanotubes in the polymeric matrix. They can be aligned by electric and magnetic fields [20], [66], by hot-pressing [21], [64], of by shear forces [42]. In other cases, surface modification techniques are needed to improve their compatibility and thus, dispersion into the polymer. Surface modifications treatments (covalent and non-covalent) of BNNTs are covered in the next section.

Styrene-butadiene rubber (SBR) is a synthetic rubber that posses a high abrasion resistance as well as high tensile and impact strength [1], [2], [59], able to withstand high deformability when external forces are applied. Due to these properties, it is one of the key components in tire formulations [1], [2], [3]. However, it possesses a low thermal conductivity, which can be translated as a low heat dissipation material. Different fillers such as carbon black [11], [12], silica [4], [76], [77], clays [13] and carbon-based nanomaterials [14], [5] have been used to improve the thermal conductivity and mechanical properties of the SBR matrix. The incorporation of BN nanostructures in rubbers have been limited to BNNS or h-BN [42], [70]. This could be attributed to the fact that the synthesis method it still expensive for the fabrication of high-quality nanotubes, in comparison to other BN nanostructures. In addition, a surface treatment or alignment was required for their incorporation into rubber, making the fabrication longer and more expensive.

2.3 Characterization of rubber compounds for tire applications

Three main properties are of interest to evaluate the performance of tires: rolling resistance, wet traction (or wet grip) and abrasion resistance (tire wear) [9], [78] which are known as the "magic triangle" [8]. Rolling resistance refers to the energy needed for the movement of the tire. It is related to the total fuel consumption, and thus, to the car efficiency. On the other hand, wet grip is related to safety and abrasion resistance, to the durability of the tire [9]. Usually, the improvement of one of these properties leads to a decrement in the other two. An ideal filler would be able to improve the three aforementioned properties at the same time.

As mentioned earlier, styrene-butadiene rubber is one of the main components of tires, used in the manufacturing of treads. For that reason, a great work has been devoted to study the dynamic properties of unfilled and filled rubber compounds. In order to simulate the straining cycles of tires due to rotation and braking in reinforced elastomers, dynamic strains at different temperatures and frequencies are employed [79]. Storage modulus (G'), loss modulus (G'') and tan δ curves are used to evaluate the viscoelastic properties of the material. Storage modulus refers to the elastic part of the material whereas loss modulus to the viscous part. Tan δ, also known as loss factor, expresses the ratio between G'' and G', and it is used to measure the portion of the energy that is dissipated during dynamic deformation [79].

Rolling resistance correlates with the deformation of the tire in the frequency range of 10-100 Hz, in a temperature interval of 50-80 °C [79]. On the other hand, wet grip occurs at room temperature and at frequencies in the range of 10^4 to 10^7 Hz, which are determined by the roughness of the road surface [79]. Due to the high frequencies involved in the performance of a tire, it is necessary to reduce them to a measurable level considering lower temperatures for the characterization of rubber composites. This is reached by applying the Time-Temperature Equivalence Principle, also known as WLF Temperature-Frequency Conversion [79].

According to viscoelastic properties, an ideal material used for the manufacturing of high-performance tires should have a low tan δ value in the temperature range of 50-80 °C [79] in to reduce the rolling resistance, and thus, the fuel consumption of the vehicle. In contrast, higher tan δ values in the range of -20 to 0 °C are desirable for improving the wet grip [79], [9]. An ideal tire should also be able to dissipate the heat generated internally and due to the friction of the tread with the road surface [10]. In order to fulfill those requirements, new materials are constantly sought to improve heat dissipation and elastic properties in tire treads.

2.4 Surface modification of BNNTs

Several approaches have been developed to improve the dispersion of BNNTs into polymers. They include the use of surfactants, surface modification (functionalization), polymer wrapping and sonication. [44]. The use of surfactants is a simple and cost-effective way to improve the dispersion, but it has the limitation that the compounds detach from the surfaces at low temperatures (as low as 65-70 °C) due to the fact that they are only adsorbed [80]. A similar behavior is observed when using polymer wrapping. The interactions between nanoparticles and solvents/polymers are weak (non-covalent) and they can easily separate. Sonication is used to help to disperse the nanoparticles in solvents using an external energy, but it has the disadvantage that it can damage the structure of the particle if too much energy is applied [81]. In addition, if there is no affinity between the solvent and the particle, the latter will sediment in the next few minutes after sonication.

In applications where the use of higher temperatures is required, surface functionalization shows promise. Surface functionalization can be performed in the presence of solvents (solvent/wet chemistry) or in their absence (gas phase). Solvent-based techniques often require the use of complex methodologies and multi-steps reactions, while the surface of the nanoparticles can be

damaged. In addition, the removal of unreacted species and the disposal of solvent waste can be time-consuming and complex, not to mention the management of health and safety concerns [82]. On the other hand, gas phase approaches are an alternative for the surface modification of nanoparticles. Specifically, chemical vapor deposition (CVD) shows a promising solution. There are several advantages when using gas phase techniques, compared to solvent-based methodologies. Gas phase techniques do not require the use of solvents; thus, the processes are less complex and cleaner. In addition, CVD allows the production of pure materials with high density on complex shapes. Gas techniques have the advantage that can be carried out in a continuous way instead of intermittent processes (batches) [80]. Table 2.2 shows a summary of some treatments that have been done with BNNTs. They include wet chemistry and gas phase approaches.

Table 2.2 Summary of some surface treatments of BNNTs.

Type of functionalization	**Work**	**Ref.**
Liquid phase, covalent	Covalent functionalization was achieved in BNNTs surface using stearoyl chloride. A chemical reaction between some amino groups on the edges of BNNTs (from NH_3 used in their synthesis) and the COCl from the reactive agent were expected. The resulting material was soluble in solvents with different polarity.	[83]
Liquid phase, non-covalent	Solubilization of BNNTs in aqueous and organic media was reached through functionalization of BNNTs with an amine-terminated oligomeric poly(ethylenglycol). The aqueous solution containing the functionalized material was colored brown due to the presence of the oligomer. However, after 3 days, the solution was reversible, losing its color.	[84]
Liquid phase, non-covalent	BNNTs were wrapped in poly[*m*-phenylenevinylene-*co*-(2,5-dioctoxy-*p*-phenylenevinylene)] (PmPV) using a wet chemistry approach. The functionalized material was soluble in	[27]

	organic solvents such as chloroform, tetrahydrofuran and *N,N*-dimethylacetamide.	
Liquid phase, non-covalent	BNNTs were functionalized using trialkylamine and trialkylphospine. The product of the reaction was then dispersed in organic solvents (toluene, benzene) and stable solutions were obtained.	[85]
Liquid phase, covalent	BNNTs were attached covalently to polystyrene (PS) and polymethyl methacrylate (PMMA) through a radical polymerization technique. In addition, carbon-BNNTs composites were produced using the f-BNNTs. Mechanical properties of composites were improved.	[86]
Liquid phase, covalent	BNNTs were chemically modified using isophorone diisocyanate (IPDI) molecules. The isocyanate (NCO) groups formed are capable to react with carboxylic, hydroxyl or amine groups, present in polymers or other compounds. An enhancement in mechanical properties was observed in m-BNNTs/polyvinyl alcohol (PVA) composites.	[57]
Liquid phase, non-covalent	The outer layers of BNNTs were peeled off after sonication treatments in primary alcohols. The B-N bond was weakened, producing BN nanostructures with different morphologies. Different primary alcohols were used. The alcohol with the longest alkyl chain (hexanol) gave the best results.	[81]
Liquid phase followed by gas phase, covalent	Dimethyl sulfoxide was used to weaken the B-N bond in BNNTs in order to facilitate a subsequent hydrolysis process. B-OH and N-H bonds were formed on B and N sites, respectively. Peeled shells resulted after the chemical treatment and Y junctions were formed.	[87]
Gas phase, covalent	Hydroxyl (-OH) and amine groups (-NH) were chemically attached to the BNNTs surface through a treatment with H_2O_2 at high pressure and high temperature. A subsequent esterification was carried	[58]

	out. Polycarbonate (PC) and polyvinyl butyral (PVB) composites were fabricated using modified BNNTs. Elastic modulus and tensile strength were improved.	
Gas-phase, covalent	Surface modification of BNNTs with amine groups was obtained through ammonia plasma treatment, using a microwave plasma generator. The high kinetic energy of generated N_2^+ ions (100 eV) allowed the formation of defects at the BNNTs surface (BE of h-BN of 7-8 eV). The functionalized NTs were dispersed in chloroform, forming a stable dispersion, in comparison with no dispersibility when using the pristine material.	[88]
Gas-phase, covalent	The surface of BNNTs was modified through a chemical vapor deposition approach by using a high-frequency induction furnace. The role of SO_2 gas generated during the synthesis and simultaneous surface modification of the NTs was critical. Three different morphologies (wool-like, balloon-like and collapsed nanotubes) were obtained but differences in chemical composition were not observed. The modified NTs showed higher specific area and thus an increase in the hydrogen adsorption capacity.	[61]
Gas-phase, covalent	Oxygen (O_2) plasma treatment was used to modify the surface of BNNTs. First, O_2 plasma was able to create N vacancies with subsequent addition of oxygen to BNNTs. In addition, surface functionalization of the NTs applying N_2 + H_2 plasma was performed, incorporating amide groups to the nanostructure.	[34]
Gas-phase, covalent	BNNTs films were treated with low-temperature H_2 plasma followed by CH_4/H_2 plasma. The stability of the superhydrophobic coatings was studied.	[39]
Gas-phase, covalent	Wenzel (homogeneous) and Cassie-Baxter (heterogeneous) states were studied for treated	[38]

	BNNTs using silicon as a substrate. Two approaches were used for the surface modification: UV/O_3 and high temperature plasma treatments.	
Gas phase, covalent	A room-temperature H_2/N_2 plasma treatment was used to tune the hydrophobicity of BNNTs films. A higher amount of amine functional groups were obtained when continuous wave and pulse mode (CW+P) were combined. Super hydrophilic, hydrophilic and hydrophobic surfaces were observed with little damage to BNNTs structure.	[37]
Gas-phase, covalent	Functionalization of intrinsically hydrophobic surface of BN nanostructures (including BNNTs films) was carried out in order to obtain super-hydrophilic surfaces. An ion/electron bombardment was applied to the samples in an air plasma environment.	[89]
Gas phase, covalent	Air-plasma treatment was used to control the wetting properties of BN nanostructures. The amount of grafted OH groups was crucial in determining the water wettability of the films.	[40]
Gas phase, covalent	Ammonia plasma was employed to covalently formed BNNT-NH_3. The functionalized material showed improved dispersion in water.	[90]
Gas phase, covalent	Low temperature oxygen plasma was used to functionalize the BNNTs. Different degrees of wettability were obtained at different treatment times.	[91]

As could be seen, liquid-phase functionalizations are carried out in several steps, making the process longer. In addition, a purification process is often required to remove any unreacted/undesired product. Gas-phase approaches have solved some of these issues. However, these treatments often require great amounts of energy, making the process expensive. A surface

treatment, ideally in the gas phase operating at low energy, is needed to tailor the surface properties of BNNTs.

2.5 Photo initiated chemical vapor deposition

Chemical vapor deposition (CVD) is a film deposition process that employs gases to carry out chemical reactions, which occur due to dissociation or excitement of the gaseous reactants in an activated environment [92]. Depending on the energy source used to start the reaction, CVD can be classified in thermally activated CVD (TACVD), plasma-enhanced CVD (PECVD) and photoinitiated CVD (PICVD). The use of heat, electrons, or light, respectively, is needed to initiate the reactions [92]. A comparison between these CVD techniques is shown in Table 2.3.

Table 2.3 Comparative table of CVD techniques [82], [94].

CVD technique	**Advantages**	**Drawbacks**
TACVD	✓ Simple operation ✓ Mature technique ✓ Large scale treatment ✓ High deposition rates ✓ Control of functionality	• High temperature required • Vacuum required • Limited range of monomers • Expensive • Low energy efficiency
PECVD	✓ Elevated deposition rates ✓ Mature technique ✓ Large scale treatment ✓ Different monomers can be used ✓ Control of functionality	• Vacuum requirement • High energy consumption • Expensive • Contamination in functional coating • Low cross linking • Low energy efficiency
PICVD (syngas/UVC)	✓ Operation at room temperature ✓ Operation at atmospheric pressure ✓ Inexpensive UV lamp ✓ Low energy consumption ✓ Inexpensive monomers and photo-initiators	• Photosensitivity of precursors is required • Slower deposition rate than PECVD • Technique in development • Control of $Fe(CO)_5$

	✓ Low cost ✓ Potential for scalability ✓ High crosslinking	• Reactor setup

Photo-initiated chemical vapor deposition (PICVD) employs light to start the chemical reactions. Single precursors or mixtures can be used. The precursors should be able to absorb UV light to allow complete or partial dissociation of constituent bonds of the absorbing precursor(s) or react with other excited species/radicals formed by the absorption of UV light of other precursors. The use of binary mixtures extends the degree and type of functionalities that can be obtained, by adjusting operational parameters [95], [96], [97], [82]. For example, Kasparek et al. [96] obtained different concentration of thiol (SH-) groups by varying the gas ratio of C_2H_2 and H_2S, while Grujicic et al. [97], optimized the synthesis of carbon nanotubes by tunning the mole fraction of methane in a mixture of CH_4 and H_2.

Syngas, or synthesis gas, is a mixture of carbon monoxide (CO) and hydrogen (H_2), obtained from biomass and waste gasification processes [98], [99]. Photochemistry of syngas has been studied by Dion et al. [80], Farhanian et al. [100] and Hosseininisab et al. [101] in photo-initiated chemical deposition processes. Based on those studies, commercial UVC germicidal lamps, with a main emission peak at 253.7 nm and a secondary peak at 185 nm allowed the decomposition/excitation of the aforementioned precursors for the deposition of oxygenated and carbon-based coatings [80], [100].

Syngas PICVD has been applied for the coating of copper coupons [80] and silicon wafers [100]. It has also been used for the coating of polymers such as high-density polyethylene (HDPE), polyethylene terephthalate (PET) [102] and polystyrene-divinylbenzene (PS-DVB) [103]. Regarding the modification of nanoparticles, the surface properties of cellulose nanocrystals (CNCs) [104], CNTs [82], and nanoparticles from ash powder [105], have been treated with this gas-phase technique. It has also been used for the encapsulation of magnetic iron oxide nanoparticles [106] and for the coating TiO_2 nanoparticles [107].

Due to the synthesis of nanoparticles such as CNTs and BNNTs are performed in the gas phase, it results pertinent to consider a subsequent functionalization step also in the gas phase. So far, gas-phase approaches operate at high temperature and/or under vacuum, using expensive equipment,

and thus, making the process expensive. Syngas PICVD, operating under normal conditions and at low energy requirements, is a promising scalable approach for modification of nanomaterials.

2.6 Solubility parameters

Solubility parameters, Hildebrand parameters, or cohesion parameters can be used to correlate and estimate the cohesive and adhesive energies of solvents and polymers considering the properties of individual species [108]. Cohesion parameters rely on the famous principle "like dissolves like", where homogeneous mixtures will be formed when polymers (or solid particles) are dissolved in liquids with similar parameters to them. Solubility parameters relates to the energy required to evaporate a liquid, and thus, the energy *E* required to keep the molecules together [109], [110]. This energy of vaporization, *E*, can be divided into three components: dispersive (E_D), polar (E_P) and hydrogen bonding (E_H) forces, as can be appreciated in equation 1. Diving each term by its molar volume, the energy of vaporization can be expressed as a cohesive energy density, *E/V* (equation 2). The Hildebrand parameter δ_t can be calculated as the root square of the cohesive energy density (equation 3), and can be divided into three components, related to the dispersion (δ_d), polar (δ_p) and hydrogen bonding (δ_h) interactions, which represent the Hansen solubility parameters (HSP) (equation 4). They are related to intermolecular interactions and determine the degree of solubility of a solute in a specific solvent [109], [110], [111]. Dispersion or London forces, present in all molecules, relate to the variations in the atomic dipole, formed by a positive nucleus surrounded by electrons. Polar interactions, including dipole-dipole (Keesom) and dipole-induce dipole interaction (Debye), refer to the non-uniform distribution of the electronic charge. Other interactions, mainly hydrogen bonding can also be present in certain molecules [110].

$$E = E_D + E_P + E_H \tag{1}$$

$$E/_V = {E_D}/_V + {E_P}/_V + {E_H}/_V \tag{2}$$

$$\delta = (E/V)^{1/2} \tag{3}$$

$$\delta_t{}^2 = \delta_d{}^2 + \delta_p{}^2 + \delta_h{}^2 \tag{4}$$

The units more often used for δ_t and the HSP are $MPa^{1/2}$, although it can also be expressed in $(cal/cm^3)^{1/2}$ [109].

Based on Hansen solubility theory, it is possible to plot the solutes and solvents in a three-dimensional (3D) space (Hansen space) with their corresponding HSP (δ_d, δ_p and δ_h) as coordinates (Figure 2.5). The center of the solubility sphere is determined by the solute coordinates with an experimental radius, R_o. The solvents located inside the sphere will dissolve the solute, with higher solubility for the solvents that are closer to the center of the sphere. The distance between the solvent and the solute, R_a, in the Hansen space can be determined applying the following expression (equation 5):

$$R_a{}^2 = 4(\delta_{d1} - \delta_{d2})^2 + \left(\delta_{p1} - \delta_{p2}\right)^2 + (\delta_{h1} - \delta_{h2})^2 \quad (5)$$

The ratio between R_a and R_o (equation 6), known as relative energy difference (RED), can be determined in order to estimate the position of the mixture in the solubility sphere. A RED < 1 indicates that the solvent will dissolve the solute. For RED = 1, partial dissolution is expected and for RED > 1, the solute will not dissolve in the solvent. HSP values can be used to predict the solubility of nanomaterials in specific solvents, by correlating their Hansen solubility parameters. In addition, not only single solvents can be used but also binary mixtures of solvents (co-solvents) [44].

$$RED = \frac{R_a}{R_o} \quad (6)$$

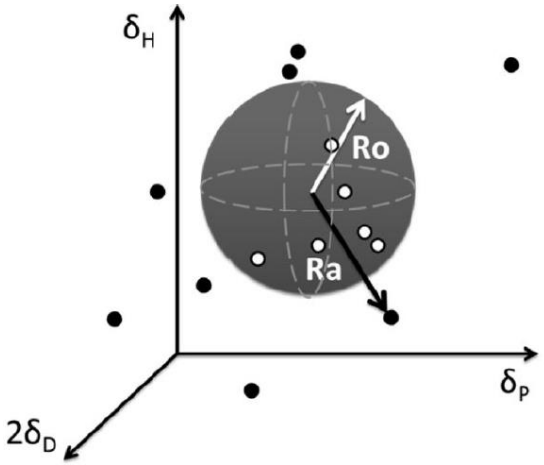

Figure 2.5 Graphical representation of the Hansen. Good solvents (white points) are inside the sphere while bad solvents (black points) are outside, taken from Ma et al. (2013) [112].

2.6.1 Characterization of polymers

Different approaches exist to determine the HSP of polymers. These include dissolution, swelling [113], [114], [115], determination of the melting point, measurements of viscosity, evaluation of environmental stress cracking (ESC), permeation measurements or chemical resistance evaluations [109], [111]. Among these methods, the simplest one is the evaluation of the dissolution of the polymer. Solvents able to dissolve the polymer will have HSP closer to the polymer, while solvents presenting low degree of solubility (or no solubility), will have parameters further away [109], [111]. This method requires that a certain amount of polymer is put into a fixed amount of solvent, and then, after a certain time, the dissolution state is evaluated qualitatively (visually), classifying the solutions as “good” or “bad”. The data are entered into the computer program (*HSPiP*) [116] to obtain the HSP of the polymer in question.

2.6.2 Characterization of nanoparticles

Hansen solubility method has been used to characterize surfaces such as pigments, fibers and fillers. Small quantities of the particles are deposited in tests tubes containing a fixed volume of liquid. Then, agitation is required and sedimentation or its absence can be observed. If the particle

size of the solid is large (> 5 μm), the surface effects are less significant in comparison with particles with smaller size (< 0.01 μm). A relative sedimentation time (RST) can be used instead of absolute sedimentation time to compensate for differences in density and viscosity (equation 7) [109].

$$RST = t_s\left(\frac{\rho_p - \rho_s}{\eta}\right) \quad (7)$$

where ρ_p and ρ_s refer to the densities of particle and the solvent and η is the viscosity of the solvent. The use of purified nanoparticles is important to ensure a constant density through the sample. Impurities present in the material would lead to different densities, and thus, different sedimentation rates. Similarly, the viscosity and density of the solvents affect the sedimentation rates.

HSP of BNNTs have been determined previously. As a first attempt, Mutz et al. [43] determined the total solubility parameter (δ_t) for unpurified multi-walled BNNTs, based on static light scattering measurements and, on the Flory, and Hildebrand–Scatchard solution theories. They listed potential good solvents to disperse the BNNTs based only on δ_t, which is not enough to predict reliable solvents, because polar and hydrogen bonding interactions are not considered. Tiano et al. [44], improved the characterization by considering the dispersive, polar and hydrogen bonding interaction of BNNT in different organic media. Although they considered the three types of interaction, their limitation relies on that unpurified material was used as well, affecting the sedimentation rated of their dispersion, due to the presence of boron and other impurities that could have sedimented faster than the purified nanotubes. Measurement of the dispersibility based on solubility parameters and HSP determination of other nanoparticles such as cellulose nanocrystals (CNCs) [117], [118], CNTs [112] [119], [120], graphene [121], graphene oxide [122], reduced graphene oxide [123], halloysite nanotubes [124], titanium carbide nanosheets [125], and exfoliated metal nanosheets [126] has also been conducted.

CHAPTER 3 OBJECTIVES AND ORGANIZATION OF THE ARTICLES

The literature review presented in the previous chapter highlights that a proper characterization of the dispersibility of pristine boron nitride nanotubes has yet to be presented. Indeed, although a few works have been reported in the literature, a reliable characterization was lacking. Such understanding, which is a proxy to expressing BNNT surfaces properties, is necessary knowledge to improve the incorporation of BNNTs into polymers.

Once the surface properties are determined, surface modification techniques (in the liquid or gas phase) can be performed. Depending on the final application, gas-phase or liquid-phase approaches are preferred. One main drawback of the liquid-phase methods is that they are multi-step processes, which requires purification steps, elevating the operational costs. Thus far, the only reported gas-phase modification techniques for BNNT covalent functionalization have been based on plasma – while functional, these pose difficulties from scalability and cost points of view. A low-cost gas phase technique is missing for large-scale functionalization of BNNTs.

The partial ionic B-N bond imparts mild polar characteristics to BNNTs, making them suitable for incorporation into mildly polar media. However, some applications involve the use of non-polar polymers, such as SBR. Thus, a facile approach for improving compatibility between these two materials is needed for fabrication of polymer composites with improved properties.

3.1 Objectives

3.1.1 General objective

The main objective of this work is to identify and validate a method to incorporate BNNTs into elastomer formulations, to improve thermal conductivity.

3.1.2 Specific objectives

In order to achieve the general objective, the following subobjectives are pursued:

SO1. Determine the relationship between the surface chemistry of pristine BNNTs and their dispersibility in organic solvents.

SO2. Propose and demonstrate an alternate, cost-effective gas phase method for BNNT surface modification.

SO3. Develop a method to incorporate the BNNTs into styrene-butadiene rubber to fabricate nanocomposites with improved thermal conductivity.

3.2 Organization of the articles

In order to fulfill the above-mentioned objectives, three scientific articles are presented. Chapters 4 to 6 show the main results of this research work.

Chapter 4 presents the first publication of this dissertation entitled: "*Chemical affinity and dispersibility of boron nitride nanotubes*". This work studies the dispersibility of BNNTs in a wide set of organic solvents. This characterization, based on Hansen solubility theory, allowed us to determine the Hansen solubility parameters of purified nanotubes, considering differences in densities of the nanoparticles and solvents, as well as viscosities of the solvents. With these physical properties, a corrected sedimentation time was calculated. The previous works in the literature did not consider these properties, which may lead to unprecise results. When determining the sedimentation times, the purity of the nanoparticle plays a key role. If other components are present (such as contaminants) possessing higher or lower densities, different sedimentation rates will be observed, and thus, heterogeneous dispersions will be formed. This paper was published in *Nanoscale Advances,* **2020***, 2,* 2497 (DOI: 10.1039/d0na00136h).

Chapter 5 describes the second publication of this study entitled "*Covalent functionalization of boron nitride nanotubes through photo-initiated chemical vapour deposition*". This article presents how we were able to tailor the chemistry of BNNTs towards hydrophilic surfaces, employing photo-initiated chemical vapor deposition. This low-cost technique operating a room temperature and near atmospheric pressure, is a promising approach for surface modification of nanoparticles. X-ray photo electron spectroscopy showed a highly oxidized BNNT surface after treatment. In addition, a decrease in water contact angle and an increase in surface energy were observed for the treated material. These results open new possibilities to incorporate hydrophilic BNNTs surfaces

into polar polymers or other matrices of interest. This paper was published in the *Canadian Journal of Chemical Engineering*, **2022** (DOI: 10.1002/cjce.24440).

Chapter 6 presents the third part of this research with the paper entitled: "*Thermally conductive styrene-butadiene rubber/boron nitride nanotubes*". This work shows how solubility theory can be used to predict suitable solvents for different materials, such as nanoparticles and polymers. Based on this theory, we were able to improve the affinity of BNNTs for the polymeric matrix (styrene-butadiene rubber), by mixing both components in a binary mixture. No chemical functionalization or additional treatments were required for this particular test case. The solvent casting technique followed by hot-pressing was chosen as the fabrication method. The thermal conductivity of the nanocomposites was improved of up to 35 wt% and a 235 % increase in storage modulus was obtained when a BNNTs loading of 10 wt% was used. This paper was published in the *Journal of Composite Science*, **2022** (DOI: 10.3390/jcs6090272)

CHAPTER 4 ARTICLE 1 : CHEMICAL AFFINITY AND DISPERSIBILITY OF BORON NITRIDE NANOTUBES

Cristina Sofia Torres Castillo, Charles Bruel, Jason. R. Tavares

Department of Chemical Engineering, École Polytechnique de Montréal, P.O. Box 6079, Station Centre-Ville, Montreal, Quebec, H3C 3A7, Canada

Published in:

Nanoscale Advances, 2020, Vol. 2, pp 2497-2506

https://doi.org/10.1039/D0NA00136H, Publication Date: May 2020, Available online 5 May 2020,

KEYWORDS :

Boron nitride nanotubes; dispersibility; solubility parameters

Abstract

Boron nitride nanotubes (BNNTs) are electrically insulating nanoparticles that display highly competitive elastic modulus and thermal conductivity. Long presented as potential fillers for nanocomposite applications, their poor dispersibility in most commodity polymers has, however, limited their spread. In this work, the chemical affinity of purified BNNTs, measured in terms of Hansen solubility parameters (HSP), was obtained through sedimentation tests in a wide set of organic solvents, taking into account relative sedimentation time. The parameters obtained were $\{\delta_d; \delta_p; \delta_h\} = \{16.8; 10.7; 14.7\} \pm \{0.3; 0.9; 0.3\}$ $MPa^{1/2}$, with a Hildebrand parameter, $\delta_t = 24.7$ $MPa^{1/2}$ and a sphere radius of 5.4 $MPa^{1/2}$. The solubility parameters were determined considering complete dispersion of the purified nanomaterial, as well as the viscosity and density of the host solvent. These factors, combined with the high purity of the BNNTs, are crucial to minimize the uncertainty of the HSP characterization. Such refined values provide necessary insights both to optimize the solvent casting of unmodified BNNTs, and to orient the surface modification efforts that would be needed to integrate these nanomaterials into a wider range of host matrices.

4.1 Introduction

Boron nitride nanotubes are counterparts to carbon nanotubes (CNTs) in which C atoms are replaced by alternating B and N atoms in a honeycomb network (Figure 4.1) [23], [19], [18], [15]. First synthesized in 1995 [18], these nanomaterials have properties that may outmatch those of CNTs for high temperature or electrical insulation related applications. Compared with CNTs, BNNTs display a competitive Young modulus (~ 1.18 TPa) and thermal conductivity (up to ~ 350 Wm/K). Contrary to CNTs, they have a high thermal stability (up to 1100 °C in air) [15] and are electrical insulators, with a constant band gap of ~ 5.5 eV. CNTs degrade from ~ 500 °C in air and are conductive or semi-conductive materials [23], [18]. The two nanotube types also differ in their physical appearance: pure BNNTs present a white color while CNTs are black [18].

The partially ionic B–N bonds in BNNTs bring about their unique properties [18], [15]. A difference in electronegativity between B and N atoms leads to the formation of local dipole moments, providing BNNTs with a polar behavior [18].

BNNTs find potential applications as reinforcing agents in polymeric and ceramic materials [15] and, due to their high surface area, are good candidates for hydrogen storage devices [18], [61]. In addition, because of their unique combination of thermal conductivity and electrical insulation, BNNTs can be used for heat dissipation in electronics and computers [30], [21], [62]. However, in spite of these attractive properties, their incorporation into composites has been hindered mainly by production limitations: few methods exist to produce large quantities and high-quality material (high crystallinity, small diameter and few walls) [19], [18]. In 2013, the National Research Council of Canada patented an industrially-scalable approach for the increased production (20 g h^{-1}) of few-walled and small diameter (~ 5 nm) BNNTs [33], [127], [128]. In brief, hexagonal boron nitride (h-BN), N_2 and H_2 are used as precursors in a thermal plasma reactor. These are dissociated into individual atoms (B, N and H) and recombine as BNNTs. Hydrogen acts as a catalyst and is crucial in reaching a high production rate for BNNTs. It enables the formation of nitrogen reactive species and impedes the formation of N_2 as a side product [33]. While high production rates have therefore become possible, there remains little available knowledge to reliably disperse BNNTs in solvents and polymers.

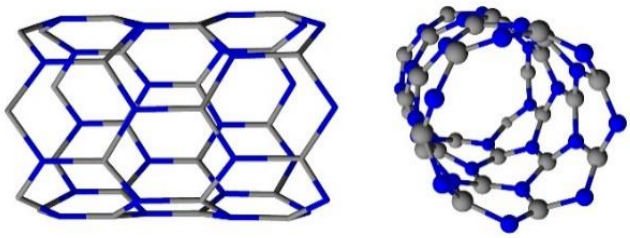

Figure 4.1 Structure of single-walled BNNTs. Boron atoms are in blue, nitrogen atoms in grey.

As a starting point to predict dispersion behaviour, Mutz et al. [43] determined the Hildebrand solubility parameter of BNNTs, on the basis of the Hildebrand-Scatchard Solution Theory. Using this parameter, they proposed a list of potential good solvents for dispersing these nanotubes. However, predicting chemical affinity by considering only the Hildebrand solubility parameter (δ_t) is not reliable, unless the chemical in question displays a purely non-polar behavior, such as saturated aliphatic hydrocarbons [109]. Otherwise, dispersive, polar, and hydrogen bonding interactions should be considered.

In another work, Tiano et al. [44] determined the Hansen solubility parameters (HSP) of few-walled BNNTs (up to three walls) through sedimentation tests. They used as-synthesized material without any further purification, containing boron nanoparticles as impurities. These impurities not only have different surface chemistry than the nanotubes but also different density (~ 2.3 vs 1.4 g/ml), which significantly modifies the sedimentation rate. In addition, some discrepancies are found in their work regarding the determination of good solvents.

Solubility parameters of purified BNNTs are necessary to orient surface modification efforts. Indeed, according to the literature, several covalent [83], [58], [57], and non-covalent [129], [130], [84], [85], [131] functionalization methods have been carried out on BNNTs in attempts to properly disperse them in a specific medium. However, in most cases, the methodology applied is not specifically tailored or targeted, relying instead on general assumptions to promote dispersion. Given that surface modification approaches can be complicated and time consuming, that they employ costly molecules as surfactant/modifier agents and that, in the case of covalent functionalization, the intrinsic properties of BNNTs are often modified (initial sp^2 structure altered), these efforts must be guided by a strong initial knowledge of the BNNTs dispersion to target the most appropriate surface treatment.

In order to have a proper characterization of the dispersibility of purified BNNTs, here, we apply the Hansen solubility theory, taking into account differences in density and viscosity of the solvents, to characterize the surface properties of BNNTs through sedimentation tests. Having defined their HSP, three scenarios may be addressed. First, surface modification may be performed depending on the chemical affinity (or lack of it) between the BNNTs and the polymeric matrix. Second, if the functionalization method is solvent-based, then, knowing the proper solvents to disperse BNNTs will allows us to select the best media in which to conduct surface modification. Third, when using solvents casting techniques, the selection of an appropriate solvent will improve nanocomposite fabrication.

4.2 Theory

Solubility parameters rely on the principle that “like seeks like”, which states that liquids with similar parameters will form homogeneous mixtures [109]. Transposed to particles, this principle means that solvents will better disperse particles with similar surface chemistry. The Hansen

solubility method has been successfully used to characterize solid surfaces such as pigments, [124] fibers, nanoparticles [44], [120], [119], [132], [133], [121], [118], [117], and fillers.

Solubility parameters, also known as *cohesion parameters*, can be related to the amount of energy necessary to evaporate a liquid [109]. This is a measure of the total energy required to keep the molecules of a liquid together, expressed as the cohesive energy density (E/V) (eq. 1):

$$\delta_t = (E/V)^{1/2} \qquad (1)$$

Where δ_t ($MPa^{1/2}$), V (mol/cm^3), and E (kJ/mol), are the Hildebrand solubility parameter, the molar volume of the solvent and its latent heat of evaporation, respectively [109].

The Hildebrand solubility parameter can be divided in three components related to dispersion (δ_d), polar (δ_p) and hydrogen bonding (δ_h) interactions [109]. These are known as Hansen solubility parameters (HSP) (eq. 2) and provide a measure of the strength of the interactions that a chemical may form in a specific solvent [109].

$$\delta_t{}^2 = \delta_d{}^2 + \delta_p{}^2 + \delta_h{}^2 \qquad (2)$$

Dispersion forces (δ_d), produced by atomic interactions, accounts for non-polar London interactions [109]. Polar forces (δ_p) are present when permanent dipole-permanent dipole interactions are formed. These interactions occur at the molecular level and the dipole moment is used to determine this type of attractions [109]. Like in polar forces, hydrogen bonding interactions (δ_h) take place at a molecular level. δ_h has been generally used to describe the capability of electron exchange determined by Lewis' acid and base theory [134]. δ_h has been divided into sub-parameters such as acid-base, dispersion, induction, orientation, as well as proton-donors and proton-acceptors. However, the use of a single parameter to describe hydrogen bonding interactions has been proven to give satisfactory results [109].

Based on Hansen solubility theory, it is possible to plot the particle of interest and solvents in a three-dimensional (3D) space (Hansen space) with their corresponding HSP {δ_d; δ_p; δ_h} as coordinates. The center of the solubility sphere is determined by the particle coordinates with an experimental radius, R_o. The solvents with coordinates located inside the sphere will disperse the particle, with higher dispersibility for the solvents that are closer to the center of the sphere [109].

The distance between the solvent and the particle, R_a, in the Hansen space can be determined applying eq. 3:

$$R_a{}^2 = 4(\delta_{d1} - \delta_{d2})^2 + \left(\delta_{p1} - \delta_{p2}\right)^2 + (\delta_{h1} - \delta_{h2})^2 \quad (3)$$

$$RED = \frac{R_a}{R_o} \quad (4)$$

The ratio between the R_a and R_o (eq. 4), known as the relative energy difference (RED), estimates the position of the solvent in the solubility sphere [109]. RED < 1 indicates that the solvent will disperse the particle. For RED = 1, partial dispersion is expected and for RED > 1, the particle will not disperse in the solvent. HSP can also be used for binary mixtures of solvents (co-solvents).

When determining the HSP of nanoparticles, several factors should be considered, owing to different interactions that may occur. For instance, Bergin et al. [120] demonstrated that increasing the diameter of the nanotubes decreases δ_t by reducing the surface to volume ratio: this structural link between δ_t and morphology is also expected for BNNTs (eq. 5).

$$\delta_t = 2\sqrt{\frac{E_{S,T}}{D}} \quad (5)$$

Where $E_{S,T}$ and D correspond to the total nanotube surface energy and to the nanotube diameter, respectively. Exploring this in the context of CNTs, they demonstrated that the Hildebrand parameter decreases when D increases [120].

Empirically, HSP may be determined by depositing small quantities of particles in test tubes containing a fixed volume of liquid and subsequently agitating [109]. Stability is assessed based on the presence of agglomerates in suspension, assessed visually or through spectroscopic means. If the particle size of the solid is large (> 5 μm), surface effects are less significant compared to particles with smaller sizes (< 0.01 μm). Nonetheless, viscosity and buoyancy effects can impede proper analysis of a solid suspension. To compensate for differences in density and viscosity, a

relative sedimentation time (RST) can be used instead of absolute sedimentation time, t_{sed}, (eq. 6) [109].

$$RST = t_{sed}\left(\frac{\rho_p - \rho_s}{\eta}\right) \qquad (6)$$

where ρ_p and ρ_s refer to the densities of particle and the solvent and η is the viscosity of the solvent. For the determination of solubility parameters, the HSPiP software is typically used [116]. A description of the mathematical analysis is presented in the ESI (Appendix B).

4.3 Experimental part

4.3.1 Materials and methods

Purified BNNTs were provided by Tekna Plasma Systems, Inc. (Sherbrooke, Qc, Canada) in the form of buckypapers (2cm x 2cm). They were obtained from the previously described induction thermal plasma process [33], [135]. The as-obtained BNNTs possessed a beige color, attributed to the presence of amorphous boron [33], [56]. These impurities were removed through the purification method described by Cho et al. [56]. Briefly, the as-obtained BNNTs were dried for 3 h at 150 °C. They were then pre-heated in a quartz tube at 105 °C in an Ar atmosphere, keeping the temperature constant for 20 min. The quartz tube was then filled with Cl_2. The temperature was raised to 750 °C, under a flow of 1 standard liter per min of Cl_2. The exposure time was set at 1 min per gram of as-obtained BNNTs. These selective chlorine etching conditions were used to remove boron allotropes, including $B_xN_yH_z$ derivatives [56]. The system was then purged with N_2 and allowed to cool under a steady flow of N_2. The purified material was subsequently bath sonicated in methanol. Despite the purification process, SEM images suggest that some BN hollow cages are, however, still present in the material [33], [56]. These structures are also visible on our TEM images (Figure *4.2*C and D).

Organic solvents were obtained by chemical suppliers and were used without any further purification. Most of them were of high purity (≥ 99%) with exception of d-limonene (96%) and ethanol (95%). The list of solvents employed, as well as their physical properties (density, viscosity and molar volume) and HSP, are available in Table 4.1 and Table B.1. Solvent selection considered

the list of solvents proposed by Hansen for sedimentation tests, for which solubility parameters have been validated experimentally [109], and expanded with a few additional solvents: ethyl benzoate, d-limonene and heptane, whose HSP values were determined through modelling.

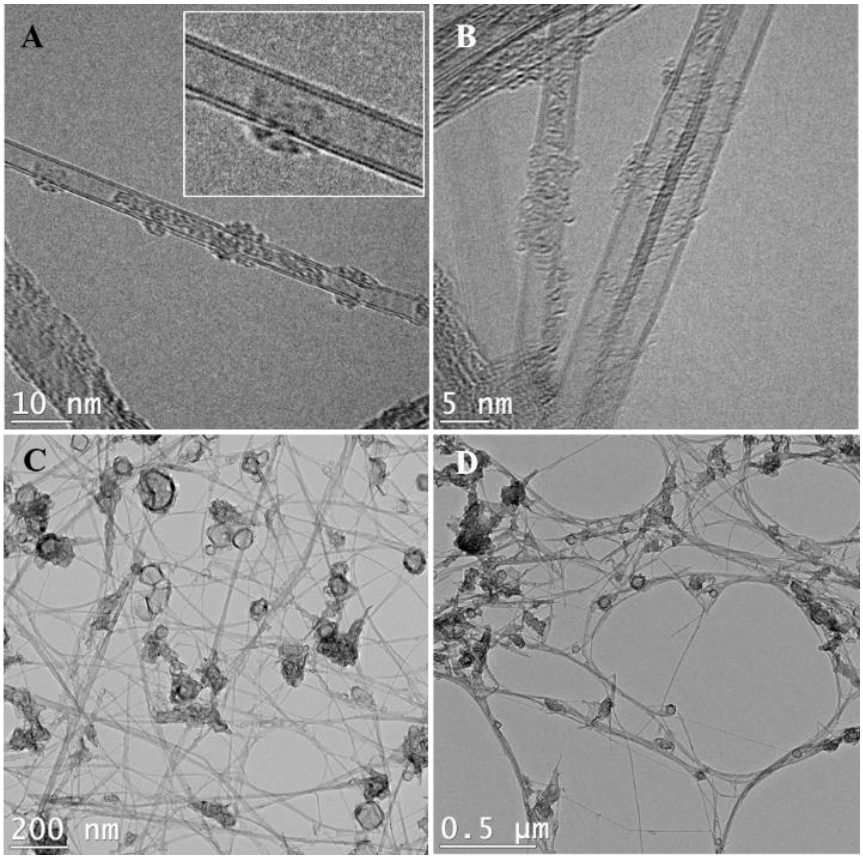

Figure 4.2 Representative TEM images of BNNTs dispersed in ethanol. (A and B) BNNTs have a diameter of approximately 5 nm. The inset in (A) shows they are double walled. (C and D) BNNT length is on the order of a few µm, and some BN hollow cages remain in the material.

4.3.2 Microscopy

TEM analysis was performed in BNNT dispersions using ethanol as a solvent. In brief, 1 mg of BNNTs was added to 10 mL of anhydrous ethanol and the resulting mixture was sonicated with a probe sonicator supplying 500 J of energy. A drop of the solution was deposited on a copper TEM grid and dried overnight. The analyses were performed using a Jeol JEM 2100F transmission electron microscope in bright field imaging mode, operating at 200 kV.

4.3.3 Sedimentation tests

10 mL of solvent were added to 1 mg of BNNTs in a glass vial of diameter 2.5 cm. This concentration was chosen as an intermediate value to form stable BNNTs dispersions in different solvents, according to previous works [43], [44].

To disperse the nanoparticles, a Cole–Parmer probe sonicator was employed with an operation frequency of 20 kHz using a cylindrical probe (type 410–08). The treatment consisted of pulsations operating with 5 s ON/2 s OFF cycles set at 30% of amplitude and a power in the range of 20–30 W. A total energy of 500 J mgBNNTs^{-1} was used, which is high compared to typical standards for nanomaterial dispersion (e.g. 10 J mg^{-1} required to disperse cellulose nanocrystals in water) [136], attributable to the BNNTs high aspect ratio. To prevent any overheating, the vials were kept in an ice bath during sonication. The resulting suspensions were kept in a quiescent state at room temperature to allow the nanoparticles to sediment. The density of BNNTs was obtained from the literature [43], [137] and an average of 1.5 g cm^{-3} was used. A relative sedimentation time (RST) of 1.03 x 10^{11} s^2 m^{-2} was considered, corresponding to an absolute sedimentation time (t_{sed}) of 48 h in N,N'-dimethylacetamide (DMAc). This solvent was chosen as a reference because it remained in a good dispersion state even after two days. The calculated absolute sedimentation time for each solvent is shown in Table 4.1.

4.4 Results and discussion

4.4.1 Ultrasonication and dispersion

According to TEM images (Figure 4.2), the BNNTs used in the dispersions are doubled-walled (Figure 4.2A and B) with a diameter of ~ 5 nm and a length of a few micrometers (Figure 4.2C and D). These dimensions agree with the results reported by Kim et al. [33] where nanotubes with 2, 4 or 5 walls were obtained. The most common damages induced by ultrasonication treatments to BNNTs are peeling, shortening, and formation of Y-junctions or nanoribbons. All these phenomena are detectable through TEM, [81], [138], [87] namely for dispersion in ethanol, the solvent that was used in the preparation of the TEM grids, which has been reported to induce peeling under some circumstances [81]. However, based on our own images and on a comparison with those prior to sonication [33], we have no reasons to believe that our ultrasonication conditions

may cause significant damages to the BNNTs. The effect of a more severe ultrasonication, as performed in benzyl alcohol and ethylene glycol, was not investigated and we cannot rule out that some morphological damages occurred under these harsher conditions. That being said, the main driver for morphological changes, cavitation, is notoriously less efficient in viscous media [139].

Table 4.1 HSP, sedimentation time, dispersion state, Ra, and RED of the solvents used in sedimentation tests. Solvents are classified based on their dispersion states at the end of the sedimentation period (Figure B.4).

Solvent	**δ_d ($MPa^{1/2}$)**	**δ_p ($MPa^{1/2}$)**	**δ_h ($MPa^{1/2}$)**	**Sedimentation time (h)**	**R_a**	**RED**
Good dispersion state						
N,N′-Dimethylacetamide	16.8	11.5	10.2	48.0	5.36	1.00
N,N′-Dimethylformamide	17.4	13.7	11.3	42.6	4.69	0.88
Ethanol	15.8	8.8	19.4	51.3	5.45	1.00
2-Propanol	15.8	6.1	16.4	78.5	5.30	0.97
Intermediate dispersion state						
Acetone	15.5	10.4	7.0	14.1	8.13	1.51
Acetonitrile	15.3	18.0	6.1	14.0	11.7	2.16
Ethyl acetate	15.8	5.3	7.2	20.6	9.46	1.75
Ethyl benzoate	17.9	6.2	6.0	114	10.0	1.87
Methanol	15.1	12.3	22.3	23.8	8.83	1.62
Methyl ethyl ketone	16.0	9.0	5.1	15.8	9.88	1.83
Propylene carbonate	20.0	18.0	4.1	267	14.4	2.67
Tetrahydrofuran	16.8	5.7	8.0	25.8	8.36	1.55
Poor dispersion state						
Acetic acid	14.5	8.0	13.5	65.8	5.47	1.00
tert-Butanol	15.2	5.1	14.7	139	6.45	1.19
Chloroform	17.8	3.1	5.7	529	12.0	2.22
Cyclohexane	16.8	0	0.2	39.7	18.0	3.34
Dichloromethane	17.0	7.3	7.1	72.3	8.34	1.55
Dimethyl sulfoxide	18.4	16.4	10.2	142	7.94	1.48
1,4-Dioxane	17.5	1.8	9.0	81.4	10.7	1.98
Ethylene glycol[a]	17.0	11.0	26.0	1573	11.3	2.09
Formamide	17.2	26.2	19.0	255	16.1	2.98
Heptane	15.3	0	0	13.7	18.4	3.42
d-Limonene	17.2	1.8	4.3	38.9	13.7	2.54
Toluene	18.0	1.4	2.0	26.8	15.9	2.96
Additional solvents						
Benzyl alcohol[a,b]	18.4	6.3	13.7	342	5.53	1.02
Water[b]	15.1	20.4	16.5	50.6	10.4	1.93

[a]Reaching a good dispersion state required a stronger sonication. [b]Additional test solvent but not considered for the HSP analysis.

Pictures of the dispersions were taken immediately after sonication (Figure B.1) and after their respective sedimentation time (Figure B.4). According to Figure B.1, nine solvents were able to form good BNNT dispersions. These solvents were: ethanol (EtOH), propylene carbonate, 2-propanol (IPA), dimethyl acetamide (DMAc), dimethyl formamide (DMF), ethyl benzoate, dimethyl sulfoxide (DMSO), formamide and tetrahydrofuran (THF). All are Lewis bases, and are hence susceptible to interact with B atoms in the BN structure by sharing a pair of electrons. Over time, however, BNNTs progressively lost part or all their stability in propylene carbonate, ethyl benzoate, DMSO, formamide, and THF. This suggests that other phenomena may be at play besides Lewis acid–base interactions. Results presented in Table 4.1 report the dispersion observed at the end of the sedimentation time. At this point, only four solvents remain good: DMAc, DMF, EtOH, and IPA.

Dispersions in methanol (MeOH), methyl ethyl ketone (MEK), acetonitrile, acetone and ethyl acetate showed some dispersed particles at the top of the vial, while some sedimented at the bottom. On the other hand, when using ethylene glycol (EG), agglomerates of BNNTs were observed. The formation of these agglomerates most probably happened because the energy provided during sonication was not sufficient in such a highly viscous solvent (20.9 mPa s). In order to properly disperse the nanotubes, the dispersion was repeated, applying higher energy during sonication. An energy of 1800 J mgBNNTs^{-1} was used. This new system is shown in Figure B.2 and, given its good dispersion behaviour after applying higher energy, EG has been added to the list of good media (thus bringing the total to 10 solvents).

In toluene, cyclohexane and heptane, BNNTs lost their stability and stuck to the glass right after sonication (Figure B.1). These solvents are the three least polar and, in this case, our results align with those of Tiano et al. [44] for hexane. The instability of BNNTs can be attributed to a large difference in polarity between the nanotubes and the solvent. Due to a difference in electronegativity between B and N atoms, BN structures possess a dipolar moment.

This finding concurs with previous works on hexagonal boron nitride (h-BN) films, showing these are hydrophilic, with water contact angles of 50–55° [140], [38]. However, there is controversy concerning the hydrophilicity of BNNTs films. Some studies have determined that BNNTs films are superhydrophobic, with contact angles in the range of 145–167° [38], [37], [141]. However, morphological characteristics in the films such as the packing density, length and alignment of the

nanotubes [38] as well as the roughness and surface chemical heterogeneities [142] have an impact on the wettability of BNNTs films. In addition, theoretical studies have demonstrated that the spreading of a liquid over a highly curved surface is different from that on a flat surface [140], with high surface curvature being associated with more hydrophobic behavior [38].

4.4.2 Time-dependent dispersion state

In order to evaluate the evolution of the dispersions, three solvents were studied over a period of 150 h: propylene carbonate, ethyl benzoate and DMSO. These were chosen because, while their dispersion state was good immediately after sonication (Figure B.1), it worsened over time (Figure B.3). This emphasizes the need to determine a normalized sedimentation time in order to make objective evaluations of the dispersions.

The interval of time after which observation is performed varies due to differences in viscosity and density for each solvent. In order to compensate for these variations, a corrected relative sedimentation time (RST) (eqn (6)) is employed [109]. The calculated absolute sedimentation times, t_{sed}, for ethyl benzoate, DMSO and propylene carbonate were 114, 142 and 267 h, respectively. At 114 h, the dispersion state in ethyl benzoate showed a cloudy region at the top of the vial (around 20% of the volume) and the rest (80% of the volume) are swollen particles (Figure B.3B, B.4A and B.4B). For DMSO, at 142 h after sonication, phase separation can be observed. In the case of propylene carbonate, the dispersion state observed at 267 h (Figure B.4A and B.4B) is similar to that observed at 150 h (Figure B.3A). Given these observations at t_{sed}, these 3 solvents can no longer be considered "good" as they were for t = 0 observations in the previous section. It is worth noting that the cloudy agglomerates formed by BNNTs over time may easily be redispersed by simply hand mixing the vials.

4.4.3 Dispersion end state

The quality of the dispersions was evaluated after their respective sedimentation time, t_{sed} (Table 4.1). The dispersions were classified as good, intermediate or poor (Figure 4.3). Good solvents were able to form dispersions that were cloudy, but uniformly throughout the whole vial (Figure 4.3A). Intermediate solvents presented dispersed material at the top of the vial while having

sedimented BNNTs at the bottom (Figure 4.3B). Poor solvents led to the formation of phase separation, with transparent regions at the top of the vial (Figure 4.3C).

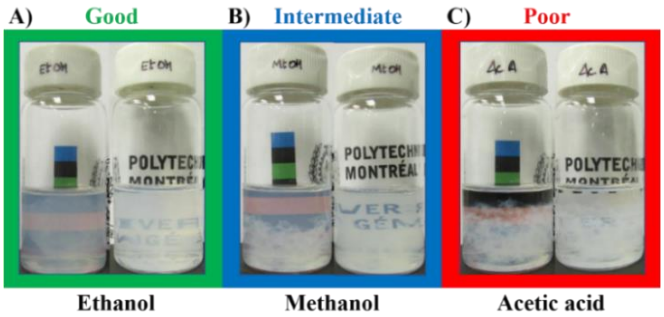

Figure 4.3 Dispersibility of BNNTs at tsed in A) ethanol, B) methanol, and C) acetic acid.

24 organic solvents were used for these sedimentation tests (Table 4.1). Dispersion in water was also conducted, but this solvent was not considered for the analysis because it has a strong tendency to structure itself in clusters, which may alter its HSP [109]. Four solvents were able to form cloudy and uniform dispersions of BNNTs (Figure B.4): DMAc, DMF, ethanol and 2-propanol. These solvents contain amide or hydroxyl groups on their structure, which may lead to hydrogen bonding interactions with the nanotubes. In fact, these four are Lewis bases, characterized by the ability to donate a pair of electrons. On the other hand, B atoms on BN nanostructures present an electron deficiency, and thus, make them vulnerable to interactions with Lewis bases such as amines [85], [143]. These interactions have in fact been specifically exploited by researchers aiming to noncovalently surface modify BNNTs. Xie et al. [84] used diamine-terminated polyethylene glycol (PEG) to functionalize the surface of BNNTs in order to disperse them in water. Similarly, Pal et al. [85] used trioctylamine and tributylamine to modify the BNNTs, while Maguer et al. [144] employed quinuclidine for modification, and Iannitto et al. [90] exploited similar chemistry in an ammonia plasma system.

As can be seen in Table 4.1, the calculated RED (eqn (4)) for these four good solvents was in the range of 0.88–1.0, which indicates that the solvents will be located inside or in the borders of the sphere. N,N’-Dimethylformamide and 2-propanol were found inside the sphere while N,N’-dimethylacetamide and ethanol were in the border.

Intermediate solvents were acetone, methanol, THF, ethyl acetate, acetonitrile, ethyl benzoate, MEK and propylene carbonate, with calculated RED values (eqn (4)) in the range of 1.51–2.67. These solvents possess δ_d and δ_p similar to the solvents classified as "good", but a significantly lower δ_h (Table 4.1). Low values of this parameter would prevent hydrogen bonding interactions required to obtain total dispersion of BNNTs. The exception to this was methanol, with an extremely high δ_h. For acid–base Lewis interactions to happen, a certain compatibility between the donor and acceptor is necessary. When the donor is much stronger than the acceptor, the former may prefer to interact with itself. In the case of methanol (the donor), it is likely that its molecules might have been able to self-associate, hiding most of their OH groups within itself and leaving the CH_3 groups exposed at the surface of the clusters [116]. The HSP of "clustered" methanol have been reported as $\{\delta_d; \delta_p; \delta_h\}_{Cluster}$ = {14.7; 5; 10} $MPa^{1/2}$ [116], where δ_d and δ_h are significantly lower compared to the standard HSP of methanol $\{\delta_d; \delta_p; \delta_h\}_{MeOH}$ = {15.1; 12.3; 22.3} $MPa^{1/2}$. Therefore, these CH_3 groups should not been able to interact with the BNNTs.

It is worth noting that different types of interparticle forces are expected during the assembly of nanoparticles. These include van der Waals forces, magnetic and electrostatic forces, repulsive steric, confining or jamming forces, solvation, structural and depletion forces, capillary forces, convective forces and friction and lubrication forces [145]. Their study would require a more detailed analysis, beyond the scope of the present work.

Dispersions with phase separation (i.e. "poor") at t_{sed} were observed in chloroform, acetic acid, DMSO, toluene, cyclohexane, heptane, D-limonene, formamide, 1,4-dioxane, ethylene glycol, tert-butanol and dichloromethane (DCM). The highest RED values (RED > 3) were obtained when non-polar solvents were used, reaching values of 3.34 and 3.42 for cyclohexane and heptane, respectively.

4.4.4 HSP analysis

Having probed the dispersibility of BNNTs in a large set of solvents, it becomes possible to determine their HSP using the HSPiP software. Solvents are classified as good (score = 1) or bad (score = 0) and their respective score ("0" or "1") is inputted into the HSPiP software. Calculations are performed based on the maximisation of a desirability function, FIT, that relies on the HSP distance, R_a [116]. FIT reaches a maximum of 1.0 when a sphere of center $\{\delta_d; \delta_p; \delta_h\}$ and of radius

R_0 may be fitted to simultaneously include all the good solvents while excluding all the bad ones. When this is impossible, FIT is decreased by a factor that considers the various HSP distances. In circumstances where several combinations yield the same FIT, the software calculates an uncertainty on the true position of the sphere's center. Details and equations are provided in ESI (Appendix B) and in Table B.2.

Since we witnessed three categories of behavior for the dispersions (good, intermediate, and poor), various combinations may be considered for the fitting. In the following paragraph, we will first attribute the grade 1 to good solvents only (DMF, DMAc, ethanol and 2-propanol), and grade 0 for intermediate and poor ones. Then, the grade 1 to good and intermediate solvents alike and grade 0 for poor solvents only. Two sets of HSP coordinates will thus be determined, corresponding to a main and to an extended chemical affinity, respectively.

Attributing the grade 1 to good solvents (green circles) only, the Hansen space for the BNNTs has them distributed inside the sphere, while the intermediate (blue triangles – grade 0) and poor solvents (red squares – grade 0) are located outside (Figure 4.4). 2D plots (Figure 4.5) help to visualize the data presented in Figure 4.4. These provide upper and lower bounds for the various HSP. From Figure 4.5A and B it can be concluded that the dispersive component (δ_d) of the BNNTs is in the range of 15.8–17.4 $MPa^{1/2}$. From Figure 4.5A and C, the polar component (δ_p) should be in the interval of 6.1–13.7 $MPa^{1/2}$.

The hydrogen-bonding component (δ_h) can be determined from Figure 4.5B and C, in the range of 10.2–19.4 $MPa^{1/2}$. The dispersion state versus the Hildebrand parameter (δ_t) is plotted in Figure 4.5D. Good solvents for the dispersion of BNNTs will be those with a δ_t in the range of 22.4–26.5 $MPa^{1/2}$, that also respect conditions for R_a (eqn (3)) and RED (eqn (4)) such that RED < 1. However, as mentioned before, the selection of potential solvents should be done based on the HSP distance (eqn (3)) considering the three HSP: dispersive, polar and hydrogen bonding interactions, not just the Hildebrand parameter.

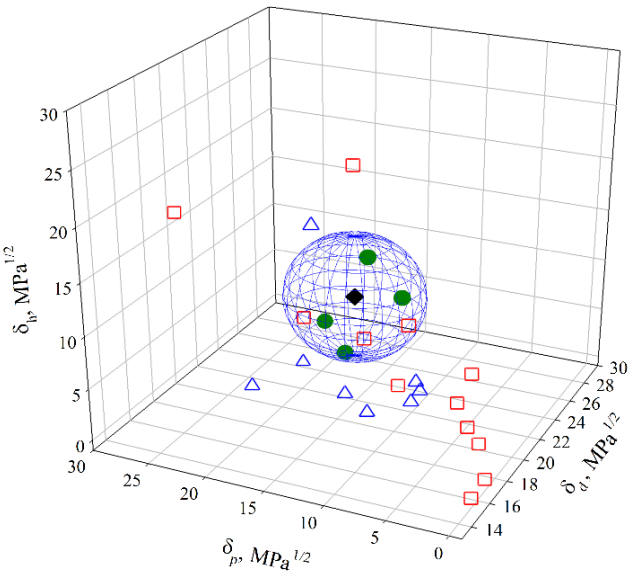

Figure 4.4 Hansen space of BNNTs. The green circles correspond to the good solvents, the blue triangles to intermediate ones and the red squares to poor ones. The black diamond represents the centre of the sphere. Full symbols correspond to solvents inside the sphere while empty symbols to solvents outside.

The first set of calculated HSP for BNNTs is: $\{\delta_d; \delta_p; \delta_h\}_{main} = \{16.8; 10.7; 14.7\} \pm \{0.3; 0.9; 0.3\}$ $MPa^{1/2}$. The radius of the sphere is $R_0 = 5.4$ $MPa^{1/2}$ and the $\delta_t = 24.7$ $MPa^{1/2}$. A FIT = 1.0 was obtained, meaning that all the grade 1-solvents were located inside the sphere and all the grade 0-solvents outside. The HSP of BNNTs obtained in this work differ from those obtained by Tiano et al. [44]. In their work, the center of the sphere was determined by $\{\delta_d; \delta_p; \delta_h\}_{Tiano} = \{16.8; 10.7; 9.0\}$ $MPa^{1/2}$ with a $\delta_t = 21.8$ $MPa^{1/2}$ and $R_0 = 4.3$ $MPa^{1/2}$. They used as-synthesized material containing boron nanoparticles as impurities), affecting not only the surface chemistry of the nanotubes but also their density. They determined 4 good solvents: DMAc, DMF, acetone and N-methyl-2-pyrrolidone (NMP). However, based on their vial pictures, the dispersion in acetone should not be qualified as “good”, as a large fraction of nanotubes are sedimented after settling for 1 week. This behaviour is corroborated in our experiments, where just after sonication some nanotubes sedimented while other fractions were suspended (Figure B.1). In addition, when comparing the HSP of acetone $\{\delta_d; \delta_p; \delta_h\}_{ACE} = \{15.5; 10.4; 7\}$ $MPa^{1/2}$ with the intervals proposed in the present work to estimate good solvents for BNNTs, only the δ_d value is within its

corresponding interval and a RED = 1.51 (eq. 4) was obtained. This indicates that acetone is not a good solvent to disperse the BNNTs. Regarding NMP, with $\{\delta_d; \delta_p; \delta_h\}_{NMP} = \{18; 12.3; 7.2\}$ $MPa^{1/2}$, similar to acetone, only δ_p is within the interval proposed, while δ_d and δ_h are outside the range provided. The calculated RED = 1.49 (eq. 4) indicates that NMP is situated outside the sphere, and thus considered as a poor solvent. In both cases, a low value of δ_h prevents some hydrogen bonding interactions from happening, impeding complete dispersion of BNNTs.

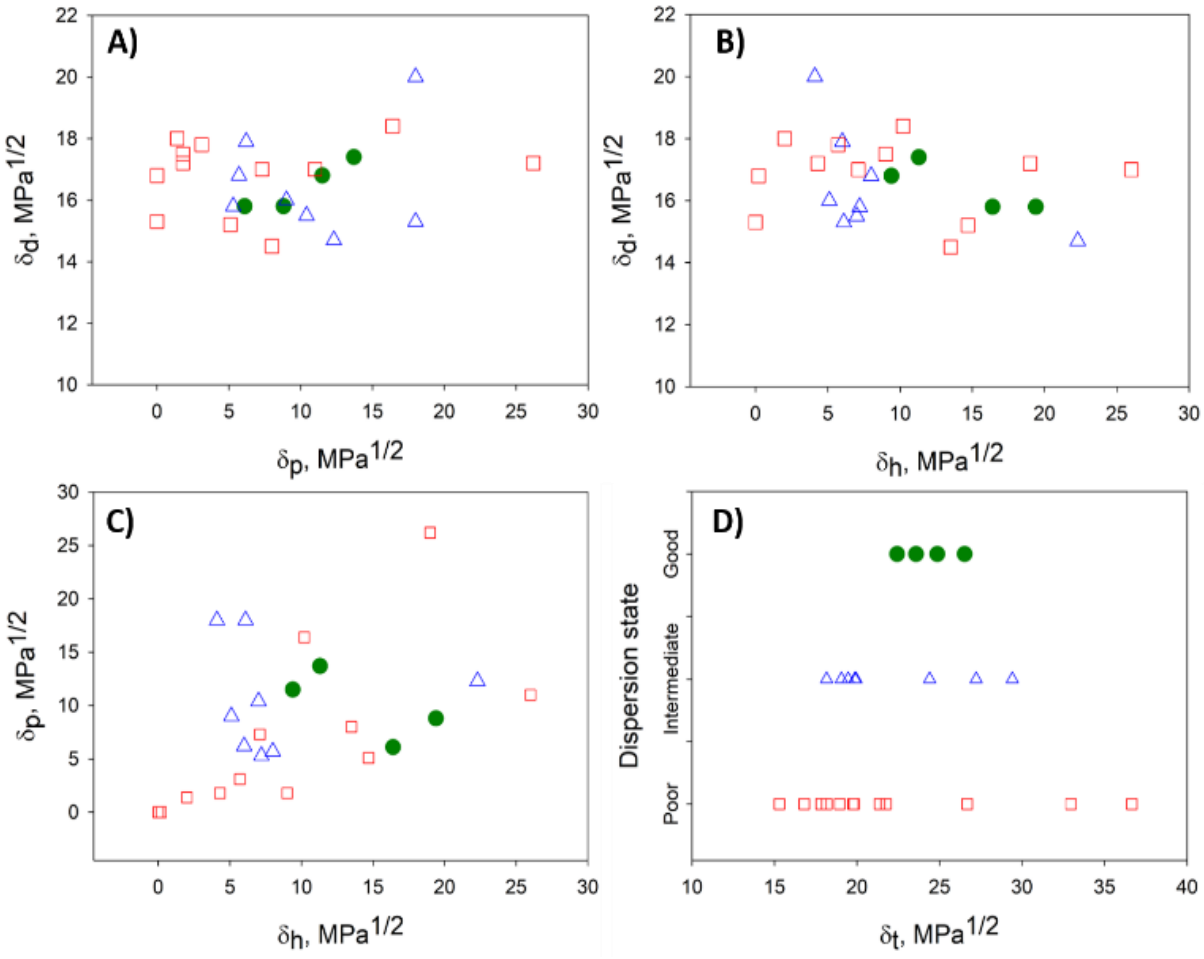

Figure 4.5 2D projections to help with the visualization of the data presented in fig 4. A) δd vs δp, B) δd vs δh, C) δp vs δh and D) dispersion state vs δt. Good, intermediate and bad solvents are represented by green, blue and red circles, respectively.

An explanation for the deviations between Tiano's results [44] and those presented in this work could be the concentration (0.25 mg/mL, compared with 0.1 mg/mL in this work). It may have caused some dispersions to oversaturate and thus, favored a sedimentation of the BNNTs. Another factor arises from the sedimentation time: their analysis considered an absolute sedimentation time of 1 week for all the dispersions. As discussed earlier, the use of a normalized sedimentation time, t_{sed}, is preferred. Variations in chemical composition, as well as in length and diameter of the nanotubes could also affect the HSP determination [44], [120]. Tiano et al. [44] concluded that their HSP correlate well with the BNNTs used. However, they stated that dispersions should be repeated if different methods of synthesis and/or purification processes are used, being this the main limitation of their work.

In the present study, we minimized the uncertainty in the HSP values by using purified material and compensating for differences in density and viscosity of the solvents. Nonetheless, the uncertainty of ± {0.3; 0.9; 0.3} $MPa^{1/2}$ with which the HSP of BNNTs were determined means that the border of the sphere is a soft one. With an HSP radius of R_0 = 5.4 $MPa^{1/2}$, it translates in an uncertainty of roughly ± 0.2 on RED values: any predictions made on solvents whose RED is comprised between 0.8 and 1.2 must be considered with caution. This may be highlighted by investigating the behaviour of BNNTs in a solvent like benzyl alcohol. With HSP of $\{\delta d; \delta p; \delta h\}_{BA}$ = {18.4; 6.3; 13.7} $MPa^{1/2}$, benzyl alcohol has a RED value (eq. 4) of ~ 1.02, meaning that it is located right at the outer edge of the border of the BNNTs' Hansen sphere. With a RED strictly above 1, it should thus be a poor solvent. However, it is right in the middle of the uncertain area for RED values. Experimentally, it was found to be a good solvent (Figure B.4). This proves the soft nature of the border between good and poor solvents when RED values are close to 1. Calculating the RED according to Tiano's results yields a value of 1.33, which suggests that their range of uncertainty regarding RED values was probably even larger than ours. It is worth noting that because of its high viscosity (5.47 mPa s), a higher energy (1,600 J/mgBNNTs) was applied during sonication to properly disperse the BNNTs in benzyl alcohol. Our analysis is performed based on the assumption that the BNNTs were not damaged by this more intense ultrasonication step.

To make a graphical comparison between the Hansen space obtained by Tiano et al. [44] and the one obtained in this work, a 3D graph containing both spheres was plotted (Figure

4.6). The blue sphere corresponds to the results obtained in this work, $\{\delta_d; \delta_p; \delta_h\}_{main}$ = {16.8; 10.7; 14.7} $MPa^{1/2}$, while the black one to Tiano's, $\{\delta_d; \delta_p; \delta_h\}_{Tiano}$ = {16.8; 10.7; 9.0} $MPa^{1/2}$. Even though δ_d and δ_p are the same in both cases, the differences in δ_h and R_0 cause the spheres to locate in different regions. A partial overlap is observed in the space limited by δ_d = 15.8 - 17.8 $MPa^{1/2}$, δ_p = 7.3 – 13.7 $MPa^{1/2}$ and δ_h = 9.4 – 14.7 $MPa^{1/2}$. These HSP values are within the intervals proposed in this work for the prediction of good solvents for BNNTs. The center of the intersection region was found at $\{\delta_d; \delta_p; \delta_h\}_{intersection}$ = {16.8; 10.6; 11.5} $MPa^{1/2}$. Only two solvents were found in that space: DMF, located within the overlapped region, and DMAc, located in the border. On the other hand, 2-propanol and benzyl alcohol were found inside the blue sphere, centered at $\{\delta_d; \delta_p; \delta_h\}_{main}$, while ethanol was in the border. DCM and acetone were located inside the black sphere, with center at $\{\delta_d; \delta_p; \delta_h\}_{Tiano}$. Three of the four expected solvents (DMF, DMAc and acetone) were located inside this sphere. The fourth one, NMP, with coordinates $\{\delta_d; \delta_p; \delta_h\}_{NMP}$ = {18; 12.3; 7.2} $MPa^{1/2}$, was not used as a test solvent in the present work. Instead, DCM, with $\{\delta_d; \delta_p; \delta_h\}_{DCM}$ = {17; 7.3; 7.1} $MPa^{1/2}$, was found to be inside the black sphere. Although δ_d and δ_h possess similar values, a difference of 5 $MPa^{1/2}$ is observed in the polar component, δ_p. According to Tiano's results, the dispersion in DCM was not good and a phase separation was observed 30 min after sonication, with swollen particles at the bottom of the vial. These results are in agreement with the ones obtained in the present work.

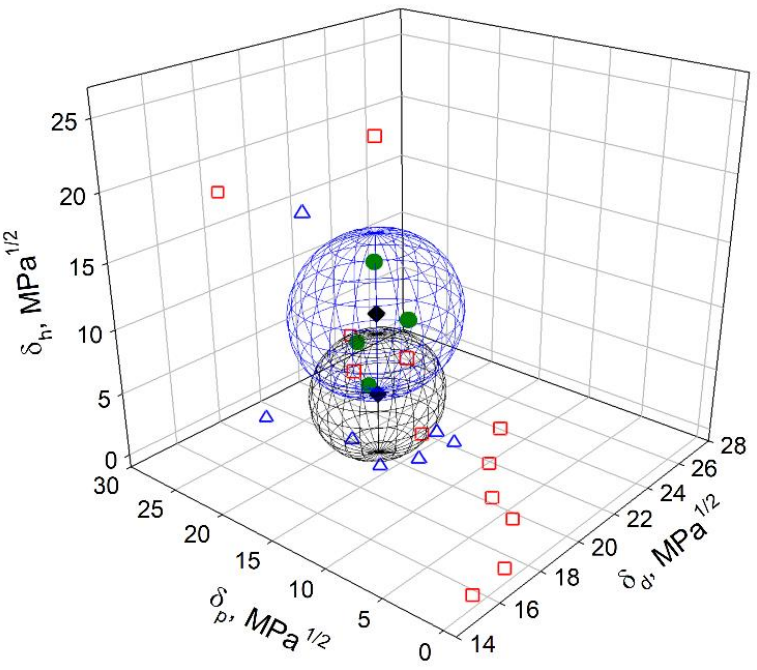

Figure 4.6 Hansen space of BNNTs obtained in this work (blue sphere) and the results obtained by Tiano et al. [44] (black sphere). The green circles, blue triangles and red squares correspond to good, intermediate and poor solvents determined in this work.

To visualize the influence of partial dispersibility in the Hansen space, a second analysis was performed, expanding the list of good solvents (scored 2) with the intermediate ones (scored 1, Table 4.1). These solvents were acetone, methanol, THF, ethyl acetate, acetonitrile, ethyl benzoate, MEK and propylene carbonate. They were scored as "1" and added to the list of good solvents previously defined (DMAc, DMF, EtOH and IPA). The "poor" solvents were kept scored "0". The resulting Hansen sphere (gray sphere) is shown in Figure 4.7. The Hansen space determined previously, considering total dispersibility of BNNTs (blue sphere) and the one obtained by Tiano et al. [44] (black sphere) are also plotted. As can be seen in the figure, the blue and black spheres are located inside the gray one. This trend was expected because good solvents should remain suitable when good and intermediate solvents are considered [109]. However, the addition of more solvents to the list of "good" ones will modify the coordinates and radius of the Hansen sphere. In this

case, the solvents added to the list of good ones possess a wide range of HSP, covering different spaces in the Hansen space but leaving some uncovered regions.

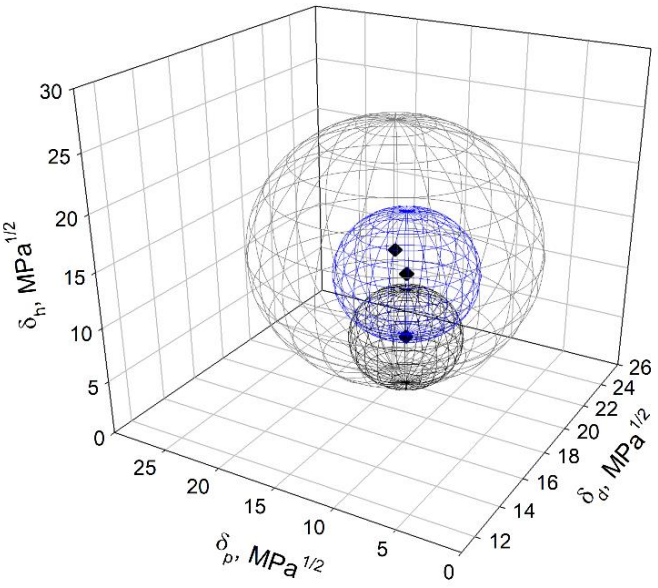

Figure 4.7 Hansen space of BNNTs obtained in this work considering total dispersibility (blue sphere), partial dispersibility (gray sphere) and Tiano's results (black sphere).

The Hansen solubility parameters of the gray sphere were {18.8; 13.9; 14.4}$_{\text{extended}}$ ± {0.2; 0.4; 0.3} MPa$^{1/2}$, with a radius R_0 = 11.4 MPa$^{1/2}$. A *FIT* = 0.434 was obtained, meaning that some good solvents were located outside the sphere while some poor ones are inside (see supporting information). DCM, acetic acid, DMSO and tert-butanol, considered as bad solvents (Table 4.1), were located inside this gray Hansen sphere while methanol, MEK, acetonitrile, ethyl benzoate and ethyl acetate (good solvents) are located outside. This relocation of the solvents by the *HSPiP* software could have happened due to the large differences in their HSP, making difficult to get a good FIT. Low values in the *desirability function* FIT will provide less reliable values of the HSP of the particle in question.

As mentioned earlier, Mutz et al. [43] determined the total solubility parameter, δ_t = 18.53 MPa$^{1/2}$, using static light scattering and the Flory and Hildebrand-Scatchard Solution Theories. The BNNTs used had a diameter in the range of 30-100 nm, in comparison with

the 5 nm diameter nanotubes used in our work. Based on the expression developed by Bergin et al. [120] for CNTs (eq. 5), larger nanotubes have lower δ_t values. We suggest it may be the reason why our δ_t is higher than the one reported by Mutz et al. [43]. Based on that, Mutz et al. proposed a list of *potential* good solvents: ethyl acetate, isophorone, diamyl phthalate, vinyl toluene and *cis*-1,2-dichloroethyelene. However, as mentioned before, the prediction of solvents considering only the Hildebrand solubility parameter (δ_t) is not reliable for particles presenting polar and hydrogen interactions [109]. In addition, it is pertinent to note that one of the good solvents predicted was ethyl acetate, which is indeed able to partially disperse the BNNTs, as demonstrated in this work (intermediate score).

4.5 Conclusions

In this work, the Hansen solubility parameters of purified BNNTs were determined for the first time through sedimentation tests accounting for relative sedimentation time. The HSP obtained were $\{\delta_d; \delta_p; \delta_h\} = \{16.8; 10.7; 14.7\} \pm \{0.3; 0.9; 0.3\}$ $MPa^{1/2}$. The radius of the sphere was $R_0 = 5.4$ $MPa^{1/2}$ and the Hildebrand parameter $\delta_t = 24.7$ $MPa^{1/2}$. Evaluation of the dispersion state in different organic solvents was done after an appropriate relative sedimentation time, taking into account differences in density and viscosity of the solvents. However, the method of synthesis used, the presence of impurities and the diameter of the nanotubes play an important role when determining their HSP. Four solvents were able to form uniform dispersions of BNNTs. These were DMF, DMAc, ethanol and 2-propanol. It is thought that the hydrogen bonding interactions between the solvents and the nanotubes are crucial for good dispersion. Having defined the HSP of BNNTs more precisely, this data can now be used to guide dispersion into host matrices, as well as methodologies for surface treatment.

Conflicts of interest

There are no conflicts to declare.

Acknowledgements

The authors would like to acknowledge the Natural Sciences and Engineering Research Council of Canada (NSERC), Prima Québec, the Mexican National Council for Science and Technology (CONACyT), Tekna Plasma Systems, Michelin Canada and Polytechnique Montréal. The Fonds de Recherche du Québec - Nature et Technologies (FRQNT) provided C. Bruel with a scholarship (number 208324). Mr. Paul-Henri Verger and Ms. Alekhya V. Veerubhotla are also thanked for their valuable contributions to the early versions of this work.

CHAPTER 5 ARTICLE 2 : COVALENT FUNCTIONALIZATION OF BORON NITRIDE NANOTUBES THROUGH PHOTO-INITIATED CHEMICAL VAPOUR DEPOSITION

Cristina Sofia Torres Castillo, Jason. R. Tavares

Department of Chemical Engineering, École Polytechnique de Montréal, P.O. Box 6079, Station Centre-Ville, Montreal, Quebec, H3C 3A7, Canada

Published in:

The Canadian Journal of Chemical Engineering, 2022, pp 1-11

https://doi.org/10.1002/cjce.24440, Publication Date: June 2022, Available online 7 May 2022,

KEYWORDS :

Boron nitride nanotubes, chemical vapour deposition, covalent functionalization, photochemistry

Abstract

Boron nitride nanotubes (BNNTs) are analogous nanostructures to carbon nanotubes (CNTs), possessing similar properties such as Young's modulus and thermal conductivity, but superior resistance to oxidation and thermal stability. In addition, BNNTs are insulating materials, whereas CNTs are electrically conductive. They could be used as reinforcements in polymeric matrices as heat dissipators or as protective coatings in harsh environments. However, when incorporating them into polymers, one main drawback is their tendency to agglomerate. To improve their dispersion, covalent surface modification can be applied, with solvent-free approaches being preferred. Herein, we used syngas photo-initiated chemical vapour deposition (PICVD) to incorporate oxygen functionalities on the surface of BNNT. X-ray photoelectron spectroscopy analysis showed a highly oxidized BNNT surface after treatment. In addition, a decrease in water contact angle and an increase in surface energy were observed for the treated material. These results open new possibilities to incorporate hydrophilic BNNTs surfaces into polar polymers or other matrices of interest.

KEYWORDS

boron nitride nanotubes, chemical vapour deposition, covalent functionalization, photochemistry

5.1 Introduction

Boron nitride nanotubes (BNNTs) are attractive nanomaterials; they possess an analogous structure to carbon nanotubes (CNTs), where C atoms have been replaced by alternating B and N atoms [23], [19], [18], [15]. Both nanomaterials possess a theoretical Young's modulus as high as ~1.2 TPa and a thermal conductivity of 200–300 W/m · K. However, BNNTs show both higher thermal stability (up to 1100°C in air) and chemical stability than CNTs [15]. In addition, BNNTs have a band gap in the range of 5–6 eV, independent of diameter but as a function of tube chirality, compared to the semiconductor behaviour of CNTs. BNNTs find potential applications as reinforcing agents in polymers [21], [58], [57], [146] and, due to their high surface area, are good candidates for hydrogen storage devices [18], [61]. In addition, because of their unique combination of thermal

conductivity and electrical insulation, BNNTs can be used for heat dissipation in polymer composites [21], [146], [20], [30], [32] and in electronic devices [62].

To avoid agglomeration and to transfer the extraordinary properties of BNNTs to polymeric matrices, a surface treatment is needed. Surface modification can be performed through two main approaches: non-covalent and covalent. Non-covalent interactions often involve the use of a polymer to wrap the surface of BNNTs [84], [27], [85]. Although the chemical structure of the nanotubes is preserved, their application in high-temperature environments is not possible due to detachment of the surfactant from the nanotubes at temperatures as low as ~70°C [84], [147]. To address this shortcoming, covalent functionalization approaches can be employed. These can be divided into two categories: solvent chemistry and gas-phase techniques. In the liquid phase, several works have successfully covalently modified the surface of BNNTs (Table 5.1).

Table 5.1 Comparison of some covalent functionalization approaches of boron nitride nanotubes (BNNTs) in the liquid phase.

Reactants	**Steps**	**Resulting BNNT**	**Ref.**
Stearoyl chloride	1) Reflux at 100°C for 120 h 2) Washing	BNNT with long alkyl chains	[83]
Chloroacetyl chloride, styrene, CuCl, 4,4'-dinonyl-2,2'-dipyridyl, xylene	1) Mixing at 150°C for 120 h 2) Washing 3) Mixing at 130°C for 48 h 4) Washing	PS-grafted BNNTs	[86]
Isophorone diisocyanate (IPDI)	1) Mixing on a N_2 atmosphere at 100°C for 120 h 2) Washing	IPDI–BNNTs	[57]

	3) Functionalization with COOH, OH and NH_3 containing species.		
Nitric acid, 3-aminopropyl-triethoxysilane (APTES), ethanol	1) Oxidation with HNO_3 2) Washing 3) Silanization with APTES	NH_2-terminated BNNTs	[148]
Folic acid, nitric acid, *N*,*N*-dimethylacetamide, *N*-(3-dimethylaminopropyl)-*N*'-ethylcarbodiimide hydrochloride (EDC), 4-(dimethylamino) pyridine (DMAP)	1) Oxidation with HNO_3 2) Washing 3) Functionalization with folic acid 3) Washing	Folate-grafted BNNTs	[149]
Sulfuric acid, nitric acid, glycol dimethacrylate (TEGDMA),	1) Oxidation 2) Washing 3) Functionalization with TEGDMA 4) Washing	TEGDMA-BNNTs.	[150]

As can be seen, solvent chemistry approaches often use toxic compounds, multi-steps reactions, long reaction times, and can require extensive purification processes, making the functionalization process hazardous, intermittent, and time consuming. To circumvent some of these issues, gas

phase techniques, mainly plasma treatments, have been developed to covalently modify the surfaces of BNNTs in one-step processes and are friendlier towards the environment (Table 5.2).

Table 5.2 Comparison of some covalent functionalization approaches of boron nitride nanotubes (BNNTs) in the gas phase.

Reactants	**Reaction conditions**				**Ref.**
	Reactor	**Temperature**	**Pressure**	**Power**	
Dimethyl sulfoxide (DMSO)	Autoclave	180°C for 6 h	High pressure (not specified)	Not specified	[87]
Ammonia (NH_3)	Microwave plasma	200°C	<0.3 Pa	200 W	[88]
Hydrogen peroxide (H_2O_2)	Autoclave	120°C for 24 h	High pressure (not specified)	Not specified	[58]
N_2+H_2, O_2	Plasma	Not specified	0.3-10 Pa	10-100 W	[34]
N_2+H_2	Plasma	Room temperature	5.5 Pa	100 W	[37]
Air (O_2+N_2)	Plasma	Room temperature	Ambient pressure	45 W	[40]
Ammonia (NH_3)	Plasma	Not specified	267 Pa	100 W	[90]
Oxygen (O_2)	Plasma	Low temperature	Not specified	400 W	[91]

H_2/CO	Quartz tube (PICVD)	Room temperature	Near-ambient pressure	30 W	This work

Table 5.1 and Table 5.2 show a summary of some covalent functionalization approaches in both, liquid and gas phases. However, other covalent and non-covalent modification techniques can be found in the literature [151], [152], [153], [154], [68], [155].

Although successful covalent modification has been performed in the gas phase, the use of high energy consumption equipment, high temperature, or vacuum make the functionalization of BNNTs an expensive process. Thus, a technology operating at low cost and near-atmospheric pressure is needed.

Photo-initiated chemical vapour deposition (PICVD) is a gas-phase technique that employs light to start the deposition reactions. The precursors can be single molecules or mixtures of gases and radicals or excited species that are produced when the former are exposed to ultraviolet (UV) light [80], [100], [82]. Hydrogen and carbon monoxide, known as synthesis gas or syngas, can be excited in the presence of UV light and thus produce radicals or reactive species [80], [100], [82], [101]. Syngas PICVD has been applied for the deposition of thin films on copper coupons [80] and silicon wafers [100]. It has also been used for the surface treatment of polymers such as high-density polyethylene (HDPE), polyethylene terephthalate (PET) [102], and polystyrene-divinylbenzene (PS-DVB) [103]. Regarding surface modification of nanoparticles, PICVD has been applied to tailor the surface properties of cellulose nanocrystals (CNCs) [104], CNTs [82] and for the functionalization of nanoparticles from ash powder [105]. The process has also been scaled up for the encapsulation of magnetic iron oxide nanoparticles [106] and for the modification of TiO_2 nanoparticles in a fluidized bed geometry [107]. Due to the versatility of syngas PICVD, herein, we employed this technique to covalently modify the surface of BNNT films.

5.2 Materials and methods

5.2.1 Materials

Purified BNNT films (squares of ~2 cm × 2 cm) with a thickness of 75 ± 25 μm were provided by Tekna Plasma Systems. The BNNT content is higher than 75%, with elemental free B less than 1%. The balance comprises hexagonal boron nitride (h-BN) and B-N-H derivatives. The nanotubes are highly crystalline and few walled, with diameters of ~5 nm and lengths of a few micrometres. Their synthesis and purification processes are explained in detail elsewhere [33], [56]. Carbon monoxide (CO), hydrogen (H_2), and ultra-pure (99.999%) compressed argon (Ar) were supplied by Air Liquide Canada. Hydrogen peroxide (H_2O_2) at 50% was purchased from Fisher Chemical. Formamide (99%) and diiodomethane (99%) were obtained from Alfa Aesar. All reactants were used as received without further purification.

5.2.2 Methods

BNNT films were treated using syngas PICVD. Before the reaction, the BNNT film was dried in an oven for 2 h at 100°C to remove any traces of moisture. Figure 5.1 shows a schematic of the PICVD reactor. CO and H_2 were used as precursors. The reactor consisted of a quartz tube of 90 cm in length and 25 mm in internal diameter, with a total volume of 441.8 cm^3. Two UVC lamps (200–280 nm) at a power of 30 W were used as a light source, with the main emission peak at 253.7 nm and a secondary peak at 185 nm. Argon was fed to the reactor for 3 min at a rate of 3 standard ft^3/h (0.084 95 m^3/h) before and after treatment to ensure an inert atmosphere. Then, a molar ratio of 0.5:1 of H_2:CO was fed to the reactor. Hydrogen peroxide (1 ml/h) was used as a photo-initiator. The reaction time was 1 h, and the reactor pressure was −10 kPa (gauge). The sample was located at ~20 cm from the gas inlet. The films were treated on both sides (1 h per side). These treatment conditions are based on prior work showing that hydrophilic surfaces can be obtained by applying a slight vacuum to the system, positioning the sample near the inlet of the gases, and using hydrogen peroxide [80], [82].

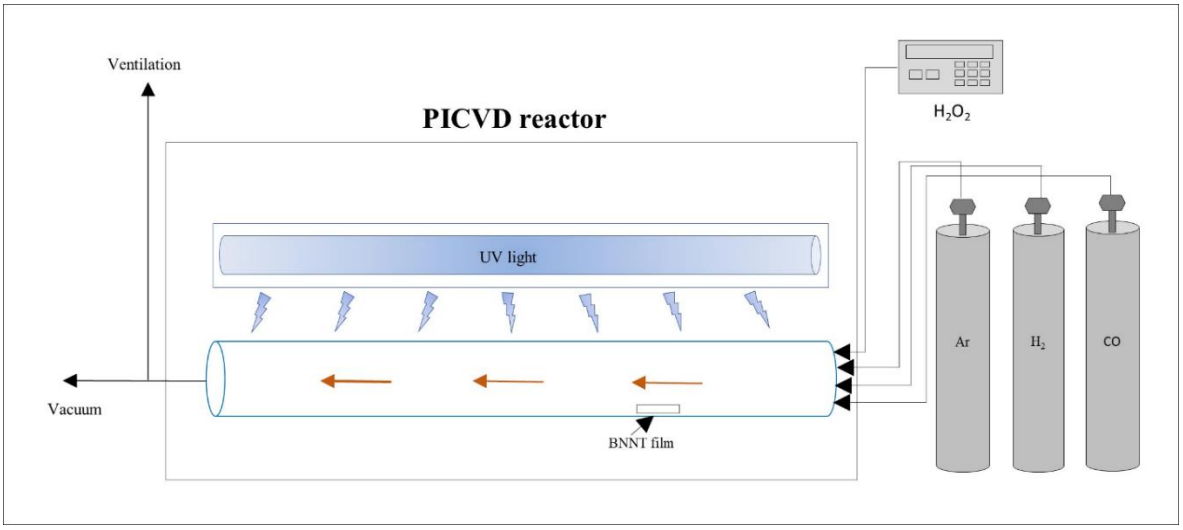

Figure 5.1 Schematic of the PICVD reactor.

X-ray photoelectron spectroscopy (XPS) measurements were done in a VG ESCALAB 3 MKII apparatus, with a Mg Kα source, a power of 300 W, and a pressure of $3.0 \times 10{-}9$ Torr. For the survey scans, an energy step size of 1.0 eV and a pass energy of 100 eV were employed. Fourier-transform infrared (FTIR) spectroscopy was performed on a Thermo Scientific NICOLET iS5 spectrometer, equipped with an attenuated total reflectance (ATR) module. Contact angle (CA) measurements were performed using an FDS OCA Data Physics TBU 90E tensiometer. The sessile drop method was used to measure the static contact angles of the test solvents and the films. In brief, 2 µl of solvent was placed on the surface of the BNNT films. Then, the static CA was measured. Advancing and receding contact angles (ARCA) were also performed to evaluate the effect of roughness, chemical heterogeneity, and/or swelling behaviour of the BNNTs films. In this case, 6 µl of solvent was used. The pendant drop method was used to determine dispersive and polar components of the surface tension of formamide and water, due to variabilities presented in the literature. This was done to minimize the variance in the surface energy calculations where those parameters are used (Equation (1)). The surface energies for both untreated and treated BNNTs were determined by applying the Owens, Wendt, Rabel, and Kaelble (OWRK) method [142]. The temperature and relative humidity (RH) during the measurements were 23°C and 46%, respectively. When diiodomethane was used, the RH was 64%. For water ARCA measurements, the temperature was in the range of 21.5–23.1°C with a RH between 65% and 74%. Then, the

contact angle hysteresis (CAH) was calculated considering the polar and dispersive components of water, as well as its advancing and receding contact angles. Finally, dispersions of treated BNNTs (1 mg/10 ml solvent) were done in a Cole-Palmer probe sonicator using a cylindrical probe, with operation cycles of 5 s ON/2 s OFF and an amplitude of 30%. The operation frequency was 20 kHz.

5.3 Results and discussion

Figure 5.2 shows the physical appearance of purified and treated BNNTs. Untreated films had a characteristic white colour (Figure 5.2A), while after the PICVD treatment, the film colour changed to yellow (Figure 5.2B). A uniform deposition was observed after 1 h of treatment. Similar behaviour was observed by Dorval Dion et al. [80] and Farhanian et al. [100] when conducting PICVD treatments on copper coupons and silicon wafers, respectively.

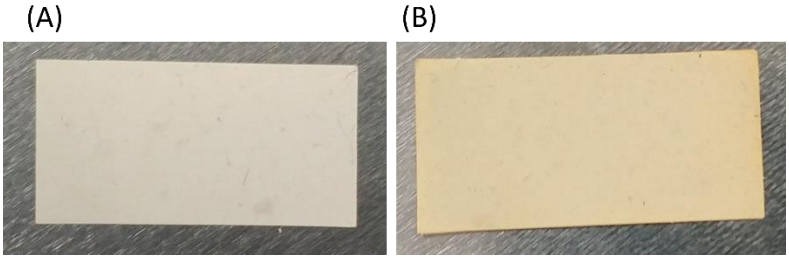

Figure 5.2 (A) Untreated and (B) treated boron nitride nanotubes (BNNT) films (rectangles of ~ 2 cm x 1 cm).

5.3.1 X-ray photoelectron spectroscopy

X-ray photoelectron spectroscopy was employed to elucidate the chemical structure of the BNNTs. Table 5.3 shows the atomic composition of both samples. The untreated material is composed of 42.5% B (from B1s) and 45.7% N (from N1s), with a small content of C (from C1s, 4.0%) and O (from O1s, 7.8%). This agrees with the literature [57], [149], [40], [91], [156], [157]. The presence of carbon could be attributed to adsorbed C during XPS measurements [157] or to the adsorption of airborne hydrocarbons [158] due to the curvature of the BNNTs on the films [38]. On the other hand, the presence of oxygen could be related to by-products formed between air/moisture and reactive species during the synthesis of the nanotubes [56] or to the adsorption of O_2 on the surface and/or to hydroxyl groups [159]. For the treated material (t-BNNTs), a decrease of ~12% in the B1s was observed, and a more significant decrease of 22.7% was obtained for N1s. An increment

of 29.3% was observed for the O1s. A 2.2% addition of iron (from Fe2P3) was obtained for the t-BNNT.

Table 5.3 Atomic composition of untreated and treated boron nitride nanotubes (BNNTs).

Name	**BE (eV)**	**At. %**	
		Untreated	**Treated**
B1s	191.9	42.5	30.6
C1s	285.1	4.0	7.0
N1s	399.2	45.7	23.0
O1s	533.8	7.8	37.1
Fe2p3	712.1	-	2.2

Figure 5.3 shows the high-resolution XPS spectra for both untreated and treated BNNT. For the untreated material, the B1s spectrum (Figure 5.3A) shows an intense peak at 190.8 eV, corresponding to the BN bond [58], [34], [91]. Additionally, a small shoulder is seen at 189.5 eV. Cho et al. [56], showed that during the purification of BNNT at high temperatures (in the range of 750–1050°C), the B-N bond originally located at ~190.4 eV moved to a lower value of binding energy (BE) (~189.8 eV). Thus, we speculate that the secondary peak at 189.5 eV present in our untreated BNNTs was formed during the purification process. It could also be related to hydrogenated BN (H-BN) or to B-N-H derivatives [56], intermediate species formed during synthesis, because a decrease in BE indicates bonding to a less electronegative element. For the treated BNNT (Figure 5.3B), the signal at 190.8 eV decreased and thus the amount of BN bonds. In contrast, the appearance of a new peak at 192.9 eV was observed, attributed to B-O bonds [148], [91] possibly due to the attachment of OH groups to B [58]. However, a broad and shifted B-O peak to higher BE means that B was subjected to strong oxidation [34], [91], with BE of 192.8 eV

corresponding to $B(OH)_3$, and energies of 193.1 eV are attributable to B_2O_3 [34]. Thus, we speculate that the surface of our treated BNNT is composed of $B(OH)_3$. N1s spectra are shown in Figure 5.3C,D. Both spectra show a dominant peak at 398.4 eV, corresponding to the BN bond [58], [148], and a secondary peak at 396.8 eV, related to B-C-N bonding [157], generated during the synthesis. The intensities of both peaks decreased for the treated BNNT, suggesting that N sites were substituted by oxygen after the treatment, which agrees with the literature [91]. O1s spectra are shown in Figure 5.3E,F. A strong peak is observed at 532.7 eV, corresponding to adsorbed O_2 or surface hydroxyl groups [159], [160]. For the treated material, this peak increased considerably to double its intensity, meaning that an oxidation process took place, and more B-OH bonds were formed [160]. Additionally, a new peak appeared at 531.3 eV, corresponding to C-OH bonds, $Fe(OH)_3$, or O=C-O-Fe bonds [82]. C1s spectra are shown in Figure 5.3G,H. For the untreated sample (Figure 5.3G), the peak at 283.6 eV could be attributed to B-C-N bonds, while the peak at 285.0 eV corresponds to C-C bonds [82] or to C contamination (284.6 eV), due to the exposure to air [34]. For the treated sample, the intensity of the peak at 285.0 eV increased, meaning more C-C bonds were formed during the treatment or contamination took place during treatment or XPS analysis. These new C-C bonds may be part of a hydrocarbon chain formed due to the reaction of CO and H_2 [100]. Additionally, a peak at 287.2 eV appeared, related to B-C-N-O bond or to OH groups [82]. Finally, a slight peak at 289.5 eV is attributed to O-C=O bonds, related to COOH groups [82]. Figure 5.3I shows the Fe2p2 XPS spectrum for the treated BNNT. Iron pentacarbonyl, $Fe(CO)_5$, is generated over time in pressurized CO cylinders due to the reaction of Fe from the steel tank with CO gas, increasing its concentration with time [156], [161]. In previous work, Nasri Lari et al. [162] studied the decomposition of $Fe(CO)_5$ under UVC light. They showed that after exposure to the UVC lamp at 253.7 and 185 nm, the formation of $Fe(CO)_n$ is expected. The peaks at 712.1, 715.1, and 719.5 eV (Figure 5.3I) can be attributed to Fe_2O_3, FeO(OH), and Fe_3O_4, respectively [82]. Similar results were obtained by Hosseininasab et al. [82] and Farhanian et al. [100] when CNTs and silicon wafers were subjected to syngas PICVD reactions.

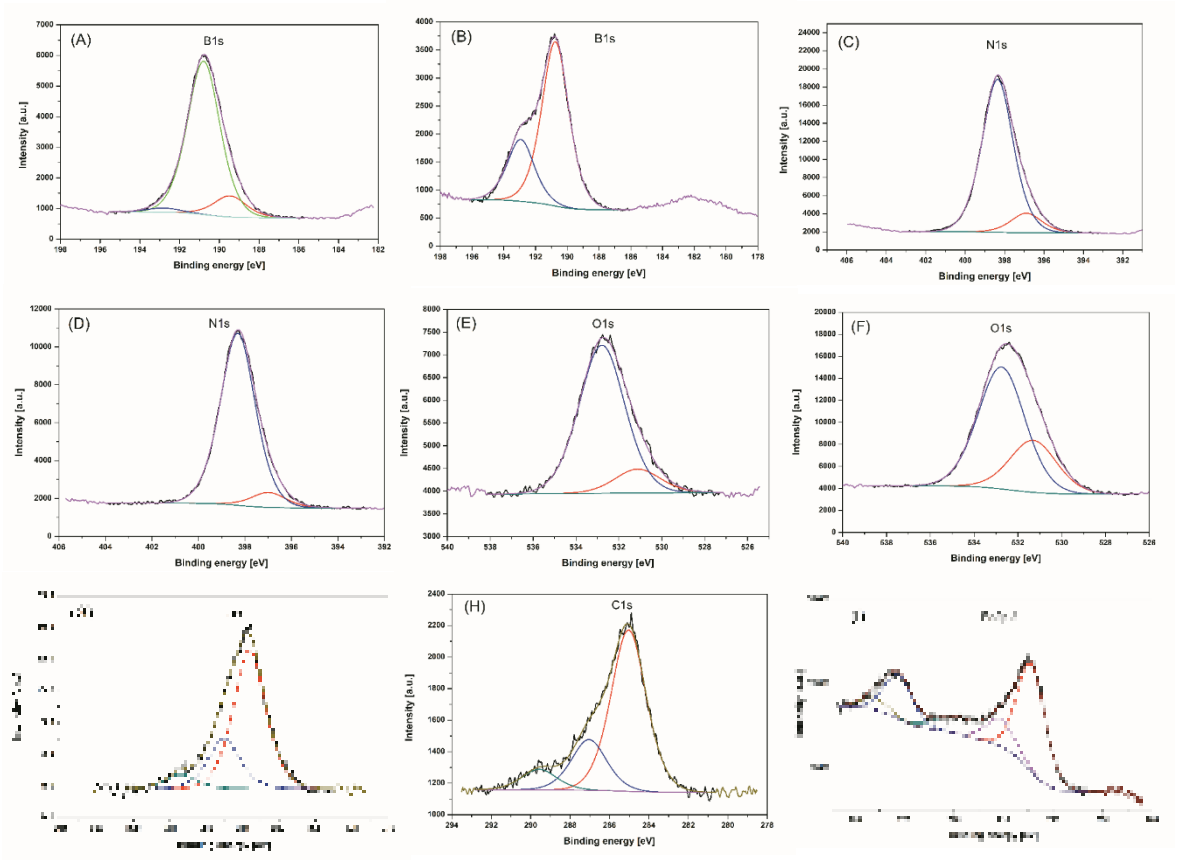

Figure 5.3 (A) B1s, (C) N1s, (E) O1s, and (G) C1s high-resolution spectra for untreated boron nitride nanotubes (BNNTs), and (B) B1s, (D) N1s, (F) O1s, (H) C1s, and (I) Fe2p2 high-resolution spectra for treated BNNTs.

The relevance of this work relies on the low cost and low energy consumption technology employed to oxidize the surface of BNNTs. The cost for a 1 h treatment is only $0.3921 CAD (Appendix C), with ~ 0.5% of this cost attributed to the energy consumption of the UV lamps, 14.2% to the consumption of the gases (CO, H_2, and Ar) and 85.3% to the cost of H_2O_2. In treatments where H_2O_2 is not needed, and considering the same reaction conditions, the operational cost would be as low as $ 0.0575 CAD/h. We increased the O_2 atomic content from 7.8% from the untreated sample to 37.1% for the treated one. This level of oxidation is higher than the 16% obtained by Dai et al. [34], when using an O_2 plasma treatment for 20 min, and the 24.3% reported by Jakubinek et al. [91], when another O_2 plasma treatment was used for a period of 10 min. We have calculated the cost of the energy consumption of the plasma treatments in the works of Dai et

al. [34] and Jakubinek et al. [91] for comparison purposes with this work (Appendix C). However, these estimates do not account for the increased infrastructure cost associated with plasma systems.

5.3.1 Fourier-transform infrared spectroscopy

FTIR spectra were obtained for both untreated and treated BNNT films (*Figure 5.4*). The peak at 1350 cm^{-1} is attributed to the in-plane B-N mode of the BNNTs, while the peak at 800 cm^{-1} is linked to the B-N-B bending vibration [58], [88], [163]. For the t-BNNT, the addition of a broad peak centred at 3325 cm^{-1} is seen, corresponding to the adsorption of water molecules from the environment [163]. The measurements were done at a RH of 46%. Hołysz et al. [45] studied the effect of relative humidity on water contact angles deposited on unoxidized and oxidized silicon wafers. In both cases, the CA changed with the relative humidity, but this change was more significant in oxidized surfaces, where the adsorption of water is higher.

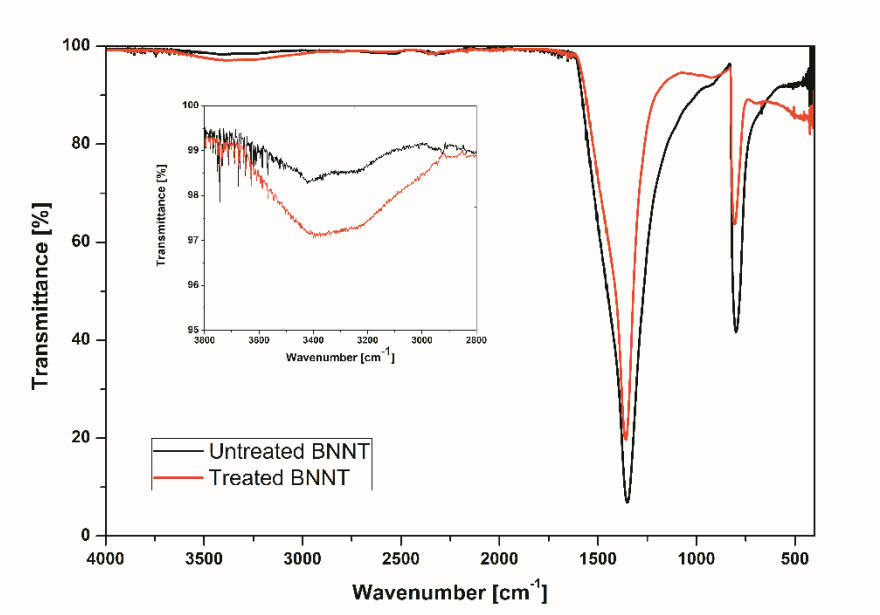

Figure 5.4 FTIR spectra of (A) untreated and (B) treated BNNTs. The inset shows a zoom in the 2800 – 3800 cm-1 range.

5.3.2 Contact angle measurements and surface energy

Water contact angles were measured in both untreated and treated BNNTs (Figure 5.5). The untreated film showed an average water contact angle of ~88°, in comparison to the 16.8° (static) contact angle after the PICVD treatment, which continued to shrink to almost 0° after 3 s. This indicates that the surface treatment increased the affinity of the BNNT for water, thus increasing its hydrophilicity. Similar water CA results were obtained by Pakdel et al. [40] and Jakubinek et al. [91], when an oxygen-plasma treatment was used to oxidize the surface of BNNT films.

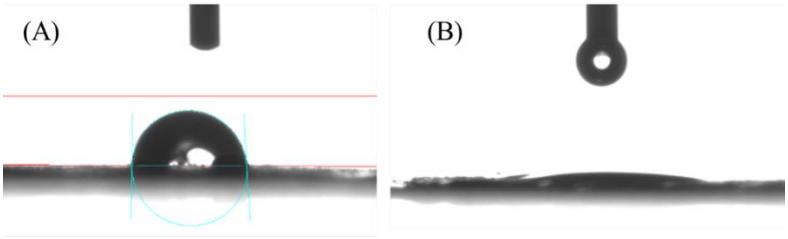

Figure 5.5 Water contact angle of (A) untreated and (B) treated BNNTs.

Surface energies for both materials were determined applying the OWRK method, as indicated in Equation (1), where γ_l^d and γ_l^p are the dispersive and polar components of the test solvents and θ_w their corresponding contact angle. Water, formamide and diiodomethane were used as polar, intermediate polarity and non-polar solvents, respectively. Then, the total surface energy of the films (γ_s) and its dispersive (γ_s^d) and polar (γ_s^p) components were calculated, as shown in Equation (2). For the untreated material, a surface energy γ = 55.43 mJ/m^2 was obtained, being mainly of a dispersive nature. On the other hand, an increment in surface energy of ~12 mJ/m^2 was observed for the treated BNNT, with a dispersive component (γ_d) of 30.56 mJ/m^2 and a polar component (γ_p) of 37.11 mJ/m^2 (Table 5.4). This supports our XPS results, where an oxidized surface was obtained. An increment in surface energy is related with an increment on the polarity of the films.

$$\gamma_{sl}\left(\frac{1+cos\theta_w}{2}\right) = (\gamma_s{}^d\gamma_l{}^d)^{0.5} + (\gamma_s{}^p\gamma_l{}^p)^{0.5} \quad (1)$$

$$\gamma_s = \gamma_s{}^p + \gamma_s{}^d \quad (2)$$

Table 5.4 Static contact angle and surface energy of BNNT films.

Sample	CA (°)			Surface energy (mJ/m^2)		
	Water	**Formamide**	**Diiodomethane**	**Total**	**Dispersive**	**Polar**
Untreated BNNT	87.8 ± 7.1	33.0 ± 4.0	22.2 ± 3.8	55.43	55.01	0.41
Treated BNNT	16.8 ± 1.3	15.6 ± 3.1	12.9 ± 3.1	67.67	30.56	37.11

Advancing and Receding contact angles were performed using water as a test solvent to consider the effect of roughness, chemical heterogeneities, swelling behavior and/or reorientation of functional groups on the BNNTs surfaces [142], [45]. Then, a second value of surface free energy (γ_S) was determined based on the Contact Angle Hysteresis approach (CAH), as can be seen in Equation (3), where θ_a and θ_r are the advancing and receding water contact angles, and γ_L its total surface tension The new surface energy was determined following the equation proposed by Chibowski et al. [164]. A surface free energy γ_s = 50.15 mJ/m^2 was obtained for the untreated BNNT and a γ_s = 71.55 mJ/m^2 for the treated film. Even though the absolute values are different (Table 5.5), the delta remains constant. Liquid penetration of the solvents was observed during the measurements, due to the porosity presented by the films. This could affect mainly the receding angles, because of a prolonged exposure of the droplet on the film. In this work, we believe that surface roughness is the dominant role on the wettability of the films (over chemical heterogeneities). Thus, we have speculated that the wetted BNNT films experiences a homogeneous wetting regime (Wenzel state) [142]. A decrease in the advancing and receding CA angle was observed during the dynamic measurements compared to the static values.

$$\gamma_S = \gamma_L(cos\theta_r - cos\theta_a)\frac{(1+cos\theta_a)^2}{(2+cos\theta_r+cos\theta_a)} \qquad (3)$$

Table 5.5 Water ARCA and SE for untreated and treated BNNT.

Sample	Water ARCA (°)		Total Surface energy (mJ/m^2)
	Advancing	Receding	
Untreated BNNT	65.9 ± 0.8	56.2 ± 3.4	50.15
Treated BNNT	21.2 ± 1.6	12.6 ± 1.7	71.55

5.3.3 Dispersion tests

Dispersion tests of treated BNNTs were done in water, methanol, and glacial acetic acid. In previous work [25], we determined the Hansen solubility parameters (HSP) of untreated BNNTs employing a wide range of organic solvents. Briefly, the HSP consider dispersive (δ_d), polar (δ_p), and hydrogen bonding (δ_h) interactions that a particle (solid or liquid) may have [165]. The determined HSP for the untreated BNNTs were $\{\delta_d; \delta_p; \delta_h\} = \{16.8; 10.7; 14.7\} \pm \{0.3; 0.9; 0.3\}$ $MPa^{1/2}$, with a Hildebrand parameter (δ_t) equal to 24.7 $MPa^{1/2}$ [25]. These values indicate that the particle in question possesses a mild polarity and agrees with the partial ionic bonds present in the BNNTs [18], [15]. The discrepancies between the HSP of the untreated BNNT films (which suggest a polar surface) and the surface energy (SE) values (low polarity surface) determined in the present work arise from the morphology of the sample used. In the first case, the films were dispersed in organic solvents by the means of sonication, while in the latter, the measurements were done directly on BNNT films. The alignment of the nanotubes, packing density, curvature, roughness, porosity, and chemical heterogeneities have a significant effect on the hydrophilicity/hydrophobicity of the BNNTs films [37], [38], [140], [166]. The more vertically aligned nanotubes in the film, the more voids will be present, and more air will fill the free space, making the surface more hydrophobic [40], [140], [166]. Other factors such as the temperature used during the synthesis also contribute to the hydrophobicity of the resulting BNNT films [40].

HSP indicate where the dispersibility sphere (Hansen sphere) of a particle, in this case the BNNTs, is in a 3D space. Then, one can plot the HSP of a solvent of interest and see where it is located with

respect to the BNNTs. With the HSP of the solvent, the distance between the solvent and the particle, R_a, can be calculated, and a relative energy difference (RED) for each solvent can be determined. For RED < 1, the solvent will be considered 'good' to disperse the particle in question. For RED > 1, the solvent will show poor dispersion, and for RED = 1, the solvent will be partially able to disperse the particle [109].

Water, methanol, and acetic acid were chosen for the dispersions of t-BNNTs because they were classified as intermediate (water and methanol) or poor (acetic acid) for the untreated material (Figure 5.6) [25]. The reasoning behind this was to compare the dispersion state of untreated and treated BNNTs. Digital pictures of t-BNNTs (Figure 5.7) were taken at 0, 48, and 120 h after sonication. In our cited previous work [25], absolute sedimentation times (t_{sed}) for dispersions in water, methanol, and acetic acid were calculated, considering the density of BNNTs and the viscosity of the solvents. The t_{sed} were 50.6, 23.8, and 65.8 h for water, methanol, and acetic acid, respectively. As we can see in Figure 5.7A, the dispersion state immediately after sonication for the t-BNNTs is classified as intermediate in the three cases. However, in the case of water (Figure 5.7B), only 48 h after sonication, which is approximately the same as t_{sed} (50.6 h), there is a separation of BNNTs, where some of the nanoparticles are dispersed forming a cloudy region, some are sedimented at the bottom of the vial, and a few of them are located at the solvent-air interface. It can be observed that the number of particles at the water–air interface decreased for the t-BNNTs, in comparison with the untreated material (Figure 5.6A), meaning that the particles migrated to the liquid phase, improving their affinity for water. In the case of methanol, the dispersion state of t-BNNTs at its t_{sed} (23.8 h) was not taken, but just after sonication the particles were well dispersed (Figure 5.7A). However, after 48 h (Figure 5.7B), they formed two regions: a cloudy one and a sedimented one. For the dispersion in acetic acid, no significant change was observed between the t-BNNTs at 48 and 120 h after sonication (Figure 5.7B,C) and the untreated material at t_{sed} (65.8 h) (Figure 5.6C).

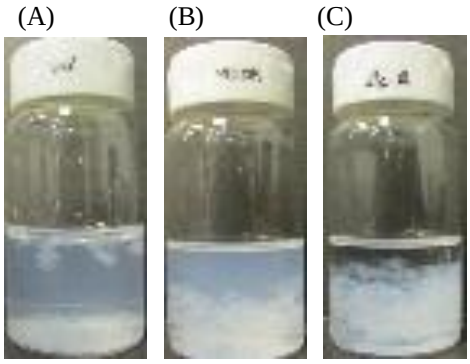

Figure 5.6 Dispersions of untreated BNNTs in (A) water, (B) methanol, and (C) acetic acid after having elapsed their respective sedimentation time, tsed.

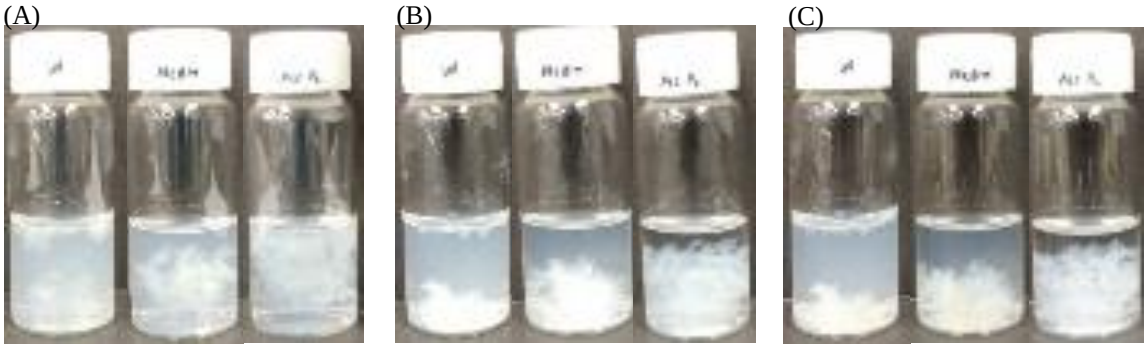

Figure 5.7 Dispersions of t-BNNTs in water, methanol and acetic acid taken (A) immediately after sonication, (B) 48 h, and (C) 120 h after sonication.

5.4 Conclusions

Covalent functionalization of purified BNNTs with oxygen functionalities was achieved using a room temperature, near ambient pressure, and low energy consumption process- syngas photo-initiated chemical vapour deposition. The energy consumption of the light source (UVC lamp operating at 30 W) was 0.03 kWh, translating into a cost of ~ $0.002 CAD, while the cost of the fed gases (CO, H_2 and Ar) was $0.055 6 CAD for 1h treatment. This extremely low-cost process

makes syngas PICVD a promising approach for surface modification at large scale, with energy consumption lower than those of plasma processes carried out by Dai et al. [34], and Jakubinek et al. [91]. An increase in the atomic oxygen from 7.8 to 37.1% was observed after treatment. This level of oxidation is higher than the ones reported in the literature using plasma treatments. A potential application of the treated BNNTs would be their incorporation into polar polymers, with the goal of improving their mechanical and thermal properties. PICVD has been shown to impart a wide range of functionalities in the past, but on BNNT, it is currently limited to hydrophilic treatments. Work is being done in order to control $Fe(CO)_5$, a non-intentional photo-active compound generated over time in pressurized CO tanks.

Acknowledgments

The authors would like to thank the Natural Sciences and Engineering Research Council of Canada (NSERC), Prima Québec, Tekna Plasma Systems, Michelin Canada and Polytechnique Montréal for their contributions. C. S. Torres-Castillo is also thankful to the Mexican National Council for Science and Technology (CONACyT) for the scholarship provided (number 739894).

CHAPTER 6 ARTICLE 3 : THERMALLY CONDUCTIVE STYRENE-BUTADIENE RUBBER/BORON NITRIDE NANOTUBES COMPOSITES

Cristina Sofia Torres Castillo, Jason. R. Tavares

Department of Chemical Engineering, École Polytechnique de Montréal, P.O. Box 6079, Station Centre-Ville, Montreal, Quebec, H3C 3A7, Canada

Published in:

Journal of Composites Science, 2022, Vol. 6 (9), pp 272

https://doi.org/10.3390/jcs6090272, Publication Date: September 2022 Available online 14 September 2022,

KEYWORDS :

boron nitride nanotubes; styrene-butadiene rubber; thermal conductivity; nanocomposite

Abstract

The use of boron nitride nanotubes (BNNTs) for fabrication of thermally conductive composites has been explored in the last years. Their elevated thermal conductivity and high mechanical properties make them ideal candidates for reinforcement in polymeric matrices. However, due to their high tendency to agglomerate, a physical or chemical treatment is typically required for their successful incorporation into polymer matrices. Our previous study about the dispersibility of BNNTs allowed determination of good solvents for dispersion. Here, we performed a similar characterization on styrene-butadiene rubber (SBR) to determine its solubility parameters. Although these two materials possess different solubility parameters, it was possible to bridge this gap by employing a binary mixture. The solvent casting approach followed by hot pressing was chosen as a suitable method to obtain thermally conductive SBR/BNNT composites. The resulting nanocomposites showed up to 35% of improvement in thermal conductivity and a 235% increase in storage modulus in the frequency sweep, when a BNNT loading of 10 wt% was used. However, the viscoelastic properties in the amplitude sweep showed a negative effect with the increase in BNNT loading. A good balance in thermal conductivity and viscoelastic properties was obtained for the composite at a BNNT loading of 5 wt%.

Keywords: boron nitride nanotubes; styrene-butadiene rubber; thermal conductivity; nanocomposite

6.1 Introduction

Boron nitride nanotubes are ceramic nanoparticles with outstanding thermal conductivity, with theoretical values of up to 3000 W/(m K) and experimental values around 350 W/(m K) [21], [167]. Like their carbon counterparts, the thermal conductivity varies according to the number of walls, with fewer walls corresponding to higher conductivity. In contrast with carbon nanotubes (CNTs), BNNTs are electrical insulators, which make them suitable for applications where thermal conductivity and electrical insulation are required, such as in devices for heat dissipation. BNNTs possess impressive mechanical properties (Young's modulus of 1.2 TPa) [15], good chemical stability, and high thermal resistance, up to 900 °C in air [17]. Thermally conductive nanocomposites have been obtained with the incorporation of BNNTs and other BN nanostructures in polymeric matrices. Table 6.1 shows a summary of some previous studies.

Table 6.1 Summary of polymer/BN nanocomposites with improved thermal conductivity (TC).

Matrix	BN material	Aligned or modified	Loading	TC composite (W/mK)	% TCE (W/mK)	Ref
PS PMMA PEVA PVB	BNNTs	No	35 wt% 24 wt% 37 wt% 18 wt%	3.61 3.16 2.5 1.81	1905 2006 1370 654	[21]
PVF PVA	BNNTs m-BNNTs	No Yes	10 wt% 3 wt%	0.45 ~ 0.30	150 267	[65]
PVA	(O)BNNTs	Yes	10 wt%	0.54	237	[20]
Epoxy	BNNTs-BNNSs	Yes	2 wt%	0.47	147	[30]
Epoxy	BNNTs	Yes	30 wt%	2.77	1285	[62]
Epoxy	BNNTs	No	30 wt%	2.9	1350	[32]
TPU	BNNTs	No	1 wt%	14.5	≥ 400	[55]
PC	BN plates	Yes	18.5 vol%	3.09	115	[64]
Epoxy	BN platelets	Yes	50 wt%	6.09	2800	[168]
Epoxy resin	h-BN	Yes	44 vol%	9.0	4400	[169]
Polysiloxane	BNNSs	Yes	15 vol%	1.56	290	[170]
SBR	BN BNNSs Si-BNNSs	Yes	10. 5 vol%	0.28 0.43 0.57	82 119 253	[70]
SBR	(R)BNNSs (O)BNNSs (R)PRh-BNNSs (O)PRh-BNNSs	Yes	27.5 vol%	0.55 1.08 0.75 1.50	189 468 295 689	[42]

Si-BNNSs refers to silane-modified BNNSs; PRh-BNNSs represents polyrhodanine@BNNSs nanostructure; (R) and (O) stands for random and oriented nanostructures.

As can be seen, special treatments, alignment or surface modification of BN nanostructures are required to further increase thermal conductivity. These additional treatments imply not only longer processing times and subsequent purification steps, but also higher energy consumption, when the nanotubes have to be aligned by any means. Regarding SBR/BN composites, the incorporation of BN nanostructures has been limited to boron nitride nanosheets (BNNSs). This could be attributed to the more expensive methods required for the synthesis of high quality BNNTs. It was also observed that chemical functionalization with a silane agent [70] or coating with polyrhodanine [42] was needed to improve the compatibility of BNNSs with a rubber matrix. A more straightforward approach is missing for the fabrication of thermally conductive SBR/BN nanocomposites.

The incorporation of nanoparticles into polymers is often carried out in the liquid phase, by dispersing both materials in a suitable solvent. Thus, a solvent compatible with both the targeted polymer and nanomaterial should be used. The appropriate selection can be performed based on the solubility of the polymer and the filler.

Solubility parameters, also known as cohesion parameters, can be used to correlate the cohesion energies of polymers and liquids, by assessing the properties of individual compounds. Solubility parameters rely on the principle that "like seeks like", which means that a polymer will be dissolved in a liquid when the solubility parameters of both are alike [109]. The energy required to hold together the molecules of a material is known as the cohesive energy. This energy is divided into three components, accounting for dispersive, polar, and hydrogen bonding interactions (Equation (1)). Dividing each component by molar volume, we obtain the cohesive energy density. The square root of the cohesive energy density is known as the Hildebrand solubility parameter (δt), as can be seen in Equation (2):

$$\frac{E}{V} = \frac{E_d}{V} + \frac{E_p}{V} + \frac{E_h}{V} \qquad (1)$$

$$\delta_t = \sqrt{{\delta_d}^2 + {\delta_p}^2 + {\delta_h}^2} \qquad (2)$$

where δ_d, δ_p, and δ_h are the Hansen solubility parameters. There are several ways to determine the Hansen solubility parameters (HSPs) of a polymer, such as dissolution, swelling, or viscosity changes [109], [110]. The simplest way is to dissolve a certain amount of polymer in a specific volume of solvent. Then, after a period of time, the dissolution state is evaluated qualitatively by classifying the solutions in good or bad [109], [111]. It is possible to represent the solubility space for the polymer and the solvents in a 3-D space (Hansen space). The center of the sphere is determined by the HSPs of the polymer, with coordinates $\{\delta_d; \delta_p; \delta_h\}$ and a calculated radius, R_0. The solvents located inside the sphere will dissolve the polymer, while the solvents found outside will not. The distance between the polymer and the solvent can be estimated by applying Equations (3) and (4):

$$R_a{}^2 = 4(\delta_{d1} - \delta_{d2})^2 + (\delta_{p1} - \delta_{p2})^2 + (\delta_{h1} - \delta_{h2})^2 \quad (3)$$

$$RED = \frac{R_a}{R_0} \quad (4)$$

where δ_{d1}, δ_{p1}, and δ_{h1} correspond to the HSPs of the polymer and δ_{d2}, δ_{p2}, and δ_{h2} represent those of the solvent. The relative energy difference (RED) indicates where the solvent is located with respect to the polymer sphere. RED < 1 corresponds to good solvents, located inside the sphere, RED > 1 indicates that the solvent is located outside, and RED = 1 indicates that the solvent may be able to dissolve the particle to a certain degree [109].

In this work, the incorporation of pristine boron nitride nanotubes into styrene-butadiene rubber was done through a simple approach. No surface modification or pre-treatment was needed. By analyzing the Hansen solubility parameters of both materials and pushing to the boundaries the solubility theory, a suitable dispersion media is described. Thermal conductivity of the resulting nanocomposites is presented, along with the mechanical properties derived from rheological testing. The present work offers a facile technique for the incorporation of BNNTs into SBR for fabrication of composites with improve thermal conductivity.

6.2 Materials and Methods

6.2.1 Materials

Purified BNNTs in the form of powder were provided by Tekna Plasma Systems. The average nanotube diameter was 5 nm +/- 2nm, with a BNNT content of >75%. They were synthesized by an induction thermal plasma process (HABS method) [33], followed by purification with a thermal method [56]. Styrene-butadiene rubber (SBR) was provided by PT Synthetic Rubber Indonesia as a light brown solid product, comprising 27% polybutadiene (itself composed of 24% vinyl-1,2 units, 30% cis-1,4 units, and 46% trans-1,4 units). Its molecular weight Mn was 118,000 g/mol, and its Mooney viscosity ML(1 + 4) was 50 MU, with a glass transition temperature of -52 °C. Organic solvents were purchased from Sigma-Aldrich and Fisher Scientific. All were of high purity (99%), except d-Limonene (96%) and ethanol (95%). All the materials were used as received.

6.2.2 Methods

SBR dissolutions were prepared in different organic solvents with validated solubility parameters. The solvents included alkanes, ketones, amides, alcohols, a chloro-compound, esters, and aromatic compounds. These solvents were chosen to have dissolutions with different polarities. In brief, 500 mg of polymer were dissolved in 5 mL of the solvent. The dissolutions were left in a quiescent state for 24 h at room temperature. Then, the dissolution states were evaluated as good, intermediate, or bad, considering if the polymer was completely dissolved, partially dissolved or no dissolution was observed.

Dispersions of BNNTs were prepared in a Cole-Palmer sonicator operating at 20 kHz and at 30% of amplitude, with cycles of 5 s ON and 2 s OFF. The power delivered to the dispersions was ~25 W. A cylindrical probe (type 410-08) was employed; 10 mg, 50 mg, or 100 mg of BNNTs were dispersed in 10 mL of solvent. To determine the adequate amount of energy needed during sonication, preliminary tests were conducted at different energies. According to the guidelines provided by Girard et al. for the dispersion of cellulose nanocrystals [171], an energy of 167 kJ/g L (grams of the material; liters of the solvent) was recommended. Based on that, we calculated the energy required to disperse the BNNTs at three different loading: 10, 50, and 100 mg. The respective energies were 16.7 J, 83.5 J, and 167 J. However, when applying this energy to our system, we observed that the dispersions were not complete, and some agglomerates could still be seen. Thus, we increased the energy up to 500 J or 1000 J to have homogeneous dispersions. We concluded that the energy applied during ultrasonication is not only a function of the amounts of the material and the volume used, but also of the type of nanoparticle to be dispersed and the properties of the solvent such as viscosity and surface tension. A total energy of 500 J (5 J/(mg mL)) was applied to 10 mg of BNNT, and 1000 J were used for 50 mg (2 J/(mg mL)) and 100 mg (1 J/(mg mL)) of BNNTs.

SBR/BNNTs nanocomposites were fabricated in a two-step process. First, SBR dissolutions and BNNT dispersions were prepared at the desired concentrations (see Table 6.2). A fixed amount of SBR was dissolved in 10 mL of the retained solvent. The dissolution was left in a quiescent state overnight, to allow the polymer to be dissolved. To reach full dissolution, the system was magnetically stirred at 500 rpm for 4 h. While stirring, BNNT suspensions were prepared at the

desired concentrations. Once the SBR and the BNNTs were fully dissolved or dispersed, they were mixed and stirred at 500 rpm for 1.5 h. The resulting mixtures were poured on 6 cm-diameter polytetrafluoroethylene (PTFE) dishes and allowed to dry at room temperature. Polymer films were obtained after 72 h of drying. The second step comprised the molding of the films. They were hot-pressed to evaporate any residual solvent and to eliminate possible bubbles/voids formed during the drying process. This was performed in a Carver press (model 3912) at a pressure of 3000 lb_f/in^2 at 120 for 5 min, with a pre-heating step at 1200 lbf/in^2 for 2 min. Then, the discs were put in a room-temperature Carver press at 1200 lbf/in^2 for 3 min to cool down the samples. A schematic of this methodology is shown in Figure 6.1.

Table 6.2 Nomenclature of composites prepared.

BNNT loading	**Mass SBR**	**Mass BNNT**
0 wt%	1 g	0 g
1 wt%	0.990 g	0.010 g
5 wt%	0.950 g	0.050 g
10 wt %	0.900 g	0.100 g

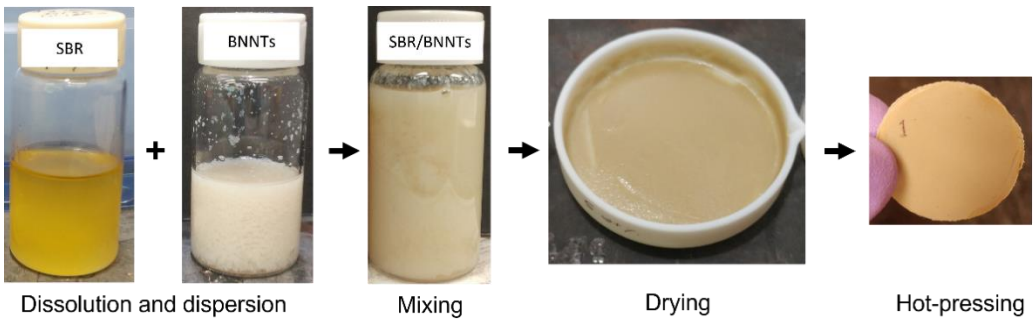

Figure 6.1 Methodology followed for the fabrication of SBR/BNNTs nanocomposites.

Transmission electron microscopy (TEM) measurements were conducted in a Jeol JEM 2100F. Prior to the analyses, the samples were encapsulated in an epoxy resin and ultramicrotomed using an EM UC7 (Leica Microsystems,Wetzlar, Germany).

Rheological properties of the composites were measured in an Anton Paar rheometer, model MCR 502. Rough parallel plates (serial number: 18289) of 25 mm in diameter were used as the measurement system. Amplitude and frequency sweeps were performed at 23 °C. Amplitude sweeps were run at a frequency of 10 Hz (62.8 rad/s) in a strain range of 0.01–100%. Frequency sweeps were performed at a constant strain *g* of 0.1% in a frequency range of 0.1–100 rad/s.

Thermal conductivity measurements were performed at room temperature using a TCi Thermal Conductivity Analyzer (model TCi-3-A) from C-Therm. The modified transient plane source (MTPS) method was employed.

6.3 Results and Discussion

6.3.1 Hansen Solubility Parameters of Styrene Butadiene Rubber

HSP were determined for SBR. Three scores were given to the dissolutions, depending on whether the dissolution was complete (score “2”), partial (score “1”) or no dissolution was observed (score “0”) (see Figure D.1). Table 6.3 shows the HSPs of each solvent, their scores, and the calculated Ra and RED numbers.

Table 6.3 HSPs, scores, and Ra and RED numbers of the solvents used for the dissolution of SBR.

Solvent	**δ_d**	**δ_p**	**δ_h**	**Score**	**R_a**	**RED**
d-Limonene	17.2	1.8	4.3	2	0.81	0.16
Chloroform	17.8	3.1	5.7	2	1.64	0.33
Toluene	18	1.4	2	2	2.90	0.58

Ethyl benzene	17.8	0.6	1.4	2	3.64	0.73
Ethyl benzoate	17.9	6.2	6	2	4.15	0.83
1,4-dioxane	17.5	1.8	9	2	4.66	0.93
Tetrahydrofuran	16.8	5.7	8	2	4.96	0.99
Cyclohexane	16.8	0	0.2	2	5.03	1.01
Ethyl acetate	15.8	5.3	7.2	1	5.09	1.02
Methyl ethyl ketone	16	9	5.1	1	7.11	1.42
Benzyl alcohol	18.4	6.3	13.7	1	10.24	2.05
Acetone	15.5	10.4	7	0	9.14	1.83
2-Propanol	15.8	6.1	16.4	0	12.93	2.59
N,N′-Dimethylformamide	17.4	13.7	11.3	0	13.15	2.63
Dimethylsulfoxide	18.4	16.4	10.2	0	15.19	3.04
Propylene carbonate	20	18	4.1	0	16.35	3.27
Ethanol	15.8	8.8	19.4	0	16.58	3.32
Methanol	15.1	12.3	22.3	0	20.92	4.18
Ethylene glycol	17	11	26	0	23.23	4.65
Formamide	17.2	26.2	19	0	27.84	5.57
Tol/EA (20/80) [1]	16.2	4.5	6.2	2	3.61	0.72

1 Additional solvent used but not considered for the HSP determination of SBR. “Tol” stands for toluene, and “EA” stands for ethyl acetate.

Once the dissolutions were scored, we proceeded to input the information in the HSPiP software to calculate the HSPs of the SBR. The HSPs were $\{\delta_d; \delta_p; \delta_h\} = \{17.4; 2.5; 4.4\} = \{0.4; 0.8; 0.6\}$ $MPa^{1/2}$, with δ_t of 18.1 and a radius R_a of 5.0 $MPa^{1/2}$. The FIT equation was 1, meaning that all the solvents that were ranked as good were inside the sphere and all the solvents ranked as bad were outside (see Figure 6.2).

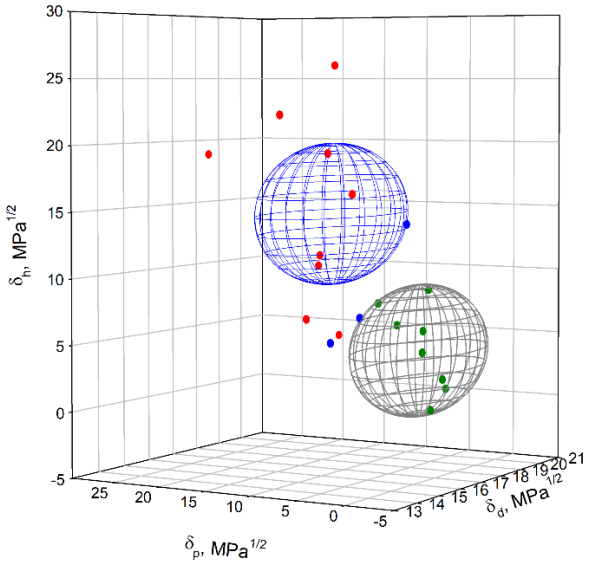

Figure 6.2 Hansen space for SBR (gray sphere) and BNNTs (blue sphere). Good solvents for SBR are represented with green dots, intermediate solvents with blue dots and bad solvents with red dots.

Liu et al. [115] previously determined the HSPs of cured SBR through swelling experiments. The obtained values were $\{\delta_d; \delta_p; \delta_h\} = \{18.0; 2.9; 2.3\}$ $MPa^{1/2}$, with a total solubility parameter, δ_t = 18.4 $MPa^{1/2}$, and R_a = 5.0 $MPa^{1/2}$. The SBR used was Buna VSL 4526-2, with a styrene content of 26 wt%, a vinyl content of 44.5 wt%, and a Mooney viscosity ML(1+4) of 5 MU. In their experiments, they observed that ethyl acetate and methyl ethyl ketone were located in a low swelling area, which agrees with our results, where they were considered as intermediate solvents to partially dissolve SBR. HSPs of SBR (brand Polysar) have been also reported in the HSP

database [109], [116]. The values are {17.6, 3.4, 2.7}, with Ra of 6.55 $MPa^{1/2}$. Although the same polymer was used in the determination of HSPs, there are some differences observed. Indeed, HSPs of polymers are sensitive to molecular weight and chemical composition. Thus, different compositions and/or proportions of the repeat units and molecular weight will lead to different HSP values [109].

As mentioned earlier, SBR and BNNTs have different surfaces energies and solubility parameters. The mild polarity of BNNTs and the non-polar behavior of SBR make them locate in different Hansen spaces (see Figure 6.2). However, based on the Hansen solubility theory, it is possible that two bad or intermediate solvents dissolve the material in question by using binary mixtures. By exploring this concept and calculating the R_a and RED numbers for binary mixtures, we were able to obtain full dissolution of SBR and good dispersion of BNNTs in short times. Based on our previous work on the dispersion of purified BNNTs [25], with HSP $\{\delta_d; \delta_p; \delta_h\} = \{16.8; 10.7; 14.7\} \pm \{0.3; 0.9; 0.3\}$ $MPa^{1/2}$ and R_a = of 5.4 $MPa^{1/2}$, we determined that the best solvents to disperse BNNTs were dimethyl formamide (DMF), dimethyl acetamide (DMAc), ethanol, and isopropanol. We also determined that some other solvents with lower polarity were able to disperse this nanomaterial for short periods, such as ethyl acetate. On the other hand, when determining the HSP of SBR (this work), we observed that ethyl acetate was able to partially dissolve this polymer, with non-polar solvents such as toluene being preferred to have full dissolution. Taking into account this information, we prepared binary mixtures of toluene/ethyl acetate at different volume ratios (see Table 6.3). Based on the results, we observed that the 20:80 volume ratio mixture we would ensure the full dissolution of SBR without compromising good BNNTs dispersion. The calculated RED number in relationship to SBR was 0.71 (RED < 1), meaning that this mixture is inside of its Hansen sphere. In relationship to BNNTs, the RED number was 1.96. Although this value is slightly higher than 1, and that the coordinate is located outside of the solubility sphere of BNNTs, the toluene/ethyl acetate mixture in a 20:80 vol % was able to form stable dispersions for short periods of time, sufficient to undertake solvent casting.

Table 6.4 Calculated HSPs and Red numbers of binary mixtures of toluene/ethyl acetate.

Tol:EA volume ratio	**δ_d**	**δ_p**	**δ_h**	**R_a**	**RED**
0/1	15.8	5.3	7.2	5.09	1.02
0.1/0.9	16.0	4.9	6.7	4.32	0.86
0.2/0.8	16.2	4.5	6.2	3.54	0.71
0.3/0.7	16.5	4.1	5.6	2.78	0.56
0.4/0.6	16.7	3.7	5.1	2.03	0.41
0.5/0.5	16.9	3.4	4.6	1.33	0.27
0.6/0.4	17.1	3.0	4.1	0.79	0.16
0.7/0.3	17.3	2.6	3.6	0.85	0.17
0.8/0.2	17.6	2.2	3.0	1.43	0.29
0.9/0.1	17.8	1.8	2.5	2.15	0.43
1/0	18	1.4	2	2.90	0.58

6.3.2 Fabrication Styrene-Butadiene Rubber/Boron Nitride Nanotubes Composites

SBR/BNNTs composites were obtained by the solvent casting technique. SBR solutions and BNNT dispersions were prepared separately and combined. Table 6.2 shows the concentrations used and the nomenclature of the samples.

The obtained films (see Figure 6.3) had a thickness of ~300 µm and a diameter of 6.3 cm. With the increase in filler loading, a more uniform color in the films was observed. The neat SBR film had a light brown/orange color (see Figure 6.3a). With the increase in concentration, darker films with more uniform color were obtained (Figure 6.3b–d).

Figure 6.3 SBR composites obtained by solvent casting containing 0 wt% (a), 1 wt% (b), 5 wt% (c), and 10 wt% (d) of BNNTs.

6.3.2.1 Rheology

Figure 6.4 shows the variation of the viscoelastic properties (G' and G'') as a function of strain, obtained using a parallel-plate rheometer. The storage modulus (G') curves are observed in Figure 6.4a. G' of neat SBR and SBR/BNNT at 1 wt% overlapped in the linear viscoelastic (LVE) region, with an earlier decreased modulus at higher strains for the composite. The low BNNT loading did not allow the formation of a filler-filler network, and thus, the storage modulus was not affected. For the composites at BNNT contents of 5 wt% and 10 wt%, G' was higher in the strain range of 0.01%–1% but was reduced in the LVE region. This can be explained by the fact that at higher contents of BNNTs, a filler network is formed and, at higher strains, this network breaks. This phenomenon, characteristic of filled elastomers, is known as the Payne effect [79] [172], [173], [14]. For unfilled rubber, the storage modulus has a linear behavior in almost of all the strain range. However, when a filler is added, a filler-filler network is formed. A decreased G' (or E' for measurements performed in the tension mode) is observed at high strains, as a consequence of the rupture/disruption of the filler network [79] [172], [173], [14]. Das et al. [14] prepared styrene-

butadiene rubber-butadiene rubber blends (SBR-BR) reinforced with CNTs at different loadings. They observed the Payne effect in all the composites, with a more abrupt decrease in the storage modulus for the highest CNT concentration used. Similarly, Zhong et al. [174] observed the Payne effect on SBR−silica composites. The curves of loss modulus (G") are appreciated in Figure 6.4b. For neat SBR and the SBR/BNNT composites at 1 wt% loading, a linear behavior occurred up to 1% strain. After this value, a small shoulder appeared. For the composites at BNNT loadings of 5 and 10 wt%, an increase in the G'' at low strains was observed. This time, the small shoulder appeared as a big peak at lower strains and with increased intensity. This behavior corroborated what is appreciated in the G' curves: some disruptions of the filler-filler network occur at low strains [79]. However, due to the great flexibility pro-vided by the rubber, the polymeric chains and the filler-filler network regenerate over time, as proven by Das et al. [14] in SBR-BR/CNTs composites. It has been widely accepted that the introduction of a filler in rubber leads to a drastic decrease in G' and this is more evident with the increase in the loading of the filler. Accompanying this behavior, a peak in the G'' curve appears in the region where the G' decreases [79], [173]. Figure 6.4c shows the complex viscosity (η*) curves of the composites. In all cases, a zero-shear viscosity (η_0) was obtained at low strains. η_0 increased with the BNNT loading, and it presented the highest value (9.7 kPa s) for the composite at 10 wt%. The linear region observed at low strains was reduced with the increase in the BNNT loadings. Shear-thinning behavior was observed for all the composites, with a decrease in η the in almost all the strain range. This is attributed to the rupture of the BNNT agglomerates (or the filler network) with strain. Shear-thinning has also been observed in carbon black suspensions [175].

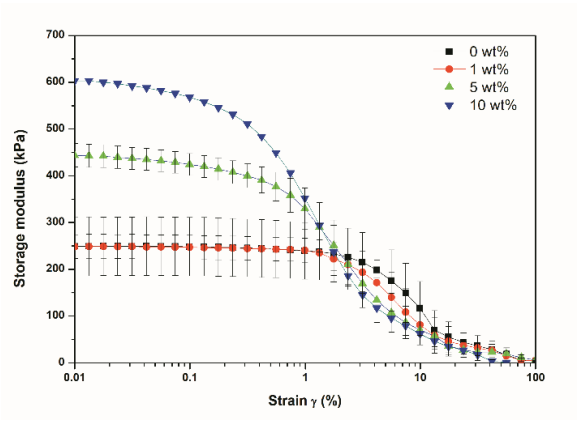

(a)

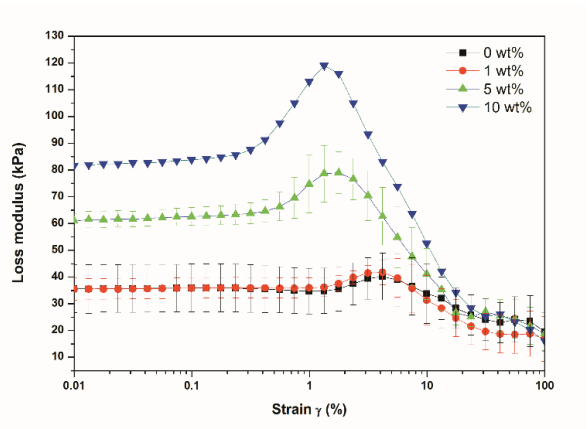

(b)

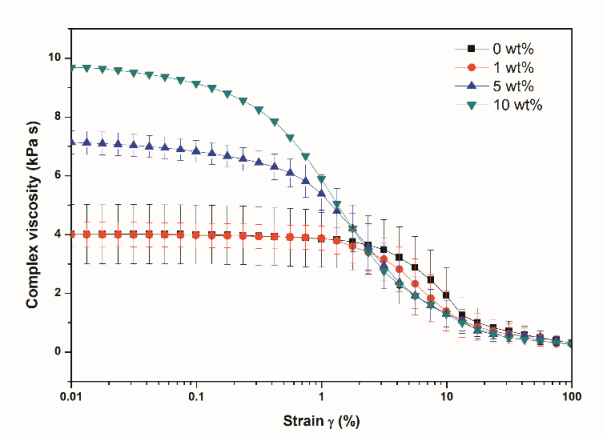

(c)

Figure 6.4 Variation of storage modulus (G') (a), loss modulus (G'') (b), and complex viscosity (η*) (c) of SBR/BNNTs composites as a function of strain. Standard deviation was calculated considering three different samples for each composite. The exception to this is the composite at 10 wt% of BNNTs, where only one measurement was performed.

Figure 6.5 shows the G', G'', and tan δ (corresponding to the G''/G' ratio) curves of the composites as a function of angular frequency. The reinforcing effect of BNNTs was evident, with an improved storage modulus for all the composites in the whole frequency range (Figure 6.5a). The highest G' was obtained for the composite at a loading of 10 wt% and at a frequency of 100 rad/s. The increase in the modulus was more pronounced at higher frequencies, with values of up to 246 kPa, 397 kPa, and 636 kPa for the composites at 1 wt%, 5 wt%, and10 wt%, respectively, at ω = 100 rad/s, in

comparison to 190 kPa obtained for the unfilled rubber. Figure 6.5b shows the G" curves for all the composites. Increases in the modulus in the composites were observed, which was related to higher energy dissipation. However, as can be seen in Figure 6.5c, the tan δ values (G''/G' ratio) were lower for the composites. Although there was an increase in loss modulus with the increase in BNNT content, the elastic portion (G') of the composites dominated in almost all the whole frequency range, with an overlapping of the curves at high frequencies. The decrease in tan δ curves of uncured SBR/carbon black composites has also been observed by Spanjaards et al. [175].

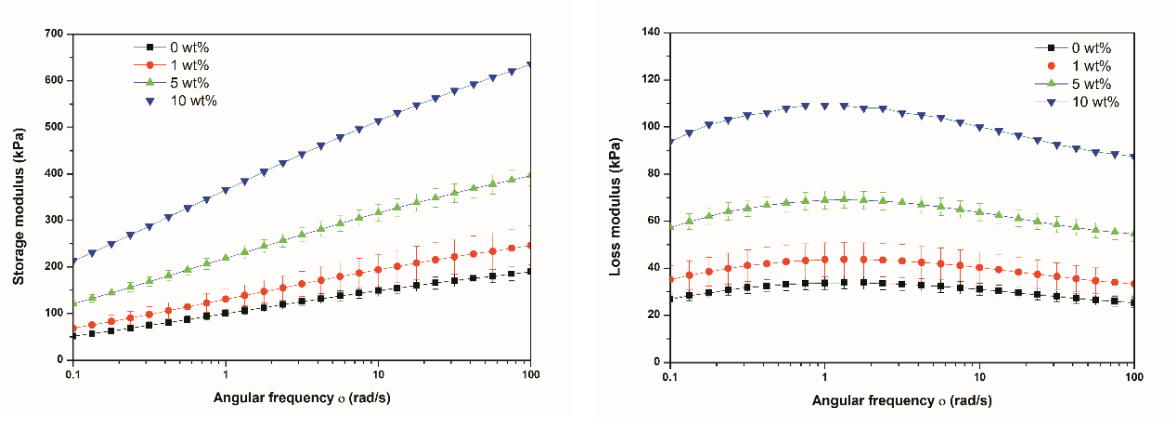

(a) (b)

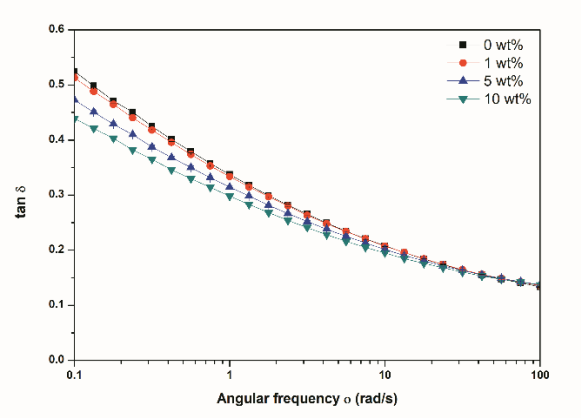

(c)

Figure 6.5 Variation of storage modulus (G') (a), loss modulus (G'') (b), and tan δ (c) of SBR/BNNTs as a function of angular frequency. Standard deviation was calculated considering three different samples for each composite. The exception to this is the composite at 10 wt% of BNNTs, where only one measurement was performed.

6.3.2.2 Transmission Electron Microscopy

Figure 6.6 shows TEM images of the cross section of SBR/BNNTs composites at a filler loading of 1 wt%. Due to its very low thickness (~300 µm), the film was encapsulated in an epoxy resin and ultramicrotomed prior to analysis. The nanotubes were dispersed but randomly distributed in the film, and small agglomerates were formed in some regions, with absence of nanotubes in others. This concentration of the filler did not lead to the formation of a BNNTs network in the polymeric film, and thus, the nanotubes did not distribute homogeneously in the entire surface of the polymer film. This agrees with the rheological results, where there was no effect in the viscoelastic properties (G' and G'') in the amplitude sweep (Figure 6.4).

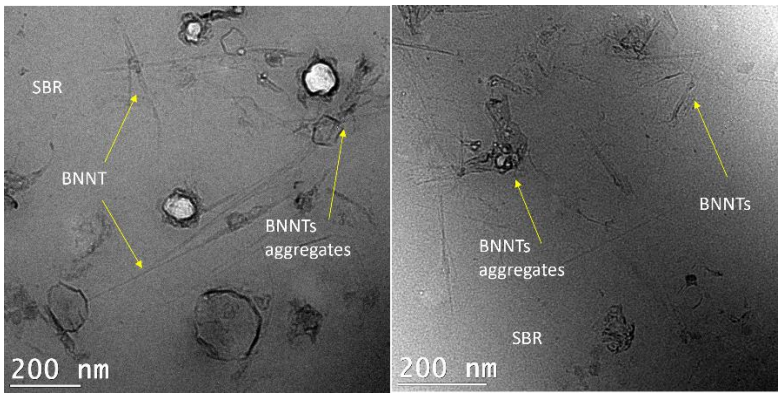

Figure 6.6 TEM images of SBR/BNNTs nanocomposites at 1 wt%. Some arrows are pointing out to individual nanotubes and others pointing out to BNNTs aggregates.

6.3.2.3 Thermal Conductivity

Thermal conductivity results are shown in Figure 6.7. For the composites containing 1 wt% of BNNT (0.64 vol%), the thermal conductivity did not change with respect to the neat polymer. This agrees with the TEM observations (Figure 6.6), where it can be seen that, at this loading, the nanotubes were not homogeneously distributed in the SBR and, consequently, some regions without nanotubes were observed in the film. For the composites at 5 wt% and 10 wt%, thermal conductivities of 0.255 W/(m·K) and 0.268 W/(m·K), with increments of 29% and 35%, respectively, were observed, in comparison with pure SBR. As inferred from Figure 6.3c,d, the BNNTs were better distributed in the SBR matrix, forming a filler network and providing a uniform

brown color along the composite. The formation of the filler network for these composites was corroborated in the rheological curves as a function of strain (Figure 6.4).

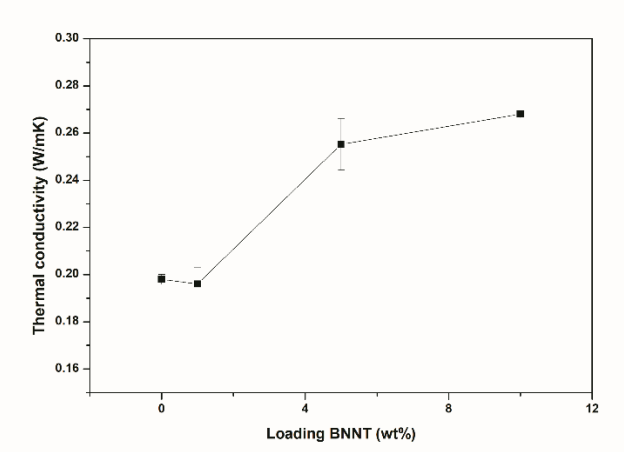

Figure 6.7. Thermal conductivity of the SBR/BNNTs nanocomposites. Standard deviation was calculated considering three different samples for each composite. The exception to this is the composite at 10 wt% of BNNTs, where only one measurement was performed.

Percolation thresholds of ~33 vol% and ~15 vol% for randomly oriented and aligned BNNTs, respectively, were determined for polyvinyl alcohol (PVA) composites [20]. A theoretical model was applied for estimating the variation of thermal conductivity as a function of BNNT loading and plotted in a graph. From that plot, the present author roughly estimated the percolation threshold of the composites, at the concentration where there was an abrupt change in that property. Although we did not reach the percolation threshold in this work, we observed a significant increment in thermal conductivity at loadings of 5 wt% (3.2 vol%) and 10 wt% (6.6 vol%). Further increases in BNNT loading and orientation of the nanotubes led to higher thermal conductivity in the rubber matrix. However, the strain-dependent viscoelastic properties (G' and G'') were diminished based on the trends observed in Figure 6.4.

The alignment of BN nanomaterial in a polymer matrix plays an important role in thermal conductivity measurements. This alignment can be reached by applying magnetic or electric fields [20], shear forces [176], tape casting [177], and hot pressing techniques [64]. Terao et al. [20] prepared PVA/BNNT composites through solvent casting and electrospinning techniques. Low loadings of aligned nanotubes were needed to reach high thermal conductivities. Xie et al. [177]

fabricated PVA/h-BN nanocomposites using the solvent casting approach. In their work, oriented h-BN microplatelets led to higher values in thermal conductivities, in comparison with randomly oriented BN. The tape casting method was responsible for the oriented platelets. Sun et al. [64] prepared polycarbonate/BN composites via hot pressing; a thermal conductivity of 3.09 W/(m·K) along the aligned direction was obtained for the composite at 18.5 vol%. Hu et al. [168] also applied the hot pressing technique for orientation of BN in epoxy resin. Their highest thermal conductivity (6.09 W/(m·K)) was obtained for oriented BN at a loading of 50%.

In this work, we did not intentionally align the nanotubes in the SBR. However, it has been reported that the solvent casting technique favors a partial alignment of the nanotubes in the polymeric matrix [177]. The hot pressing technique also has favored the alignment of the BN plates [64], [168], [21]. Thus, there might be a partial alignment in the nanotubes in our films. However, due to the moderate thermal conductivity values obtained, we believe that randomly oriented nanotubes were predominant in our composites.

Boron nitride nanomaterials have been incorporated into elastomers in order to fabricate thermally conductive composites. Cho et al. [170] fabricated poly(dimethylsiloxane) elastomer PDMS/BNNS composites. An increase of 23.5% in thermal conductivity was obtained at a BN loading of 15 vol%. Wu et al. [70] introduced BN or BNNS in SBR using the slurry approach on a conventional two-roll mill. Improvements of 82% and 119% were obtained for SBR/BN and SBR/BNNS, respectively, at a loading of 10.5 vol%. In a subsequent work, Wu et al. [42] coated BNNS with polyrhodanine to improve the compatibility with SBR. Composites with oriented nanosheets showed an improvement of up to 464% with respect to the neat matrix and a 187% improvement when randomly nanosheets were used. In both cases, the loading of BN nanostructures was 27.5 vol%.

Carbon-based nanofillers have also been used to reinforce SBR matrices. Das et al. [14] prepared SBR-BR/MWCNTs composites using a two-roll mill. A pre-dispersion of the nanotubes in ethanol was performed. An approximately 30% increase in thermal conductivity was obtained, when four parts per hundred of rubber (phr) of CNTs were used. Song et al. [5] fabricated SBR/reduced graphene oxide (RGO) composites. An improvement of 26.1% was obtained at a loading of 3 wt% of RGO. Further improvements were obtained when using functionalized CNTs (f-CNTs) and hybrid-RGO/f-CNTs as fillers. A modest increase in thermal conductivity for polymer/CNTs

composites has been reported with increasing CNTs loading [178], [179], [180]. These modest values are attributed to the interfacial resistance between the polymer and CNTs [181]. However, it is often considered that there is not a true percolation threshold for these nanotubes, but this interpretation may vary, depending on the level of improvement. For example, Kwon et al. [182] determined a percolation threshold of 1.4 vol% for CNTs in PDMS/CNTs composites when a 390% increase in thermal conductivity was obtained. On the other hand, Kapadia et al. [181] did not report a percolation threshold even at higher CNTs loadings (10 vol%).

The thermal conductivity values obtained in this work are comparable to the ones reported in the literature when using SBR/carbon-based nanomaterials. Based on the Hansen solubility theory, we were able to make the non-polar SBR matrix compatible with the mildly polar behavior of BNNTs. We validated the Hansen solubility theory. The simple solvent casting approach developed in this work paves the route for the fabrication of rubber composites with improved thermal and mechanical properties, while retaining electrical insulation (contrary to carbon nanotube systems).

6.4 Conclusions

SBR-BNNTs nanocomposites were fabricated by the solvent casting technique. Although both materials possess different surface energies, we proposed an intermediate media to mix them. A binary mixture of toluene/ethyl acetate in a 20:80 volume ratio was proposed as dispersion media, based on the Hansen solubility theory. This system allowed full dissolution of the polymer and good dispersion of the nanotubes. The nanocomposites at 10 wt% BNNT loading showed an increase in thermal conductivity of up to 35%, while the composites containing 5 wt% of BNNTs showed an increase of 29% in thermal conductivity. All the composites showed viscoelastic properties with an increase in loading of BNNTs in the frequency dependence curves. This work paves the way for subsequent incorporation of BNNTs into SBR, to eventually be followed by the vulcanization process.

Supplementary Materials: The following supporting information can be downloaded at: https://www.mdpi.com/article/10.3390/jcs6090272/s1, Figure D.1: Dissolution of SBR in organic solvents after 24 h: (**a**) cyclohexane, methanol, toluene, acetone, methyl ethyl ketone, ethylene glycol, dimethyl sulfoxide, formamide, ethyl acetate, and ethanol; and (**b**) propylene carbonate,

ethyl benzene, benzyl alcohol, dimethyl formamide, chloroform, tetrahydrofuran, ethyl benzoate, 2-Propanol, 1,4-Dioxane, and d-Limonene. Solvents were shown from left to right.

Author Contributions: "Conceptualization, C.S.T.C. and J.R.T.; methodology, C.S.T.C.; software, C.S.T.C.; validation, C.S.T.C. and J.R.T.; formal analysis, C.S.T.C.; investigation, C.S.T.C.; resources, J.R.T.; data curation, C.S.T.C. and J.R.T.; writing—original draft preparation, C.S.T.C.; writing—review and editing, J.R.T.; supervision, J.R.T.; project administration, J.R.T.; funding acquisition, J.R.T. All authors have read and agreed to the published version of the manuscript.

Funding: Research was funded by the Natural Sciences and Engineering Research Council of Canada (NSERC) (CRDPJ 499340 – 2016); and Prima Quebec (R12-13-006). C.S.T.C. would like to acknowledge the Mexican National Council for Science and Technology (CONACyT) for the scholarship provided (number: 739894).

Institutional Review Board Statement: Not applicable.

Informed Consent Statement: Not applicable.

Data Availability Statement: The data presented in this study are available in the Supplementary Information file, as well as on request from the corresponding author.

Acknowledgments: Thanks are given to Mr. Matthieu Gauthier for his assistance in the preparation of the samples for TEM. Special thanks go to Dr. Jeremy Mehlem for his guidance in the analysis of rheological data and to Mr. Gabriel Dion for his support in thermal conductivity measurements.

Conflicts of Interest: The authors declare no conflicts of interest.

CHAPTER 7 GENERAL DISCUSSION

Based on the literature review, we realized that surface modification techniques are necessary to tailor the surface properties of BNNTs for their incorporation into polymers. Covalent and non-covalent approaches are employed for this purpose, which can be performed in the liquid or gas phase. Understanding the surface properties of pristine BNNTs is crucial to establish the pathway to follow subsequent functionalization steps.

In this thesis, we aimed to study the dispersibility of pristine and functionalized BNNTs to gain knowledge about their surface properties, as well as their incorporation into a non-polar polymeric matrix.

The first objective of this work was to investigate the dispersibility of BNNT into organic solvents (article 1, chapter 4). Having defined that, two different approaches (one in the gas phase and one in the liquid phase) were chosen for their functionalization and/or modification. The second objective focused on the covalent functionalization of BNNTs though syngas PICVD (article 2, chapter 5). This gas-phase technique allowed us to deposit oxygen functionalities on the BNNTs. The third objective was centered on the incorporation of BNNTs into a non-polar polymer using a liquid-phase approach (article 3, chapter 6).

7.1 Studying dispersibility of BNNT in organic solvents

The first research objective focused on characterizing the surface properties of pristine boron nitride nanotubes in organic media. Dispersions in different organic solvents were prepared. Density and purity of the nanotubes as well as viscosity and density of the solvents play an important role in the calculation of sedimentation times. Mutz et al. [183] estimated the Hildebrand solubility parameter (δ_t) based on the Hildebrand−Scatchard Solution Theory. A list of potential solvents was proposed. However, they only considered the Hildebrand parameter, which only comprises dispersive interactions. For particles with polar components, the three HSP (δ_d, δ_p, δ_h) should be considered. Tiano et al. [44] determined the HSP of as-synthesized BNNTs containing impurities such as amorphous boron. The difference in density between the nanotubes and the impurities affects the sedimentation time, where heavier particles will sediment first. In addition,

different particles will have different chemical composition, which will alter the interaction with the solvents. Having said that, a reliable characterization was needed.

In our first publication, we determined the Hansen solubility parameters (HSP) of purified high-quality (few-walls) BNNTs [25]. The calculated HSP were $\{\delta_d; \delta_p; \delta_h\} = \{16.8; 10.7; 14.7\} \pm \{0.3; 0.9; 0.3\}$ $MPa^{1/2}$, with a Hildebrand parameter (δ_t) equal to 24.7 $MPa^{1/2}$. These HSP values suggest a mild polar surface, which agrees with the chemical nature of B-N bonds present in the BNNTs. By comparing these values with the literature, some discrepancies are found. Water contact angle measurement on BNNTs films suggest the presence of a non-polar surface, as explained in detailed chapter 2. The morphology of the BNNT films such as roughness, voids, and alignment of the tubes play a significant role in contact angle measurements, as well as the relative humidity of the room.

Another property that may affect the interactions between BNNT and solvents is the dielectric constant. BNNTs are considered electrical insulators with a dielectric constant of 5.9. In addition, they posses a bandgap of ~ 5.5 eV, which is characteristic of non-conductive materials. Based on those data, nothing led us to think that the dielectric constants would influence the interactions between solvents and the BNNTs. In fact, while doing the experiments, we did not observe a special phenomenon happening in the dispersions. However, it is worth noting that for charged particles, the effect of the dielectric constant of the solvent should be studied. For example, Bruel et al. [117] prepared organic dispersions using negatively charged cellulose nanocrystals. They observed that the electrostatic stabilization occurred in solvents having high dielectric constants.

7.2 Covalent functionalization of BNNTs

The second objective of this research focused on the covalent functionalization of BNNTs. Syngas PICVD was selected as the functionalization approach. The operational parameters were set in order to obtained non-polar surfaces, based on previous works [80], [82]. However, we observed that hydrophilic surfaces were obtained. During the development of the experiments, we identified several variables that prevent the system from operating as predicted and reach the desired

functionality: 1) operational parameters, 2) effect of $Fe(CO)_5$, 3) UVC light and its irradiance, and 4) geometry of the reactor.

1) Operational parameters

Due to a limited amount of BNNTs, we started our PICVD experiments using silicon wafers as substrates. Once we obtained the desired properties, we would transfer these conditions to the BNNTs. According to previous works [80], [82], [100] operational parameters such as gas ratio, flow rate, treatment time, pressure and position of the sample would determine the chemistry of treated samples. Hydrophilic surfaces are expected to be formed under slight vacuum (-15 kPa), using hydrogen peroxide and at a position near the inlet of the reactor. On the other hand, hydrophobic surfaces are expected to be obtained under slight pressure (15 kPa) and close the outlet of the reactor [80], [82]. We varied those parameters to see their influence on the wettability of silicon wafers. Water contact angle (CA) results for the treated samples are shown in Table 7.1. The measured CA were in the range of 60-78°, corresponding to hydrophilic surfaces. Based on these results, we observed that neither the flow rate, gas ratio (H_2/CO), treatment time or position of the sample had a significant influence in the CA values. An additional experiment was performed adding H_2O_2 as photo initiator (experiment #13 in Table 7.1), to see its effect on the treatment. This time, we positioned the sample near the inlet of the reactor (14 cm) and applied slight vacuum (-15 kPa). We observed a decreased by approximately half on the CA (~ 28°), making the surface more hydrophilic. This result agrees with the theory; the use of H_2O_2 would favour the formation of oxygenated radicals and thus, hydrophilic coatings [82].

Table 7.1 Effect of PICVD parameters on wettability of silicon wafers.

Exp #	Flow H_2 (ml/min)	Flow CO (ml/min)	H_2O_2 (1ml/h)	Pressure (kPa)	Position (cm)	Treatment time (min)	Parameter studied	Water CA (˚)
0	-	-	-	-	-	-	-	40.8
1	200	200	No	0	0	120	Reference	69.9

2	300	300	No	0	0	120	Flow rate	66.8
3	100	300	No	0	0	120	Gas ratio	70.4
4	300	100	No	0	0	120	Gas ratio	67.9
5	200	200	No	0	0	150	Treat time	-
6	200	200	No	0	0	180	Treat time	76.7
7	200	200	No	0	0	210	Treat time	70.0
8	200	200	No	0	0	240	Treat time	78.2
9	200	200	No	15	75	120	Position	71.8
10	~ 65	340	No	15	75	120	Gas ratio	60.8
11	340	~ 65	No	15	75	120	Gas ratio	65.1
12	110	240	No	15	82	120	Flow rate	68.3
13	110	240	Yes	-15	14	180	Flow rate	28.2

*Conditions: 2 spots were analyzed per sample, 1 sample per experiment.

2) Effect of $Fe(CO)_5$

Syngas PICVD was developed to tailor the surface of materials with different degrees of wettability, going from super hydrophobic to super hydrophilic surfaces. The use of a binary mixture ($CO + H_2$) and a photo-initiator (H_2O_2) would allow that. However, it was not considered

that a contaminant with a strong photocatalytic activity would alter the course of the reactions. This contaminant, iron pentacarbonyl, $Fe(CO)_5$, is generated over time in pressurized CO cylinders [161]. Based on that, we decided to study the effect of $Fe(CO)_5$ concentration in our system. For this, we used two different CO cylinders: an old one (4.8 years old) and a new one (1 month old). The operational parameters were set towards hydrophobic surfaces (slight pressure and position of the sample close to the end of the reactor). Two BNNTs samples were treated under the same conditions (pressure = 15 kPa and position = 75 cm). The only difference was the CO cylinder used. Table 7.2 shows the water CA obtained for the treated samples. When using the old CO cylinder (experiment #1), we obtained a CA of 126.7° ± 5.8°. On the other hand, when using the new cylinder (experiment #2), we obtained a more hydrophilic sample, with a decrease in the CA (78.6° ± 4.6°). Based on previous PICVD studies, we expected the opposite; a more hydrophilic sample when using the old tank, due to more concentration of $Fe(CO)_5$, and thus, more oxygenated radicals formed during the reaction. What can explain these results is the opaqueness of the quartz tube. These experiments were performed consecutively, without changing the tube, which gets yellow with time.

We performed a third reaction (experiment #3 in Table 7.2) on BNNTs films using the old cylinder and a clean quartz tube. We observed that the water CA (71.8 °) was closed the one obtained with the new cylinder (78.6 °). This result led us to consider that the use of a clean tube in each reaction is predominant over the age of the CO cylinder.

Table 7.2 Influence of CO cylinder age on PICVD treatments

Exp #	Substrate	CO tank	Flow H_2 (ml/min)	Flow CO (ml/min)	Pressure (kPa)	Position (cm)	Treat. Time (min)	Water CA (˚)
0	BNNT	-	-	-	-	-	-	83.1 ± 1.0

1	BNNT	Old	200	200	15	75	120	126.7 ± 5.8*
2	BNNT	New	200	200	15	75	120	78.6 ± 4.6 *
3	BNNT	Old	200	200	15	75	120	71.8

*2 spots same sample, 6 measurements in total

3) UVC light and its irradiance

We studied the influence of UVC light on PICVD reactions by measuring the irradiance at different heights and positions. Figure 7.1 shows a schematic of the reactor and the positions at which the measurements were done. Different irradiance values were obtained depending on the position (p) in the reactor (inlet, middle, or outlet) and on the height (h).

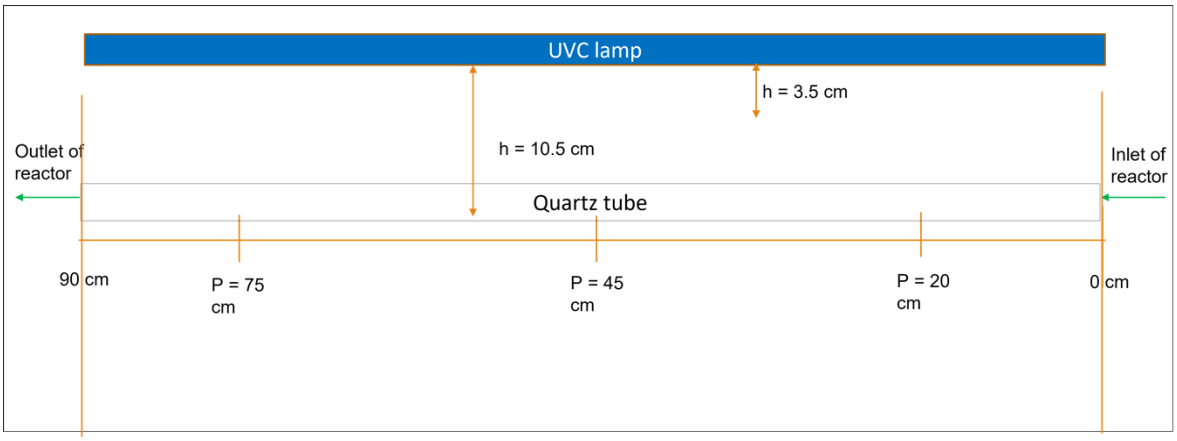

Figure 7.1 PICVD reaction system indicating position of the sample.

3.1 Irradiance at h=10.5 cm and at different positions inside the reactor

Our first experiments were conducted at a height (h) of 10.5 cm, which corresponds to the distance between the quartz tube (where the reactions take place) and the UVC light. Three positions inside the reactor were selected: 20 cm, 45 cm, and 75 cm away from the inlet. The measurements were

taken every minute, for a period of 5 min. We observed that the highest value was obtained when the sample was located at the center of the reactor (45 cm from the inlet), having an average value of 0.006 W/cm^2. Based on these results, we proceeded to measure the irradiance at a position of 45 cm for longer times, to see when it is stabilized.

3.2 Irradiance over time at a position of 45 cm and h = 10.5 cm

Figure 7.2 shows the irradiance of the UVC lamp over time at a position 45 cm without the use of syngas. After approximately 100 min of having been turned on the light, it stabilizes and reaches a plateau.

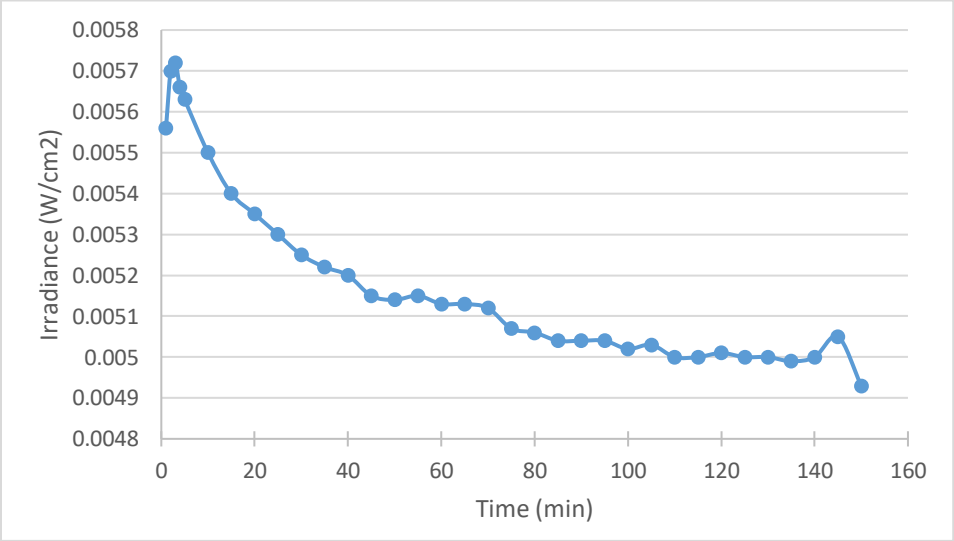

Figure 7.2 Irradiance of the UVC lamp at p = 45 cm and h = 10.5 cm.

3.3 Irradiance over time at a position of 45 cm and h = 3.5 cm

We also measured the irradiance at a height of 3.5 cm (Figure 7.3). We observed that the values were higher (0.01 W/cm^2) in comparison with the ones at h = 10.5 cm. This indicated that not only the position inside the reactor but also the distance with respect the lamp influences the light delivered to the PICVD system.

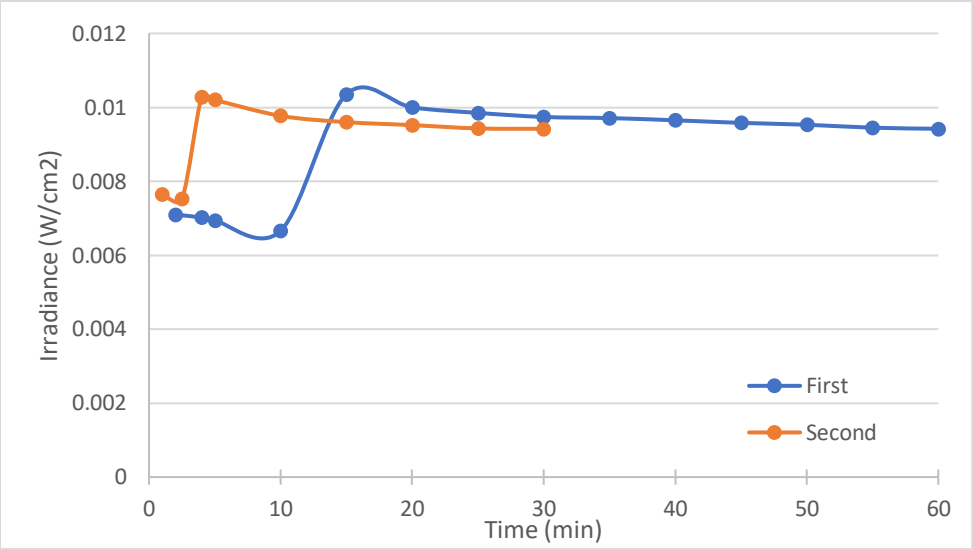

Figure 7.3 Irradiance of the UVC lamp at p = 45 cm and h = 3.5 cm.

Based on results presented in this section, the irradiance is higher at the center of the reactor (position = 45 cm), in contrast with the irradiance measured near the inlet/outlet.

4) Geometry of the reactor

The current settings of the PICVD system comprises a quartz tube of 90 cm long and 2.5 cm of diameter. However, there is no apparent need of using such a long reactor. For future work on PICVD, we propose the use of a 30 cm long reactor. Based on our findings, the position of the sample does not play a significant role in the treatment. Instead, what might have a more significant impact is the amount of light that the substrate is receiving. With the current settings, the irradiance is the highest at the center (at 45 cm from inlet). We propose to use three UVC lamps around the reactor, to maximize the surface exposed to the treatment. The proposed locations are on top and on the sides of the reactor, as can be appreciated in Figure 7.4a. The location of the samples should be at the middle of the reactor. This arrangement would allow to have the same irradiance along the sample. The second proposed configuration consist in locating the UVC lamp at the entrance of the reactor (Figure 7.4b). With this arrangement, we could vary the position of the sample and have different functionalities because the light delivered to the system would be different at the inlet and at the outlet of the reactor.

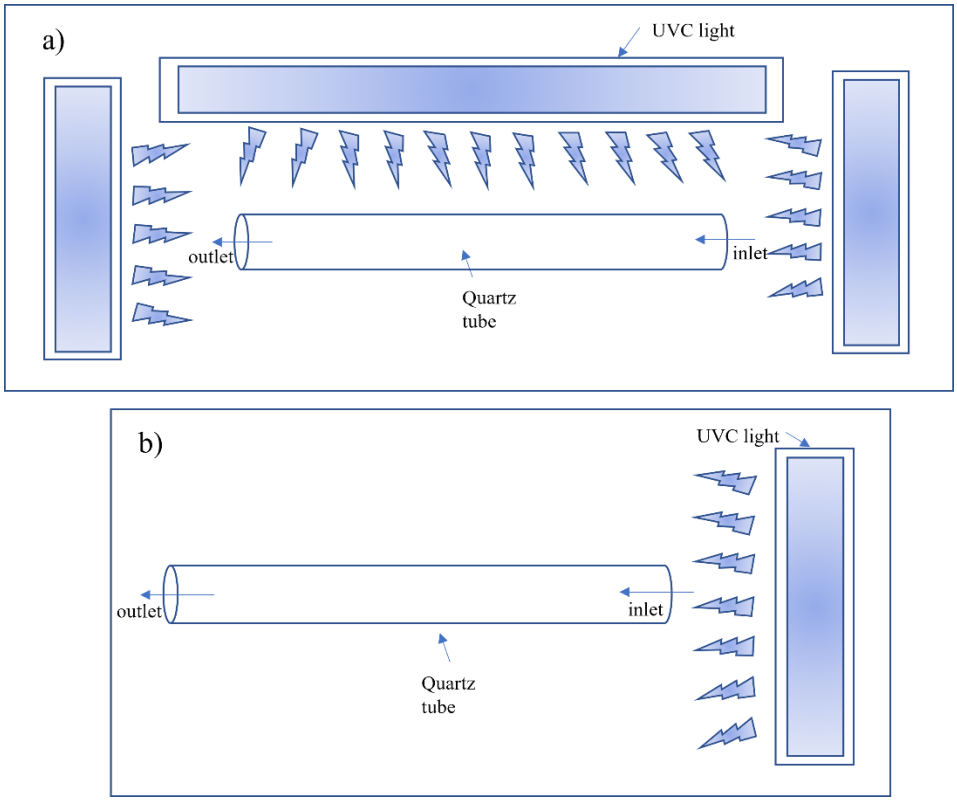

Figure 7.4 Proposed reaction configurations to optimize the light delivered to the PICVD system, a) three UVC lamps around the quartz tube, and b) one lamp at the entrance.

Despite the limitations of the PICVD system, we were able to obtain reproducible results towards hydrophilic BNNT. In the second part of our work [184], we functionalized the nanotubes with oxygen-containing groups using syngas PICVD. The level of oxidation was comparable or even higher that the one obtained in plasma processes. The contact angle for pristine BNNTs film was ~88 °. After the treatment, the water CA decreased to ~16.8 °. X-ray photoelectron spectroscopy was used to elucidate the chemical composition of untreated and treatment materials.

The functionalized BNNTs turned out to be more hydrophilic than the pristine ones, thus they could not be used for dispersion into elastomers. However, they could be incorporated into polar polymers such as polyvinyl alcohol (PVA). Other approaches were considered for surface treatment of BNNTs towards hydrophobic surfaces. We attempted the use of an amine-terminated poly(butadiene-co-acrylonitrile) (ATBN) oligomer as a compatibilizer between BNNTs and SBR.

Vacuum filtration was the selected methodology. However, due to the chemical aggressivity of this compound in damaging the filtered glass of the funnel, this approach was suspended.

7.3 Improving dispersion of BNNT into SBR

We looked back at the solubility theory and analyzed the Hansen space for the BNNTs. To determine which route to follow, we proceeded in determining the HSP of SBR as well. Once we had the two solubility spaces, we could map a route for improve their compatibilization. To determine the HSP of SBR, a certain amount of polymer was added to a fixed amount of solvent and it was left to dissolve at room temperature for 24h. This is summarized in our third paper [185]. The HSP of SBR were: $\{\delta_d; \delta_p; \delta_h\} = \{17.4; 2.5; 4.4\} \pm \{0.4; 0.8; 0.6\}$ $MPa^{1/2}$, with a $\delta t = 18.1$, and a radius $R_a = 5.0$ $MPa^{1/2}$. Having determined these values, we plotted together the Hansen spaces of SBR and BNNT, with parameters $\{\delta_d; \delta_p; \delta_h\} = \{16.8; 10.7; 14.7\} \pm \{0.3; 0.9; 0.3\}$ $MPa^{1/2}$. Figure 6.2 shows both solubility spaces.

In our previous study about the dispersibility of BNNTs [25], we identified that ethyl acetate was a good solvent to form short-time stable dispersions. On the other hand, toluene is a very good solvent for dissolving the SBR. Considering these two solvents, we explored the boundaries of the solubility theory and by calculating the *RED* numbers, we determined that a mixture of toluene/ethyl acetate at a ratio of 20:80 by volume was able to fully dissolve the polymer and form a good dispersion of the BNNTs. Then, we incorporated for the first time BNNTs into SBR through solvent casting approach without the need of a chemical or physical treatment. SBR/BNNTs composites were obtained at three different BNNT loadings. Thermal conductivity was improved 29 % and 35% for the composites at 5wt% and 10 wt%, respectively. These results are comparable to the ones obtained in SBR/carbon-based nanomaterials. The facile fabrication method used in this work opens new possibilities for large scale of SBR/BNNTs composites. A potential application would be in the tire industry, making a tire with a better heat dissipation. The storage modulus was improved by 235% for the SBR/BNNT at 10wt%. An improvement in this property would lead to a decrease in rolling resistance, and thus, a decrease in fuel consumption. In addition, the improvement in thermal conductivity would lead to higher heat dissipation, extending the lifetime of the tire. Having said that, two corners of the “magic triangle” would be improved: the

rolling resistance and the tire wear. However, with an increment in thermal conductivity there is a formation of a filler-filler network, which may diminish the viscoelastic properties. Further dynamic characterization should be performed as a function of temperature in order to evaluate the properties as in the application on tires. Crosslinked samples are recommended for this purpose. Assessment of dynamic properties as a function of temperature would be needed for a dynamic evaluation of the material.

In this research work, we used BNNTs as reinforcement in styrene-butadiene rubber in order to improve mainly the thermal conductivity. We also improve the storage modulus (G') of the composites, as observed in the figure 6.5a. However, the use of these nanotubes may have a negative effect on the loss modulus (G''), with an increase in this value in frequency-dependent curves (figure 6.5b). On the other hand, the ratio of G'' to G' (figure 6.5c) indicates that tan $\delta < 1$ in the whole frequency range when increasing the BNNT loading, meaning that the storage modulus is higher than the loss modulus. All the composites show a similar trend.

7.4 Experimental considerations

In our first publication "Chemical affinity and dispersibility of boron nitride nanotubes, we prepared BNNTs dispersions in different organic solvents to determine the chemical affinity between them. The concentration was expressed in mg of BNNTs per ml of solvent. The concentration was not specified in other terms because of the very low mass used, in the scale of milligrams. The calculation of the number of moles of BNNTs would lead to an error in their molar fraction, due to the uncertainty of their molecular weight. In addition, due to differences in densities of the solvents, variations in the concentration (for example, expressed in weight fraction) will appear. However, we could have expressed the concentration in volume fraction. Considering the density of BNNT = 1.5 g/cm^3 and a mass of 0.001 g, the corresponding volume of BNNTs would be 0.00067 ml. Then, the concentration of BNNTs in volume fraction would be 0.000067 or 0.0067 vol%.

$$V_{BNNT} = \frac{m}{\rho} = \frac{0.001\ g}{1.5\ g/ml} = 0.00067\ ml$$

$$volume\ fraction = \frac{0.00067\ ml}{10.00067\ ml} = 0.000067$$

In our second publication “Covalent functionalization of boron nitride nanotubes through photo-initiated chemical vapour deposition” the relative humidity was reported in the contact angle measurements because variations in this parameter may affect the wettability properties [45]. The humidity measured is the one present in the room, and it was not controlled or intentionally set. In addition, due to the porosity and roughness presented by our samples, two methods were used to estimate the surface energy of the BNNTs films: static contact angle (sessile drop) and Advancing and Receding Contact angle (ARCA). The static contact angle is a reliable method for estimating the surface energy of flat solid surfaces (ideal surfaces). However, when using porous films, roughness plays a role, influencing the contact angle values. For the characterization of wettability of porous/rough surfaces, the ARCA method is preferred. In our work, we observed that both methods (sessile drop and ARCA) followed the same trend, a decrease in water contact angle after the treatment.

CHAPTER 8 CONCLUSIONS AND RECOMMENDATIONS

8.1 Summary and conclusions

This work covered three different stages for understanding the surface properties and chemistry of pristine and functionalized BNNTs. First, the surface properties (dispersibility) of pristine nanotubes were characterized through sedimentation tests. The determination of solubility parameters was achieved by taking into account the purity and density of the nanotubes, as well as physical properties of the solvents. Although previous characterizations have been reported in the literature, the effect of the aforementioned variables were not considered, making the estimation of the solubility parameters unreliable.

The second part of this project consisted in the covalent modification of BNNTs through syngas PICVD. For the first time, these nanomaterials were modified employing a low-cost gas phase technique. Previous treatments in the gas phase have been performed using mainly plasma systems. However, the main drawback of plasma technology is its high energy consumption and requirement for specialized equipment. We proved that a higher degree of oxidation can be achieved through a low-cost technology, employing a waste stream (syngas) as reactants and operating at room temperature conditions.

The third part focused on the dispersion of BNNTs into styrene butadiene rubber. Even though these two materials possess different surface energies, we proposed the use of a binary mixture, based on the solubility parameters of both materials. By doing this, we were able to fully dissolve the elastomer while keeping good dispersion of the nanotubes. The fabrication of nanocomposites with improved thermal conductivity and viscoelastic properties was reached through solvent casting.

Our main objective in this research work was to introduce BNNTs into SBR, to improve mainly the thermal conductivity. This objective was successfully reached. For the incorporation of these

nanotubes into SBR, we proposed two approaches: a chemical treatment and an improved-dispersion approach. The first method, the chemical treatment, did not work as expected, due to limitations in the current settings of the PICVD reactor, namely, the presence of a photo-active contaminant. However, we paved the road for the modification of BNNTs towards hydrophilic surfaces. The second approach, the improved-dispersion technique, allowed us to properly disperse the BNNT into SBR by choosing a suitable dispersion medium for both components. Then, the solvent casting and hot-pressing techniques allowed us to fabricate the SBR/BNNTs nanocomposites. Dynamic properties such as storage and loss modulus, as well as tan δ curves were obtained from rheological measurements. The storage modulus was improved in all the composites in the whole frequency range. In addition, thermal conductivity measurements showed an improvement in the composites at 5 wt% and 10 wt% of BNNTs. These results make BNNT promising materials for their use in tires. However, as mentioned earlier, the evaluation of the tire performance is a complex process and depends on several properties, which usually are antagonistic. Subsequent work should be conducted to complete the dynamic and mechanical characterization of SBR/BNNTs composites.

8.2 Original contributions

This research work enabled the contribution to the scientific community in the following:

1) Hansen solubility parameters were determined for the first time for purified BNNTs taking into account the purity and density of the nanotubes, the physical properties of the solvents and relative sedimentation times.
2) We paved the road for subsequent modification steps for BNNTs. Having defined the solubility parameters of purified nanotubes, different directions may be taken for further modification of BNNTs, depending on the desired dispersion media.
3) Covalent functionalization of BNNTs with oxygenated functionalities was carried out using a low-cost technique (syngas PICVD) operating at room temperature under near atmospheric conditions. CO and H_2 were used as reactants, Ar as purging gas and a UVC lamp as a source light. This has never been done before on these nanomaterials. The operational cost was calculated as low as 0.058 CAD for a 1 h treatment.

4) The determination of HSP for styrene-butadiene rubber was performed. HSP characterization of polymers depends on the molecular weight, chemical composition, and number of repeating units. Determination of the solubility parameters for the elastomer used in this research work allowed us to have an accurate characterization. Having defined its HSP, binary mixtures can be prepared in order to make compatible this polymer with a filler of interest.
5) Based on HSP theory, a suitable binary mixture was proposed to incorporate the mildly polar BNNTs into the non-polar styrene-butadiene rubber. In comparison with studies reported in the literature, we were able to incorporate the nanotubes without any chemical or physical surface modification.
6) Incorporation of boron nitride nanotubes into SBR was performed for the first time.
7) Fabrication of SBR/BNNTs composites with improved thermal conductivity was done by a facile approach. Solvent casting was chosen as the processing method. The thermal conductivity of the composites is in the same range than the ones obtained with carbon-based nanoparticles. The viscoelastic properties were also improved in the SBR/BNNTs composites.

8.3 Recommendations

The following aspects are recommended for future work:

- Control and quantification of $Fe(CO)_5$ in the CO cylinder used in PICVD treatments. This will allow to apply a controlled amount of photo-initiator into the reactor and be considered as a reaction parameter.
- Optimize the geometry of the PICVD reactor. Two configurations of the reactor were proposed in chapter 7, maximizing the light delivered to the reaction system.
- The processing of SBR/BNNTs composites should be done in a two-roll mill or three-roll mill mixer. Shear forces could contribute to the orientation of the BNNTs, and thus, to an improvement in thermal conductivity.

- Sulfur or peroxide vulcanization should be performed on SBR/BNNTs nanocomposites to impart dimensional stability. This would also resemble in a better way the preparation of SBR composites in the tire industry.
- Dynamic Mechanical Analysis (DMA) should be conducted to characterize the dynamic properties of SBR/BNNT nanocomposites. Temperature sweeps from -100 °C to 80 °C are suggested to observe the variation in the storage and loss moduli, as well as the behavior of the tan δ curves.
- Mechanical testing should be performed in a universal testing machine in order to obtain the Young' modulus, the tensile strength and elongation at break of the composites.

REFERENCES

[1] B. Rodgers and W. Waddell, "The science of rubber compounding," in *The science and technology of rubber,* Houston, TX, USA, Elsevier Academic Press, 2005, pp. 420-421.

[2] "All About Sbr Rubber - Properties, Applications and Uses," Thomas Publishing Company, 20 09 2022. [Online]. Available: https://www.thomasnet.com/articles/plastics-rubber/all-about-sbr-rubber/. [Accessed 20 9 2022].

[3] G. Hou, W. Tao, J. Liu, X. Zhang, M. Dong and L. Zhang, "Effect of the structural characteristics of solution styrene–butadiene rubber on the properties of rubber composites," *J. APPL. POLYM. SCI.,* p. 45749, 2018.

[4] G. Mathew, M.-Y. Huh, J. M. Rhee, M.-H. Lee and C. Nah, "Improvement of properties of silica-filled styrene-butadiene rubber composites through plasma surface modification of silica," *Polym. Adv. Technol.,* vol. 15, p. 400–408, 2004.

[5] S. Song and Y. Zhang, "Carbon nanotube/reduced graphene oxide hybrid for simultaneously enhancing the thermal conductivity and mechanical properties of styrene -butadiene rubber," *Carbon,* vol. 123, pp. 158-167, 2017.

[6] Michelin, "https://www.michelinman.com/auto/auto-tips-and-advice/tires-101/how-are-tires-made," [Online].

[7] Michelin, "https://www.michelin.com/en/activities/tires/what-s-a-tire/," [Online].

[8] P. Weng, Z. Tang and B. Guo, "Solving “magic triangle” of tread rubber composites with phosphonium-modified petroleum resin," *Polymer,* vol. 190, p. 122244, 2020.

[9] V. Dall'Agnol Veiga, T. Marchesini Rossignol, J. Da Silva Crespo and L. Nardini Carli, "Tire tread compounds with reduced rolling resistance and improved wet grip," *J. APPL. POLYM. SCI.,* p. 45334, 2017.

[10] T. LaClair, "Chapter 12 Rolling Resistance," in *The Pneumatic Tire,* 2006, p. 476.

[11] S. S. Choi, "Effect of Bound Rubber on Characteristics of Highly Filled Styrene–Butadiene Rubber Compounds with Different Types of Carbon Black," *Journal of Applied Polymer Science,* vol. 93, pp. 1001-1006, 2004.

[12] S.-S. Choi, B.-H. Park and H. Song, "Influence of filler type and content on properties of styrene-butadiene rubber (SBR) compound reinforced with carbon black or silica," *Polym. Adv. Technol.,* vol. 15, p. 122–127, 2004.

[13] L. Zhang, Y. Wang, Y. Wang, Y. Sui and D. Yu, "Morphology and Mechanical Properties of Clay/Styrene-Butadiene Rubber Nanocomposites," *Journal of Applied Polymer Science,* vol. 78, pp. 1873-1878, 2000.

[14] A. Das, K. Stockelhuber, R. Jurk, M. Saphiannikova, J. Fritzsche, H. Lorenz, M. Kluppel and G. Heinrich, "Modified and unmodified multiwalled carbon nanotubes in high performance solution-styrene–butadiene and butadiene rubber blends," *Polymer,* vol. 49, p. 5276–5283, 2008.

[15] J. Wang, C. H. Lee and Y. K. Yap, "Recent advancements in boron nitride nanotubes," *Nanoscale,* vol. 2, pp. 2028-2034, 2010.

[16] X. Chen, L. Zhang, C. Park, C. Fay, X. Wang and C. Ke, "Mechanical strength of boron nitride nanotube-polymer interfaces," *Applied physics letters,* vol. 107, no. 253105, 2015.

[17] Y. Chen, J. Zou, S. Campbell and G. Caer, "Boron nitride nanotubes: Pronounced resistance to oxidation," *Appl. Phys. Lett.,* vol. 84, no. 13, pp. 2430-2432, 2004.

[18] C. Zhi, Y. Bando, C. Tang and D. Golberg, "Boron nitride nanotubes," *Materials Science and Engineering R,* vol. 70, pp. 92-111, 2010.

[19] M. Terrones, J. M. Romo-Herrera, E. Cruz-Silva, F. López-Urías, E. Muñoz-Sandoval, J. J. Velázquez-Salazar, H. Terrones, Y. Bando and D. Golberg, "Pure and doped boron nitride nanotubes," *Materials today,* vol. 10, no. 5, pp. 30-38, 2007.

[20] T. Terao, C. Zhi, Y. Bando, M. Mitome, C. Tang and D. Golberg, "Alignment of Boron Nitride Nanotubes in Polymeric Composite Films for Thermal Conductivity Improvement," *J. Phys. Chem. C,* vol. 114, pp. 4340-4344, 2010.

[21] C. Zhi, Y. Bando, T. Terao, C. Tang, H. Kuwahara and D. Golberg, "Towards Thermoconductive, Electrically Insulating Polymeric Composites with Boron Nitride Nanotubes as Fillers," *Adv. Funct. Mater.,* vol. 19, pp. 1857-1862, 2009.

[22] N. G. Chopra, R. J. Luyken, K. Cherrey, V. H. Crespi, M. L. Cohen, S. G. Louie and A. Zettl, "Boron Nitride Nanotubes," *Science,* vol. 269, pp. 966-967, 1995.

[23] C. Y. Zhi, Y. Bando, C. C. Tang, Q. Huang and D. Golberg, "Boron nitride nanotubes: functionalization and composites," *Journal of Materials Chemistry,* vol. 18, pp. 3900-3908, 2008.

[24] S. Kalay, Z. Yilmaz, O. Sen, M. Emanet, E. Kazanc and M. Çulha, "Synthesis of boron nitride nanotubes and their applications," *Beilstein J. Nanotechnol.,* vol. 6, pp. 84-102, 2015.

[25] C. S. Torres-Castillo, C. Bruel and J. R. Tavares, "Chemical affinity and dispersibility of boron nitride nanotubes," *Nanoscale Adv.,* vol. 2, pp. 2497-2506, 2020.

[26] V. Yamakov, C. Park, J. H. Kang, X. Chen, C. Ke and C. Fay, "Piezoelectric and elastic properties of multiwall boron-nitride nanotubes and their fibers: A molecular dynamics study," *Computational Materials Science,* vol. 135, pp. 29-42, 2017.

[27] C. Zhi, Y. Bando, C. Tang, R. Xie, T. Sekiguchi and D. Golberg, "Perfectly Dissolved Boron Nitride Nanotubes Due to Polymer Wrapping," *J. AM. CHEM. SOC.*, vol. 127, pp. 15996-15997, 2005.

[28] W. Meng, Y. Huang, Y. Fu, Z. Wang and C. Zhi, "Polymer composites of boron nitride nanotubes and nanosheets," *Journal of Materials Chemistry C*, vol. 2, pp. 10049-10061, 2014.

[29] J. S. Lauret, R. Arenal, F. Ducastelle and A. Loiseau, "Optical Transitions in Single-Wall Boron Nitride Nanotubes," *Phys. Rev. Lett.*, vol. 94, p. 037405, 2005.

[30] J. Su, Y. Xiao and M. Ren, "Enhanced thermal conductivity in epoxy nanocomposites with hybrid boron nitride nanotubes and nanosheets," *Phys. Status Solidi A*, vol. 12, p. 2699–2705, 2013.

[31] B. E. Belkerk, A. Achour, D. Zhang, S. Sahli, M. A. Djouadi and Y. K. Yap, "Thermal conductivity of vertically aligned boron nitride nanotubes," *Appl. Phys. Express*, vol. 9, no. 075002, 2016.

[32] M. B. Jakubinek, J. F. Niven, M. B. Johnson, B. Ashrafi, K. S. Kim, B. Simard and M. A. White, "Thermal conductivity of bulk boron nitride nanotube sheets and their epoxy-impregnated composites," *Phys. Status Solidi A*, 2016.

[33] K. S. Kim, C. T. Kingston, A. Hrdina, M. B. Jakubinek, J. Guan, M. Plunkett and B. Simard, "Hydrogen-Catalyzed, Pilot-Scale Production of Small-Diameter Boron Nitride Nanotubes and Their Macroscopic Assemblies," *ACS NANO*, vol. 8, no. 6, pp. 6211-6220, 2014.

[34] X. J. Dai, Y. Chen, Z. Chen, P. R. Lamb, L. H. Li, J. Du Plessis, D. G. McCulloch and X. Wang, "Controlled surface modification of boron nitride nanotubes," *Nanotechnology*, vol. 22, p. 245301 (7pp), 2011.

[35] C. Zhi, Y. Bando, C. Tang and D. Golberg, "Boron nitride nanotubes," *Materials Science and Engineering R,* vol. 70, pp. 92-111, 2010.

[36] L. W. Yin, Y. Bando, D. Golberg, A. Gloter, M. S. Li, X. Yuan and T. Sekiguchi, "Porous BCN Nanotubular Fibers: Growth and Spatially Resolved Cathodoluminescence," *J. Am. Chem. Soc.*, vol. 127, pp. 16354-16355, 2005.

[37] L. Li, L. H. Li, S. Ramakrishnan, X. J. Dai, K. Nicholas, Y. Chen, Z. Chen and X. Liu, "Controlling Wettability of Boron Nitride Nanotube Films and Improved Cell Proliferation," *The Journal of physical chemistry C,* vol. 116, pp. 18334-18339, 2012.

[38] L. B. Boinovich, A. M. Emelyanenko, A. S. Pashinin, C. H. Lee, J. Drelich and Y. K. Yap, "Origins of Thermodynamically Stable Superhydrophobicity of Boron Nitride Nanotubes Coatings," *American Chemical Society,* vol. 28, pp. 1206-1216, 2011.

[39] A. D. Aliev, L. B. Boinovich, V. L. Bukhovets, A. M. Emelyanenko, A. M. Gorbunov, A. E. Gorodetskii and A. S. Pashinin, "Superhydrophobic Coatings Based on Boron Nitride Nanotubes: The Mechanism of Superhydrophobicity and Self Regeneration of Highly Hydrophobic Properties," *Nanotechnologies in Russia,* vol. 6, pp. 723-732, 2011.

[40] A. Pakdel, Y. Bando and D. Golberg, "Plasma-Assisted Interface Engineering of Boron Nitride Nanostructure Films," *ACS NANO,* vol. 8, no. 10, p. 10631–10639, 2014.

[41] K. Yum and M. F. Yu, "Measurement of Wetting Properties of Individual Boron Nitride Nanotubes with the Wilhelmy Method Using a Nanotube-Based Force Sensor," *Nano Letters,* vol. 6, no. 2, pp. 329-333, 2006.

[42] X. Wu, Z. Yang, W. Kuang, Z. Tang and B. Guo, "Coating polyrhodanine onto boron nitride nanosheets for thermally conductive elastomer composites," *Composites: Part A,* vol. 94, pp. 77-85, 2017.

[43] M. Mutz, E. Eastwood and M. D. Dadmun, "Quantifying the Solubility of Boron Nitride Nanotubes and Sheets with Static Light Scattering and Refractometry," *J. Phys. Chem. C,* vol. 117, p. 13230−13238, 2013.

[44] A. L. Tiano, L. Gibbons, M. Tsui, S. I. Applin, R. Silva, C. Park and C. C. Fay, "Thermodynamic approach to boron nitride nanotube solubility and dispersion," *Nanoscale,* vol. 8, pp. 4348-4359, 2016.

[45] L. Hołysz, M. Mirosław, K. Terpiłowski and A. Szczes, "Influence of relative humidity on the wettability of silicon wafer surfaces," *Ann UMCS,* vol. 63, no. 18, pp. 224-239, 2008.

[46] W. Han, Y. Bando, K. Kurashima and T. Sato, "Synthesis of boron nitride nanotubes from carbon nanotubes by a substitution reaction," *APPLIED PHYSICS LETTERS,* vol. 73, no. 21, pp. 3085-3087, 1998.

[47] D. P. Yu, X. S. Sun, C. S. Lee, I. Bello, S. T. Lee, H. D. Gu and K. M. Leung, "Synthesis of boron nitride nanotubes by means of excimer laser ablation at high temperature," *APPLIED PHYSICS LETTERS,* vol. 72, no. 16, pp. 1966-1968, 1998.

[48] Y. Chen, J. F. Gerald, J. S. Williams and S. Bulcock, "Synthesis of boron nitride nanotubes at low temperatures using reactive ball milling," *Chemical Physics Letters,* vol. 299, pp. 260-264, 1999.

[49] X. Chen, X. Gao, H. Zhang, Z. Zhou, W. Hu, G. Pan, H. Zhu, T. Yan and D. Song, "Preparation and Electrochemical Hydrogen Storage of Boron Nitride Nanotubes," *J. Phys. Chem. B,* vol. 109, pp. 11525-11529, 2005.

[50] C. H. Lee, J. Wang, V. K. Kayatsha, J. Y. Huang and Y. K. Yap, "Effective growth of boron nitride nanotubes by thermal chemical vapor deposition," *Nanotechnology,* vol. 19, p. 455605, 2008.

[51] C. H. Lee, M. Xie, V. Kayastha, J. Wang and Y. K. Yap, "Patterned Growth of Boron Nitride Nanotubes by Catalytic Chemical Vapor Deposition," *Chem. Mater.,* vol. 22, p. 1782–1787, 2010.

[52] C. Tang, Y. Bando, T. Sato and K. Kurashima, "A novel precursor for synthesis of pure boron nitride nanotubes," *The Royal Society of Chemistry,* pp. 1290-1291, 2002.

[53] J. Wang, V. K. Kayastha, Y. K. Yap, Z. Fan, J. G. Lu, Z. Pan, I. N. Ivanov, A. A. Puretzky and D. B. Geohegan, "Low Temperature Growth of Boron Nitride Nanotubes on Substrates," *Nano Lett.*, vol. 5, no. 12, pp. 2528-2532, 2005.

[54] M. W. Smith, K. C. Jordan, C. Park, J. W. Kim, P. T. Lillehei, R. Crooks and J. S. Harrison, "Very long single- and few-walled boron nitride nanotubes via the pressurized vapor/condenser method," *Nanotechnology,* vol. 20, p. 505604, 2009.

[55] L. Wang, D. Han, J. Luo, T. Li, Z. Lin and Y. Yao, "Highly Efficient Growth of Boron Nitride Nanotubes and the Thermal Conductivity of Their Polymer Composites," *J. Phys. Chem. C,* vol. 122, pp. 1867-1873, 2018.

[56] H. Cho, S. Walker, M. Plunkett, D. Ruth, R. Iannitto, I. Martinez-Rubi, K. S. Kim, C. M. Homenick, A. Brinkmann, M. Couillard, S. Dénommée, J. Guan, M. B. Jakubinek, Z. J. Jakubek, C. T. Kingston and B. Simard, "Scalable Gas-Phase Purification of Boron Nitride Nanotubes by Selective Chlorine Etching," *Chem. Mater.*, vol. 32, no. 9, p. 3911–3921, 2020.

[57] S. J. Zhou, C. Y. Ma, Y. Y. Meng, H. F. Su, Z. Zhu, S. L. Deng and S. Y. Xie, "Activation of boron nitride nanotubes and their polymer composites for improving mechanical performance," *Nanotechnology,* vol. 23, p. 055708, 2012.

[58] C. Y. Zhi, Y. Bando, T. Terao, C. C. Tang, H. Kuwahara and D. Golberg, "Chemically Activated Boron Nitride Nanotubes," *Chem. Asian J.*, vol. 4, pp. 1536-1540, 2009.

[59] V. K. Thakur, J. Yan, M. F. Lin, C. Zhi, D. Golberg, Y. Bando, R. Sim and P. S. Lee, "Novel polymer nanocomposites from bioinspired green aqueous functionalization of BNNTs," *Polym. Chem.,* vol. 3, pp. 962-969, 2012.

[60] Y. Jia, T. D. Ajayi, J. Morales, M. A. R. Chowdhury, G. Sauti, S. H. Chu, C. Park and C. Xu, "Thermal properties of polymer-derived ceramic reinforced with boron nitride nanotubes," *J Am Ceram Soc.*, vol. 102, p. 7584–7593, 2019.

[61] T. Terao, Y. Bando, M. Mitome, K. Kurashima, C. Y. Zhi, C. C. Tang and D. Golberg, "Effective synthesis of surface-modified boron nitride nanotubes and related nanostructures and their hydrogen uptake," *Physica E,* vol. 40, pp. 2551-2555, 2007.

[62] X. Huang, C. Zhi, P. Jiang, D. Golberg, Y. Bando and T. Tanaka, "Polyhedral Oligosilsesquioxane-Modified Boron Nitride Nanotube Based Epoxy Nanocomposites: An Ideal Dielectric Material with High Thermal Conductivity," *Adv. Funct. Mater.,* vol. 23, p. 1824–1831, 2013.

[63] S. Zhang, W. Chen, Y. Zhao, K. Yang, B. Du, L. Ding, W. Ynag and S. Wu, "Surface NH2-functionalized by C doping of boron nitride nanotube to improve the thermal conductivity of epoxy composites," *Composites Part B,* vol. 223, p. 109106, 2021.

[64] N. Sun, J. Sun, X. Zeng, P. Chen, J. Qian, R. Xia and R. Sun, "Hot-pressing induced orientation of boron nitride in polycarbonate composites with enhanced thermal conductivity," *Composites Part A,* vol. 110, pp. 45-52, 2018.

[65] T. Terao, Y. Bando, M. Mitome, C. Zhi, C. Tang and D. Golberg, "Thermal Conductivity Improvement of Polymer Films by Catechin-Modified Boron Nitride Nanotubes," *J. Phys. Chem. C,* vol. 113, p. 13605–13609, 2009.

[66] D. Kim, M. You, J. H. Seol, S. Ha and Y. A. Kim, "Enhanced Thermal Conductivity of Individual Polymeric Nanofiber Incorporated with Boron Nitride Nanotubes," *J. Phys. Chem. C,* vol. 121, p. 7025−7029, 2017.

[67] Y. Martinez-Rubi, B. Ashrafi, M. B. Jakubinek, S. Zou, K. S. Kim, H. Cho and B. Simard, "Nanocomposite fabrics with high content of boron nitride nanotubes for tough and multifunctional composites," *Journal of materials research,* 2022.

[68] C. Zhang, R. Huang, Y. Wang, Z. Wu, S. Guo, H. Zhang, J. Li, C. Huang, W. Wang and L. Li, "Aminopropyltrimethoxysilane-functionalized boron nitride nanotube based epoxy nanocomposites with simultaneous high thermal conductivity and excellent electrical insulation," *J. Mater. Chem. A,* vol. 6, p. 20663, 2018.

[69] O. S. Kwon, D. Lee, S. P. Lee, Y. G. Kang and N. C. Kim, "Enhancing the mechanical and thermal properties of boron nitride nanoplatelets/elastomer nanocomposites by latex mixing," *RSC Advances,* vol. 6, pp. 59970-59975, 2016.

[70] X. Wu, H. Liu, Z. Tang and B. Guo, "Scalable fabrication of thermally conductive elastomer/boron nitride nanosheets composites by slurry compounding," *Composites Science and Technology,* vol. 123, pp. 179-186, 2016.

[71] Y. Zhang, J. R. Choi and S. J. Park, "Enhancing the heat and load transfer efficiency by optimizing the interface of hexagonal boron nitride/elastomer nanocomposites for thermal management applications," *Polymer,* vol. 143, pp. 1-9, 2018.

[72] Y. Zhang, Y. Fan, U. Kamran and S. J. Park, "Improved thermal conductivity and mechanical property of mercapto group-activated boron nitride/elastomer composites for thermal management," *Composites Part A,* vol. 156, p. 106869, 2022.

[73] C. Fu, Q. Li, J. Lu, S. Mateti, Q. Cai, X. Zeng, G. Du, R. Sun, Y. Chen, J. Xu and C. P. Wong, "Improving thermal conductivity of polymer composites by reducing interfacial thermal resistance between boron nitride nanotubes," *Composites Science and Technology,* vol. 165, pp. 322-330, 2018.

[74] Z. Pan, Y. Tao, Y. Zhao, M. L. Fitzgerald, J. R. McBride, L. Zhu and D. Li, "Bidirectional Modulation of Contact Thermal Resistance between Boron Nitride Nanotubes from a Polymer Interlayer," *Nano Lett.,* vol. 21, p. 7317−7324, 2021.

[75] S. Zhang, W. Chen, Y. Zhao, K. Yang, B. Du, L. Ding, W. Ynag and S. Wu, "Surface NH2-functionalized by C doping of boron nitride nanotube to improve the thermal conductivity of epoxy composites," *Composites Part B,* vol. 223, p. 109106, 2021.

[76] C. Zhang, Z. Tang, B. Guo and L. Zhang, "Significantly improved rubber-silica interface via subtly controlling surface chemistry of silica," *Composites Science and Technology,* vol. 156, pp. 70-77, 2018.

[77] B. Yoon, J. Kim, U. Hong, M. Kyeong Oh, M. Kim, S. Han, J. Nam and J. Suhr, "Dynamic viscoelasticity of silica-filled styrene-butadiene rubber/polybutadiene rubber (SBR/BR) elastomer composites," *Composites Part B,* vol. 187, p. 107865, 2020.

[78] T. Xu, Z. Jia, Y. Luo, D. Jia and Z. Peng, "Interfacial interaction between the epoxidized natural rubber and silica in natural rubber/silica composites," *Applied Surface Science,* vol. 328, p. 306–313, 2015.

[79] M. J. Wang, "Effect of Polymer-Filler and Filler-Filler Interactions on Dynamic Properties of Filled Vulcanizates," *Rubber Chemistry and Technology,* vol. 71, no. 3, p. 520–589, 1998.

[80] C. A. Dorval Dion, W. Raphael, E. Tong and J. R. Tavares, "Photo-initiated chemical vapor deposition of thin films using syngas for the functionalization of surfaces at room temperature and near-atmospheric pressure," *Surface & Coatings Technology,* vol. 244, pp. 98-108, 2014.

[81] D. Kim, S. Nakajima, T. Sawada, M. Iwasaki, S. Kawauchi, C. Zhi, Y. Bando, D. Golberg and T. Serizawa, "Sonication-assisted alcoholysis of boron nitride nanotubes for their sidewalls chemical peeling," *Chem. Commun.,* vol. 51, pp. 7104-7107, 2015.

[82] S. Hosseininasab, N. Faucheux, G. Soucy and J. R. Tavares, "Full range of wettability through surface modification of single-wall carbon nanotubes by photo-initiated chemical vapour deposition," *Chemical Engineering Journal,* vol. 325, pp. 101-113, 2017.

[83] C. Zhi, Y. Bando, C. Tang, S. Honda, K. Sato, H. Kuwahara and D. Golberg, "Covalent Functionalization: Towards Soluble Multiwalled Boron Nitride Nanotubes," *Angew. Chem. Int.,* vol. 44, p. 7932 –7935, 2005.

[84] S. Y. Xie, W. Wang, K. A. Shiral Fernando, X. Wang, Y. Lin and Y. Sun, "Solubilization of boron nitride nanotubes," *Chem. Commun.,* pp. 3670-3672, 2005.

[85] S. Pal, R. C. Vivekchand, A. Govindaraj and C. N. R. Rao, "Functionalization and solubilization of BN nanotubes by interaction with Lewis bases," *Journal of Materials Chemistry,* vol. 17, pp. 450-452, 2007.

[86] C. Zhi, Y. Bando, C. Tang, H. Kuwahara and D. Golberg, "Grafting Boron Nitride Nanotubes: From Polymers to Amorphous and Graphitic Carbon," *J. Phys. Chem. C,* vol. 111, pp. 1230-1233, 2007.

[87] Q. Huang, Y. Bando, C. Zhi, D. Golberg, K. Kurashima, F. Xu and L. Gao, "Chemical Peeling and Branching of Boron Nitride Nanotubes in Dimethyl Sulfoxide," *Angew. Chem. Int. Ed.,* vol. 45, p. 2044 –2047, 2006.

[88] T. Ikuno, T. Sainsbury, D. Okawa, J. M. J. Frechet and A. Zettl, "Amine-functionalized boron nitride nanotubes," *Solid State Communications,* vol. 142, pp. 643-646, 2007.

[89] A. Pakdel, Mori, T., Bando, Y. and Golberg, D., "Interface Engineering of Bio-inspired Boron Nitride Nano-architectures toward Controllable Hydrophobicity/Hydrophilicity," in *Nano/Micro Engineered and Molecular Systems (IEEE-NEMS 2015)*, Xian, China, 2015.

[90] R. Iannitto, H. Shin, Y. Martinez-Rubi, B. Simard and S. Coulombe, "In-Flight Plasma Functionalization of Boron Nitride Nanotubes with Ammonia for Composite Applications," *ACS Applied Nano Materials,* vol. 3, p. 294−302, 2020.

[91] M. B. Jakubinek, K. S. Kim, C. Homenick, O. Kodra, S. Walker and B. Simard, "Assessment of boron nitride nanotube materials using X-ray photoelectron spectroscopy," *Canadian Journal of Chemistry,* vol. 97, no. 6, pp. 457-464, 2019.

[92] K. L. Choy, "Chemical vapour deposition of coatings," *Progress in Materials Science,* vol. 48, pp. 57-170, 2003.

[93] C. A. Dorval Dion and J. R. Tavares, "Photo-initiated chemical vapor deposition as a scalable particle functionalization technology (a practical review)," *Powder Technology,* vol. 239, pp. 484-491, 2013.

[94] E. Kasparek, J. R. Tavares, M. R. Wertheimer and P. L. Girard-Lauriault, "Sulfur-Rich Organic Films Deposited by Plasma- and Vacuum-Ultraviolet (VUV) Photo-Polymerization," *Plasma Processes and Polymers,* vol. 13, pp. 888-899, 2016.

[95] E. Kasparek, J. R. Tavares, M. R. Wertheimer and P. L. Girard-Lauriault, "VUV Photodeposition of Thiol-Terminated Films: A Wavelength-Dependent Study," *Langmuir,* vol. 34, no. 41, p. 12234–12243, 2018.

[96] M. Grujicic, G. Cao and B. Gersten, "Optimization of the chemical vapor deposition process for carbon nanotubes fabrication," *Applied Surface Science ,* vol. 191, pp. 223-239, 2002.

[97] K. Goransson, S. U. J. He and W. Zhang, "Review of syngas production via biomass DFBGs," *Renewable and Sustainable Energy Reviews,* vol. 15, pp. 482-492, 2011.

[98] P. Lv, Z. Yuan, C. Wu and M. L. , "Bio-syngas production from biomass catalytic gasification," *Energy Conversion and Management,* vol. 48, p. 1132–1139, 2007.

[99] D. Farhanian, G. De Crescenzo and J. R. Tavares, "Kinetics, Chemistry, and Morphology of Syngas Photoinitiated Chemical Vapor Deposition," *American Chemical Society,* vol. 33, p. 1780−1791, 2017.

[100] S. Hosseininasab, N. Faucheux, G. Soucy and J. R. Tavares, "Reaction kinetics and temperature effects in syngas photo-initiated chemical vapor deposition on single-walled carbon nanotubes," *J Nanopart Res,* vol. 21, p. 114, 2019.

[101] A. Bérard, G. S. Patience, G. Chouinard and J. R. Tavares, "Photo Initiated Chemical Vapour Deposition To Increase Polymer Hydrophobicity," *Nature,* vol. 6, p. 31574, 2016.

[102] V. Labonté, A. Marion, N. Virgilio and J. R. Tavares, "Gas-Phase Surface Engineering of Polystyrene Beads Used to Challenge Automated Particle Inspection Systems," *American Chemical society,* 2016.

[103] T. Javanbakht, W. Raphael and J. R. Tavares, "Physicochemical properties of cellulose nanocrystals treated by photo-initiated chemical vapour deposition (PICVD)," *THE CANADIAN JOURNAL OF CHEMICAL ENGINEERING,* vol. 9999, 2016.

[104] D. Farhanian, C. A. Dorval Dion, W. Raphael, G. De Crescenzo and J. R. Tavares, "Combined extraction and functionalization of low-cost nanoparticles from municipal solid waste," *Journal of Environmental Chemical Engineering,* vol. 2, pp. 2242-2251, 2014.

[105] D. Farhanian, G. De Crescenzo and J. R. Tavares, "Large-Scale Encapsulation of Magnetic Iron Oxide Nanoparticles via Syngas Photo-Initiated Chemical Vapor Deposition," *Scientific Reports,* vol. 8, p. 12223, 2018.

[106] H. Nasri-Lari, J. Chaouki and J. R. Tavares, "Continuous aerosol photopolymerization to coat de-agglomerated nanoparticles," *Chemical Engineering Journal,* vol. 390, p. 124526, 2020.

[107] A. F. M. Barton, "Applications of solubility parameters and other cohesion parameters in polymer science and technology," *Pure & Appl. Chem.*, vol. 57, no. 7, pp. 905-912, 1985.

[108] C. M. Hansen, Hansen solubility parameters, A user's handbook, Boca Raton: Taylor & Francis Group, LLC, 2007.

[109] A. F. M. Barton, "Solubility Parameters," *Chemical Reviews*, vol. 75, no. 6, pp. 731-753, 1975.

[110] C. M. Hansen, "Polymer additives and solubility parameters," *Progress in Organic Coatings*, vol. 51, pp. 109-112, 2004.

[111] M. Jing and R. M. Larsen, "Comparative Study on Dispersion and Interfacial Properties of Single Walled Carbon Nanotube/Polymer Composites Using Hansen Solubility Parameters," *Appl. Mater. Interfaces*, vol. 5, pp. 1287-1293, 2013.

[112] T. B. Nielsen and C. M. Hansen, "Elastomer swelling and Hansen solubility parameters," *Polymer Testing*, vol. 24, pp. 1054-1061, 2005.

[113] J. Lara, F. Zimmermann, D. Drolet, C. M. Hansen, A. Chollot and N. Monta, "The use of the Hansen solubility parameters in the selection of protective polymeric materials resistant to chemicals," *International Journal of Current Research*, vol. 9, no. 3, pp. 47860-47867, 2017.

[114] S. S. Liu, X. P. Li, P. J. Qi, Z. J. Song, Z. Zhang, K. Wang, G. X. Qiu and G. Y. Liu, "Determination of three-dimensional solubility parameters of styrene butadiene rubber and the potential application in tire tread formula design," *Polymer Testing*, vol. 81, no. 106170, 2020.

[115] S. J. Abbott, C. M. Hansen and H. Yamamoto, "Hansen solubility parameters in practice software, ebook, datasets," [Online]. Available: https://www.hansen-solubility.com/. [Accessed 20 07 2022].

[116] C. Bruel, J. R. Tavares, P. J. Carreau and M. C. Heuzey, "The structural amphiphilicity of cellulose nanocrystals characterized from their cohesion parameters," *Carbohydrate polymers,* vol. 205, pp. 184-191, 2019.

[117] S. Gårdebjer, Andersson, M., Engström, J., Restorp, P., Persson, M. and Larsson, A., "Using Hansen solubility parameters to predict the dispersion of nano-particles in polymeric films," *Polymer Chemistry,* vol. 7, pp. 1756-1764, 2016.

[118] H. T. Ham, Y. S. Choi and I. J. Chung, "An explanation of dispersion states of single-walled carbon nanotubes in solvents and aqueous surfactant solutions using solubility parameters," *Journal of Colloid and Interface Science,* vol. 286, pp. 216-223, 2005.

[119] S. D. Bergin, Z. Sun, D. Rickard, P. V. Streich, J. P. Hamilton and J. N. Coleman, "Multicomponent Solubility Parameters for Single-Walled Carbon Nanotube-Solvent Mixtures," *ACS Nano,* vol. 3, no. 8, p. 2340–2350, 2009.

[120] Y. Hernandez, M. Lotya, D. Rickard, S. D. Bergin and J. N. Coleman, "Measurement of Multicomponent Solubility Parameters for Graphene Facilitates Solvent Discovery," *Langmuir,* vol. 26, pp. 3208-3213, 2010.

[121] D. Konios, M. M. Stylianakis, E. Stratakis and E. Kymakis, "Dispersion behaviour of graphene oxide and reduced graphene oxide," *Journal of Colloid and Interface Science,* vol. 430, p. 108–112, 2014.

[122] W. Zhu, J. Ma, X. Nan, P. O. Lartey and Y. Yang, "Study on dispersion of reduced graphene oxide on physical performance of Polyvinylidene fluoride composites by Hansen solubility parameters," *Colloid and Polymer Science,* vol. 297, p. 213–224, 2019.

[123] Z. Zhou, L. Fang, Y. Cao, W. Wang, J. Wang, Y. Yang and Y. Liu, "Determination of Hansen solubility parameters of halloysite nanotubes and prediction of its compatibility with polyethylene oxide," *Colloids and Surfaces A,* vol. 601, p. 125031, 2020.

[124] K. Maleski, V. N. Mochalin and Y. Gogotsi, "Dispersions of Two-Dimensional Titanium Carbide MXene in Organic Solvents," *Chem. Mater.*, vol. 29, no. 4, p. 1632–1640, 2017.

[125] G. Cunningham, M. Lotya, C. S. Cucinotta, S. Sanvito, S. D. Bergin, R. Menzel, M. S. P. Shaffer and J. N. Coleman, "Solvent Exfoliation of Transition Metal Dichalcogenides: Dispersibility of Exfoliated Nanosheets Varies Only Weakly between Compounds," *ACS Nano,* vol. 6, no. 4, p. 3468–3480, 2012.

[126] K. Kim, M. B. Jakubinek, Y. Martinez-Rubi, B. Ashrafi, J. Guan, K. O'Neill, M. Plunkett, A. Hrdina, S. Lin, S. Denommee, C. Kingston and B. Simard, "Polymer nanocomposites from free-standing, macroscopic boron nitride nanotube assemblies," *RSC Adv.,* p. 41186–41192, 2015.

[127] K. S. Kim, C. Kingston and B. Simard.Patent US61/813324, 2013.

[128] J. Yu, Y. Chen and B. M. Cheng, "Dispersion of boron nitride nanotubes in aqueous solution with the help of ionic surfactants," *Solid State Communications,* vol. 149, pp. 763-766, 2009.

[129] C. H. Lee, D. Zhang and Y. K. Yap, "Functionalization, Dispersion, and Cutting of Boron Nitride Nanotubes in Water," *The Journal of Physical Chemistry C,* vol. 116, pp. 1798-1804, 2011.

[130] Z. Gao, C. Zhi, Y. Bando, D. Golberg and T. Serizawa, "Noncovalent Functionalization of Disentangled Boron Nitride Nanotubes with Flavin Mononucleotides for Strong and Stable Visible-Light Emission in Aqueous Solution," *Appl. Mater. Interfaces,* vol. 3, pp. 627-632, 2011.

[131] S. Detriche, G. Zorzini, J. F. Colomer, A. Fonseca and J. B. Nagy, "Application of the Hansen Solubility Parameters Theory to Carbon Nanotubes," *Journal of Nanoscience and Nanotechnology,* vol. 8, pp. 6082-6092, 2008.

[132] S. Detriche, J. B. Nagy, Z. Mekhalif and J. Delhalle, "Surface State of Carbon Nanotubes and Hansen Solubility Parameters," *Journal of Nanoscience and Nanotechnology,* vol. 9, pp. 6015-6025, 2009.

[133] S. Süß, T. Sobisch, W. Peukert, D. Lerche and D. Segets, "Determination of Hansen parameters for particles: A standardized routine based on analytical centrifugation," *Advanced Powder Technology,* vol. 29, pp. 1550-1561, 2018.

[134] K. S. Kim, M. Couillard, H. Shin, M. Plunkett, D. Ruth, C. T. Kingston and B. Simard, "Role of hydrogen in high-yield growth of boron nitride nanotubes at atmospheric pressure by induction thermal plasma," *ACS Nano,* vol. 12, pp. 884-893, 2018.

[135] Q. Beuguel, J. R. Tavares, P. J. Carreau and M. C. Heuzey, "Ultrasonication of spray- and freeze-dried cellulose nanocrystals in water," *Journal of Colloid and Interface Science,* vol. 516, pp. 23-33, 2018.

[136] C. Zhi, Y. Bando, C. Tang and D. Golberg, "Specific heat capacity and density of multi-walled boron nitride nanotubes by chemical vapor deposition," *Solid State Communications,* vol. 151, pp. 183-186, 2011.

[137] Y. Lin, T. V. Williams, T. B. Xu, W. Cao, H. E. Elsayed-Ali and J. W. Connell, "Aqueous Dispersions of Few-Layered and Monolayered Hexagonal Boron Nitride Nanosheets from Sonication-Assisted Hydrolysis: Critical Role of Water," *J. Phys. Chem. C,* vol. 115, no. 6, p. 2679–2685, 2011.

[138] J. A. Gallego-Juarez and K. F. Graff, Power Ultrasonics Applications of High-intensity Ultrasound, Cambridge, U.K., 2014.

[139] C. H. Lee, J. Drelich and Y. K. Yap, "Superhydrophobicity of Boron Nitride Nanotubes Grown on Silicon Substrates," *Langmuir*, vol. 25, pp. 4853-4860, 2009.

[140] C. H. Lee, *Boron nitride nanotubes : synthesis, characterization, functionalization, and potential applications,* Michigan, 2010.

[141] C. Bruel, S. Queffeulou, T. Darlow, N. Virgilio and J. R. Tavares, "Experimental methods in Chemical Engineering: Contact angles," *The Canadian journal of Chemical Engineering,* vol. 97, pp. 832-842, 2019.

[142] Y. Liao, Z. Chen, J. W. Connell, C. C. Fay, C. Park, J. W. Kim and Y. Lin, "Chemical Sharpening, Shortening, and Unzipping of Boron Nitride Nanotubes," *Adv. Funct. Mater.*, vol. 24, pp. 4497-4506, 2014.

[143] A. Maguer, E. Leroy, L. Bresson, E. Doris, A. Loiseau and C. Mioskowski, "A versatile strategy for the functionalization of boron nitride nanotubes," *J. Mater. Chem.*, vol. 19, pp. 1271-1275, 2009.

[144] Y. Min, M. Akbulut, K. Kristiansen, Y. Golan and J. Israelachvili, "The role of interparticle and external forces in nanoparticle assembly," *Nature materials,* vol. 7, pp. 527-538, 2008.

[145] H. Yan, Y. Tang, J. Su and X. Yang, "Enhanced thermal–mechanical properties of polymer composites with hybrid boron nitride nanofillers," *Appl. Phys. A,* vol. 114, pp. 331-337, 2014.

[146] V. Mirjalili, M. Yourdkhani and P. Hubert, "Dispersion stability in carbon nanotube modified polymers and its effect on the fracture toughness," *Nanotechnology,* vol. 23, p. 315701, 2012.

[147] G. Ciofani, G. G. Genchi, I. Liakos, A. Athanassiou, D. Dinucci, F. Chiellini and V. Mattoli, "A simple approach to covalent functionalization of boron nitride nanotubes," *Journal of Colloid and Interface Science,* vol. 374, pp. 308-314, 2012.

[148] T. H. Ferreira, A. Marino, A. Rocca, I. Liakos, S. Nitti, A. Athanassiou, V. Mattoli, B. Mazzolai, E. M. B. De Sousa and G. Ciofani, "Folate-grafted boron nitride nanotubes:

Possible exploitation in cancer therapy," *International Journal of Pharmaceutics,* vol. 481, pp. 56-63, 2015.

[149] W. M. Da Silva, G. A. Alemão Monteiro, P. Lana Gastelois, R. G. De Sousa, W. A. De Almeida Macedo and E. M. Barros Sousa, "Efficient sensitive polymer-grafted boron nitride nanotubes by microwave-assisted process," *Nano-Structures & Nano-Objects,* vol. 15, p. 186–196, 2018.

[150] H. Shin, J. Guan, M. Z. Zgierski, K. S. Kim, C. T. Kingston and B. Simard, "Covalent Functionalization of Boron Nitride Nanotubes via Reduction Chemistry," *ACS Nano,* vol. 9, no. 12, p. 12573–12582, 2015.

[151] M. A. Fernandez-Yague, A. Larrañaga, O. Gladkovskaya, A. Stanley, G. Tadayyon, Y. Guo, J.-R. Sarasua, S. A. M. Tofail, D. I. Zeugolis, A. Pandit and M. J. Biggs, "Effects of Polydopamine Functionalization on Boron Nitride Nanotube Dispersion and Cytocompatibility," *Bioconjugate Chem.,* vol. 26, no. 10, p. 2025–2037, 2015.

[152] Q. Weng, X. Wang, X. Wang, Y. Bando and D. Golberg, "Functionalized hexagonal boron nitride nanomaterials: emerging properties and applications," *Chem. Soc. Rev.,* vol. 45, pp. 3989-4012, 2016.

[153] H. Achour, A. Achour, S. Solaymani, M. Islam, S. Vizireanu, A. Arman, A. Ahmadpourian and G. Dinescu, "Plasma surface functionalization of boron nitride nano-sheets," *Diamond & Related Materials,* vol. 77, p. 110–115, 2017.

[154] M. Foroutan, S. Jamilaldin Fatemi and S. Mahmood Fatemi, "A mini-review on dispersion and functionalization of boron nitride nanotubes," *Journal of Nanostructure in Chemistry,* vol. 10, p. 265–274, 2020.

[155] C.-Y. Su, Z.-Y. Juang, K.-F. Chen, B.-M. Cheng, F.-R. Chen, K.-C. Leou and C.-H. Tsai, "Selective Growth of Boron Nitride Nanotubes by the Plasma-Assisted and Iron-Catalytic CVD Methods," *J. Phys. Chem. C,* vol. 113, p. 14681–14688, 2009.

[156] J. Li, J. Li, Y. Yin, Y. Chen and X. Bi, "Water-assisted chemical vapor deposition synthesis of boron nitride nanotubes and their photoluminescence property," *Nanotechnology*, vol. 24, p. 365605, 2013.

[157] Z. Peng, R. Yang, M. A. Kim, L. Li and H. Liu, "Influence of O2, H2O and airborne hydrocarbons on the properties of selected 2D materials," *RSC Adv.*, vol. 7, pp. 27048-27057, 2017.

[158] J. Qu, Q. Li, C. Luo, J. Cheng and X. Hou, "Characterization of Flake Boron Nitride Prepared from the Low Temperature Combustion Synthesized Precursor and Its Application for Dye Adsorption," *Coatings*, vol. 8, p. 214, 2018.

[159] T. Sainsbury, A. Satti, P. May, Z. Wang, I. McGovern, Y. K. Gunko and J. Coleman, "Oxygen Radical Functionalization of Boron Nitride Nanosheets," *J. Am. Chem. Soc.*, vol. 134, pp. 18758-18771, 2012.

[160] R. K. Tepe, D. Vassallo, T. Jacksier and R. M. Barnes, "Iron pentacarbonyl determination in carbon monoxide," *Spectrochimica Acta Part B*, vol. 54, pp. 1861-1868, 1999.

[161] H. Nasri-Lari, D. Farhanian, D. C. Boffito, G. S. Patience, G. De Crescenzo, J. Chaouki and J. R. Tavares, "Shedding light on iron pentacarbonyl photochemistry through a CVD case study," *Catalysis Communications*, vol. 100, pp. 19-23, 2017.

[162] P. Cai, L. Chen, L. Shi, Z. Yang, A. Zhao, Y. Gu, T. Huang and Y. Qian, "One convenient synthesis route to boron nitride nanotube," *Solid State Communications*, vol. 133, p. 621–623, 2005.

[163] E. Chibowski, A. Ontiveros-Ortega and R. Perea-Carpio, "On the interpretation of contact angle hysteresis," *J. Adhesion Sci. Technol.*, vol. 16, no. 10, p. 1367–1404, 2002.

[164] C. M. Hansen, Hansen solubility parameters, A user's handbook, Boca Raton: Taylor & Francis Group, LLC, 2007.

[165] L. H. Li and Y. Chen, "Superhydrophobic Properties of Nonaligned Boron Nitride Nanotube Films," *Langmuir*, vol. 7, pp. 5135-5140, 2010.

[166] D. Golberg, Y. Bando, Y. Huang, T. Terao, M. Mitome, C. Tang and C. Zhi, "Boron Nitride Nanotubes and Nanosheets," *ACS Nano*, vol. 4, no. 6, p. 2979–2993, 2010.

[167] J. Hu, Y. Huang, X. Zeng, Q. Li, L. Ren, R. Sun, J.-B. Xu and C.-P. Wong, "Polymer composite with enhanced thermal conductivity and mechanical strength through orientation manipulating of BN," *Composites Science and Technology*, vol. 160, pp. 127-137, 2018.

[168] C. Yu, J. Zhang, Z. Li, W. Tian, L. Wang, J. Luo, Q. Li, X. Fan and Y. Yao, "Enhanced through-plane thermal conductivity of boron nitride/epoxy composites," *Composites: Part A*, vol. 98, pp. 25-31, 2017.

[169] H.-B. Cho, T. Nakayama, H. Suematsu, T. Suzuki, W. Jiang, K. Niihara, E. Song, N. S. A. Eom, S. Kim and Y.-H. Choa, "Insulating polymer nanocomposites with high-thermal-conduction routes via linear densely packed boron nitride nanosheets," *Composites Science and Technology*, vol. 129, pp. 205-213, 2016.

[170] M. Girard, D. Vidal, F. Bertrand, J. R. Tavares and M. C. Heuzey, "Evidence-based guidelines for the ultrasonic dispersion of cellulose nanocrystals," *Ultrasonics Sonochemistry*, vol. 71, no. 105378, 2021.

[171] L. Chazeau, J. D. Brown, L. C. Yanyo and S. S. Sternstein, "Modulus Recovery Kinetics and Other Insights Into the Payne Effect for Filled Elastomers," *Polymer Composites*, vol. 21, no. 2, 2000.

[172] J. L. Leblanc, "Rubber-filler interactions and rheological properties in filled compounds," *Prog. Polym. Sci.*, vol. 27, pp. 627-687, 2002.

[173] B. Zhong, Z. Jia, Y. Luo and D. Jia, "A method to improve the mechanical performance of styrene-butadiene rubber via vulcanization accelerator modified silica," *Composites Science and Technology,* vol. 117, pp. 46-53, 2015.

[174] M. M. A. Spanjaards, G. W. M. Peters, M. A. Hulsen and P. D. Anderson, "Towards the Development of a Strategy to Characterize and Model the Rheological Behavior of Filled, Uncured Rubber Compounds," *Polymers,* vol. 13, no. 4068, 2021.

[175] K. Kim and J. Kim, "Fabrication of thermally conductive composite with surface modified boron nitride by epoxy wetting method," *Ceramics International,* vol. 40, p. 5181–5189, 2014.

[176] B.-H. Xie, X. Huang and G.-J. Zhang, "High thermal conductive polyvinyl alcohol composites with hexagonal boron nitride microplatelets as fillers," *Composites Science and Technology,* vol. 85, pp. 98-103, 2013.

[177] Y. Liu and S. Kumar, "Polymer/Carbon Nanotube Nano Composite Fibers−A Review," *ACS Appl. Mater. Interfaces,* vol. 6, p. 6069−6087, 2014.

[178] A. Moisala, Q. Li, I. A. Kinloch and A. H. Windle, "Thermal and electrical conductivity of single- and multi-walled carbon nanotube-epoxy composites," *Composites Science and Technology,* vol. 66, p. 1285–1288, 2006.

[179] P. C. Ma, N. A. Siddiqui, G. Marom and J. K. Kim, "Dispersion and functionalization of carbon nanotubes for polymer-based nanocomposites: A review," *Composites: Part A,* vol. 41, p. 1345–1367, 2010.

[180] R. S. Kapadia, B. M. Louie and P. R. Bandaru, "The Influence of Carbon Nanotube Aspect Ratio on Thermal Conductivity Enhancement in Nanotube–Polymer Composites," *Journal of Heat Transfer,* vol. 136, 2014.

[181] S. Y. Kwon, I. M. Kwon, Y. G. Kim, S. Lee and Y. S. Seo, "A large increase in the thermal conductivity of carbon nanotube/polymer composites produced by percolation phenomena," *Carbon,* vol. 55, pp. 285-290, 2013.

[182] M. Mutz, E. Eastwood and D. M.D., "Quantifying the Solubility of Boron Nitride Nanotubes and Sheets with Static Light Scattering and Refractometry," *J. Phys. Chem. C,* vol. 117, p. 13230−13238, 2013.

[183] C. S. Torres-Castillo and J. R. Tavares, "Covalent functionalization of boron nitride nanotubes through photo-initiated chemical vapour deposition," *Can J Chem Eng.*, pp. 1-11, 2022.

[184] C. S. Torres-Castillo and J. R. Tavares, "Thermally Conductive Styrene-Butadiene Rubber/Boron Nitride Nanotubes Composites," *Journal of Composites Science,* vol. 6, p. 272, 2022.

[185] S. aldrich, "Sigma aldrich," [Online]. Available: https://www.sigmaaldrich.com/catalog/product/aldrich/185884?lang=en&region=CA. [Accessed 15 02 2019].

[186] Wikipedia, "Dimethylacetamide," [Online]. Available: https://en.wikipedia.org/wiki/Dimethylacetamide. [Accessed 10 02 2019].

[187] PubChem, "Isopropyl alcohol," [Online]. Available: https://pubchem.ncbi.nlm.nih.gov/compound/Isopropyl-alcohol. [Accessed 10 02 2019].

[188] Wikipedia, "Isopropyl alcohol," [Online]. Available: https://en.wikipedia.org/wiki/Isopropyl_alcohol. [Accessed 10 02 2019].

[189] PubChem, "Acetic Acid," [Online]. Available: https://pubchem.ncbi.nlm.nih.gov/compound/Acetic-acid. [Accessed 10 02 2019].

[190] Anton Paar, "Viscosity of Acetic Acid," [Online]. Available: https://wiki.anton-paar.com/en/acetic-acid/. [Accessed 10 02 2019].

[191] Fisher Scientific, [Online]. Available: https://www.fishersci.ca/ca/en/home.html. [Accessed 10 02 2019].

[192] PubChem, "Acetonitrile," [Online]. Available: https://pubchem.ncbi.nlm.nih.gov/compound/ACETONITRILE. [Accessed 12 02 2019].

[193] PubChem, "Benzyl alcohol," [Online]. Available: https://pubchem.ncbi.nlm.nih.gov/compound/Benzyl-alcohol. [Accessed 10 02 2019].

[194] [Online]. Available: www.chemicalbook.com. [Accessed 10 02 2019].

[195] [Online]. Available: http://www.trimen.pl/witek/ciecze/old_liquids.html. [Accessed 10 02 2019].

APPENDIX A METHODS OF SYNTHESIS OF BNNT

Arc discharge

This technique was the first one to be applied for the production of BNNTs in 1995, after theoretical studies. Chopra et al. [22] synthesized multi-walled BNNTs using a tungsten electrode (anode) containing h-BN powder and a copper electrode used as cathode. The resulting tubes contained metal particles at their tips and the distance between tubes was 3.3 Å. So far, there have been reported different variants of this approach, which depend on the kind of electrodes and environment conditions used. The materials obtained can be multi-walled or single-walled BNNTs and the tips of the nanotubes contain metal particles or form closed squares. In some cases, a combination of square morphology and metal tips can be found [19].

Laser ablation

This approach uses as a starting material single-crystal cubic boron nitride (c-BN). The precursors are heated with a laser during 60 seconds in a diamond anvil cell subjected to high nitrogen pressures in the range of 5-15 GPa. The nanotubes obtained are composed of just a few layers. However, the use of this technique results in a low yield of BNNTs and the presence of non-tubular species are found in the product. Subsequent work has been carried out and the fabrication of few-walled BNNTs was obtained [47].

Substitution reaction

Having hollow carbon nanotubes as a starting material and B_2O_3 powder, BNNTs can be obtained by substitution reaction. In brief, B_2O_3 powder is deposited in a graphite crucible followed by the addition of CNTs to cover the powder. Then, the substitution reaction takes place in an induction-heating system where boron oxide vapor encounters nitrogen gas in a carbon nanotubes environment at 1773 ^{o}K. The obtained BNNTs possess similar dimensions that the CNTs used, with diameters of approximately 10 nm. This technique can be applied for large production of nanotubes [46]. It is worth noting that this technique is very sensitive to experimental conditions and the substitution of all C atoms by B and N atoms is extremely difficult [19].

Chemical vapor deposition

There are many variants of chemical vapor deposition (CVD) that can be used to fabricate BNNTs [49], [50], [51]. One of them consist in using a wafer composed of $LaNi_5$/B. In brief, $LaNi_5$ and amorphous boron are mixed in a ball milling device for no less than 5 h. Then, Ni powder is added, and the new mixture is pressed. The wafer obtained is heated at 1473 ^{o}K in a resistance furnace in presence of argon flow. After that, ammonia is fed to the system. The nanotubes obtained are aligned with diameters in the range of 30-50 nm and length of the tubes in the order of microns [49].

Another approach of this technique is using boron oxide. The boron oxide chemical vapor deposition (BOCVD) method has been employed for large-scale fabrication of multi-walled BNNTs [15]. In brief, metal precursors including B and MgO are heated at a temperature higher than 1300 ^{o}C. The B_xO_y vapors created during the reactions are transported by Ar gas to allow the interaction with ammonia for the subsequent formation of BNNTs. A rapid heating and high temperature gradient are required in the induction furnace [50].

Ball milling

This technique (high temperature ball milling) is suitable to produce large quantities of nanomaterial [48]. However, the product is composed of bamboo-like structures [15]. Elemental boron and ammonia are used as reactants. The milling process is carried out at room temperature in a planetary ball mill containing steel balls. Before milling, a purge using ammonia is done and a pressure of 300 kPa is set. Having elapsed 150 h of milling, temperatures higher than 1000 ^{o}C are used for annealing of the powders in presence of nitrogen or argon gases. The amount of BNNTs and their dimensions are determined by the processing parameters [48].

Plasma-enhanced pulsed-laser deposition (PE-PLD)

The synthesis of BNNTs without the use of elevated growth temperatures has been achieved through the plasma-enhanced pulsed-laser deposition approach. The reaction takes place at 600 ^{o}C in presence of Fe catalyst. A negative substrate bias voltage induced by a nitrogen plasma allows the formation of the reactive environment for the growth of BNNTs. The obtained nanotubes possess high crystallinity and no impurities [15], [53].

Pressurized vapor condenser (PVC) method

This technique relies on the use of high temperature for the synthesis of BNNTs. It requires a forced condensation of the particles subjected at elevated pressure. In brief, a strong buoyancy force is produced due to a significant difference in density between the boron vapor generated at 4000 ^{o}C and the pressurized nitrogen gas around it [54]. Then, a cooled metal is used as a condenser to allow the homogeneous nucleation of boron droplets. After that, the creation of a loop is obtained due to the movement upwards of boron droplets. Then, the droplets reach nitrogen gas allowing the reaction between B and N_2 and thus, the formation of BNNTs. With this technique is possible to obtain gram quantities of nanotubes with extraordinary long tubes of small diameters and few walls [54].

APPENDIX B ARTICLE 1 SUPPLEMENTARY INFORMATION

This supporting information gathers the physical properties (density, viscosity and molar volume) of the solvents that were employed for the calculations of sedimentation times. It also includes the Hansen solubility parameters for each solvent.

Table B.1 Purity, supplier and physical properties of the solvents used in the sedimentation tests.

Solvent	Purity (%)	Supplier	Density[a] at 20°C (g/cm^3)	Viscosity[a] at 20°C (mPa s)	Molar volume (cm^3/mol)	Ref
N,N′-Dimethylacetamide	99.5	Anachemia	0.937 (25)	0.945 (25)	92.5	[186], [187], [116]
N,N′-Dimethylformamide	99.8	Sigma-Aldrich	0.95	0.82	77.0	[116], [109]
Acetone	≥ 99.5	Fisher Chemical	0.79	0.35	74.0	[116], [109]
Methanol	99.9	Fisher Chemical	0.79	0.59	40.7	[116], [109]
2-Propanol	99	Laboratoire MAT	0.786	1.96 (25)	76.8	[188], [189], [116]
Tetrahydrofuran	≥ 99.9	Sigma-Aldrich	0.89	0.55	81.7	[116], [109]
Chloroform	99.9	Fisher Scientific	1.48	0.37	80.7	[116], [109]
Acetic acid	≥ 99.7	Laboratoire MAT	1.049	1.037 (30)	57.1	[190], [191]

Dimethylsulfoxide	> 99.9	Alfa Aesar	1.1	1.98	71.3	[116], [109]
Toluene	99.9	Fisher Chemical	0.87	0.59	106.8	[116], [109]
Cyclohexane	99.9	Fisher Chemical	0.78	1	108.7	[116], [109]
Heptane	Not specified	Fisher Chemical	0.679	0.393	147.4	[117], [116], [109]
Ethyl acetate	99.9	Fisher Chemical	0.89	0.44	98.5	[116], [109]
d-Limonene	96	Acros Organics	0.841	0.897	162.9	[117], [116], [109]
Formamide	99	Alfa Aesar	1.13	3.3	39.9	[116], [109]
1,4-Dioxane	> 99	Alfa Aesar	1.04	1.31	85.7	[116], [109]
Acetonitrile	≥ 99.5	Laboratoire MAT	0.786(25)	0.35	52.9	[192], [193], [116], [109]
Ethylenglycol	≥ 99.8	Fisher sientific	1.12	20.9	55.9	[116], [109]
Ethanol	95	Commercial alcohols	0.82	1.22	58.6	[116], [109]
Propylene carbonate	99.5	Acros Organics	1.2	2.8	85.2	[116], [109]

Benzyl alcohol	>99	Sigma-Aldrich	1.0419 (24)	5.474 (25)	103.8	[194], [116], [109]
Ethyl benzoate	99	Alfa Aesar	1.04	1.83	144.1	[117], [116], [109]
ter-Butanol	≥99	Sigma-Aldrich	0.81 (25)	3.35	95.8	[195], [196], [116], [109]
Dichloromethane	99	Alfa Aesar	1.33	0.43	64.4	[116], [109]
Methyl ethyl ketone	≥99	Sigma-Aldrich	0.8	0.386	90.2	[117], [116], [109]
Water	DI	-	0.997	0.89	18	[117], [116], [109]

[a] When different from 20˚C, the temperature is specified in parenthesis in ˚C.

Table B.2 HSP, sedimentation time and dispersion state of the solvents used in sedimentation tests.

Solvent	HSP			Sedimentation time (h)	Dispersion state
	δ_d ($MPa^{1/2}$)	δ_p ($MPa^{1/2}$)	δ_h ($MPa^{1/2}$)		
N,*N*′-Dimethylacetamide	16.8	11.5	10.2	48.00	Good
N,*N*′-Dimethylformamide	17.4	13.7	11.3	42.6	Good
Acetone	15.5	10.4	7	14.1	Intermediate
Methanol	15.1	12.3	22.3	23.8	Intermediate
2-Propanol	15.8	6.1	16.4	78.5	Good
Tetrahydrofuran	16.8	5.7	8	25.8	Intermediate
Chloroform	17.8	3.1	5.7	529	Poor
Acetic acid	14.5	8	13.5	65.8	Poor
Dimethyl sulfoxide	18.4	16.4	10.2	141.6	Poor
Toluene	18	1.4	2	26.8	Poor
Cyclohexane	16.8	0	0.2	39.7	Poor
Heptane	15.3	0	0	13.7	Poor
Ethyl acetate	15.8	5.3	7.2	20.6	Intermediate
d-Limonene	17.2	1.8	4.3	38.9	Poor
Formamide	17.2	26.2	19	255	Poor
1,4-Dioxane	17.5	1.8	9	81.4	Poor

Acetonitrile	15.3	18	6.1	14	Intermediate
Ethylene glycol	17	11	26	1572.8	Poor
Ethanol	15.8	8.8	19.4	51.3	Good
Propylene carbonate	20	18	4.1	266.9	Intermediate
Benzyl alcohol	18.4	6.3	13.7	341.7	Good
Ethyl benzoate	17.9	6.2	6	113.8	Intermediate
tert-Butanol	15.2	5.1	14.7	138.8	Poor
Dichloromethane	17	7.3	7.1	72.3	Poor
Methyl ethyl ketone	16	9	5.1	15.8	Intermediate

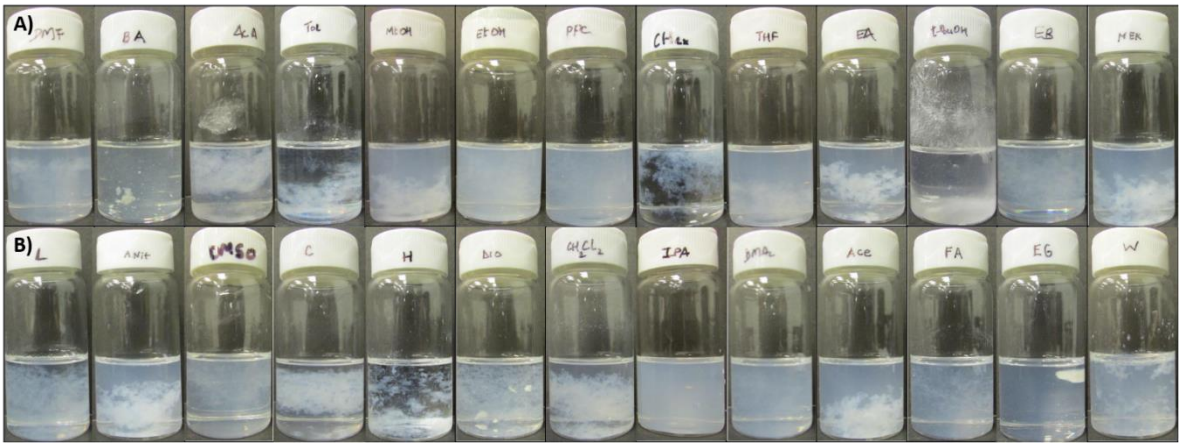

Figure B.1 Pictures of the dispersions taken immediately after sonication. Solvents from left to right are: (A) DMF, benzyl alcohol, acetic acid, toluene, methanol, ethanol, propylene carbonate, cyclohexane, THF, ethyl acetate, tert-butanol, ethyl benzoate and (B) MEK, d-limonene, acetonitrile, DMSO, chloroform, heptane, 1,2-dioxane, dichloromethane, 2-propanol, DMAc, acetone, formamide, ethylene glycol and water.

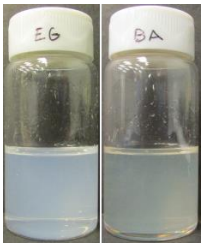

Figure B.2 BNNTs dispersions in ethylene glycol and benzyl alcohol applying high energy during sonication.

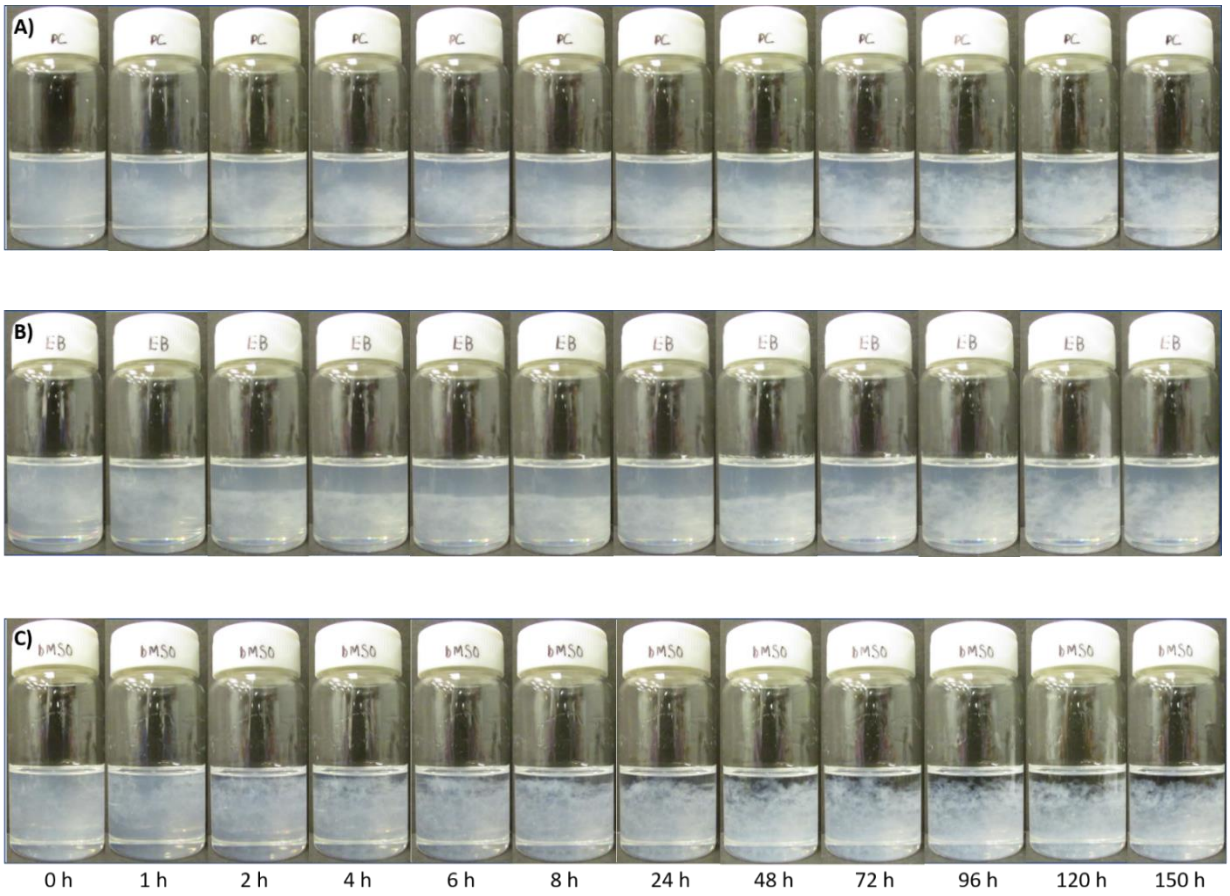

Figure B.3 Evolution of the dispersion state over time in A) propylene carbonate, B) ethyl benzoate and C) DMSO. Pictures of the vials were taken at 0, 1, 2, 4, 6, 8, 24, 48, 72, 96, 120 and 150 h after sonication.

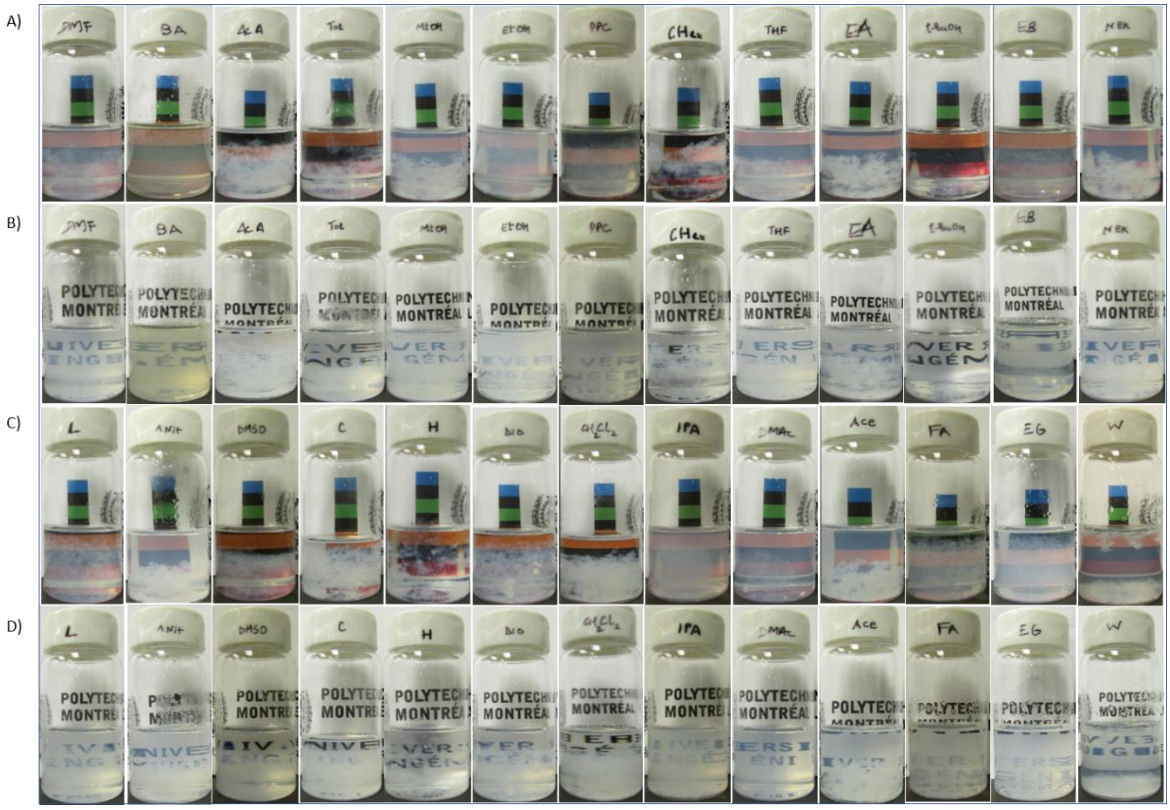

Figure B.4 Pictures of the vials taken after a relative sedimentation time (RST) of 1.0295 x 1011 s2/m2. Solvents from left to right are: (A,B) N,N'-dimethylformamide, benzyl alcohol, acetic acid, toluene, methanol, ethanol, propylene carbonate, cyclohexane, tetrahydrofuran, ethyl acetate, tert-butanol, ethyl benzoate, methyl ethyl ketone and (C,D) d-limonene, acetonitrile, dimethyl sulfoxide, chloroform, heptane, 1,4-dioxane, dichloromethane, 2-propanol, N,N'-dimethylacetamide, acetone, formamide, ethylene glycol and water.

Mathematical analysis

Classification of the dispersions in good (score = 1) and bad ones (score = 0) must be done prior the mathematical analysis. Then, "0" or "1" is inputted into the *HSPiP* software. Calculations are performed based on the *desirability function* FIT (equation S1) [109]:

$$FIT = (A_1 * A_2 * \dots A_n)^{1/n} \qquad (S1)$$

where *n* refers to the number of solvents considered in the experiment. FIT tends towards 1 when most of good solvents fit inside a sphere and most of bad solvents are excluded. The coefficient A_i can be calculated according to the equations presented in Table B.3. This coefficient will be equal to 1 when a given good solvent is inside the sphere or when a poor one is outside. The error distance refers to the separation between the solvent in error and the border of the sphere. A solvent in error happen when a good solvent is outside the sphere or when a bad solvent is inside. These errors may be attributed to low molecular volumes of the solvents [109].

Table B.3 Equation to calculate coefficient A_i.

	RED ≤ 1.0	RED > 1.0
Good solvent	$A_i = 1$	$A_i = e^{+(R_o - R_a)}$
Poor solvent	$A_i = e^{+(R_a - R_o)}$	$A_i = 1$

Taking as a starting point the average of Hansen parameters for the good solvents, the calculations are started. Then, the *SPHERE* program determines eight points, corresponding to the corners of a cube, which center is defined by the current best values. During the calculations, different radii are tested at every corner of the cube. While improving the fit, a new center of the cube is determined. This process continues until the FIT can not longer be improved [109].

While doing HSP experiments, two types of errors may occur. The first one, known as systematic error, is related to the molar volume of the species involved. The molecular size of solvent and solute considerably impacts the solubility, but also other processes such as diffusion, permeation or resistance to chemicals. Molecules with smaller sizes will tend to solubilize more than molecules with larger sizes. This is supported by Hildebrand solubility theory, where it is stated that solvents with low molar volumes are preferred over those with larger ones, despite their similarity in

solubility parameters. The Flory-Huggins theory also points out that better solubility is expected when using small molecules of solvent [109].

Beyond solute size and shape, kinetic phenomena should be considered. Diffusion occurs faster when linear and small molecules are used. In fact, it could happen that equilibrium is not reached when large and bulky molecules are used, due to a low diffusion coefficient. This situation has been observed for example, when thick rigid polymers are dispersed in organic solvents [109].

Due to the reasons mentioned above, it was thought that an extra solubility parameter based on the solvent molecular volume was needed. This was studied in some works, but it was concluded that size effects are mainly caused by kinetic phenomena and not by thermodynamic principles, on which solubility theory is based. However, there is a strong relationship between the segment size parameter (ρ) from the Prigogine theory and the dispersibility parameter (δ_D) from the Hansen solubility approach. This may lead to the conclusion that molecular size has an influence on the dispersibility parameter. For example, when δ_D is calculated for aliphatic hydrocarbons, molecules with larger molecular size such as aromatic rings possess higher δ_D. Thus, when analyzing the results obtained by HSPiP, it may happen that solvent molecular size is a significant parameter for the prediction of HSP of the solute in question [109].

The second type of error encountered when doing the HSPiP runs may be due to not expected interactions, such as reactions between solvent and solute. A common practice to minimize the errors is to analyze the output data marked with "*". When doing the calculations, the aim of the SPHERE program is to minimize the radius of the sphere while having the maximum DATA FIT (1.0) [109].

APPENDIX C ARTICLE 2 SUPPLEMENTARY INFORMATION

1.1 Cost of PICVD treatment

1.1.1 Data

Power of UVC lamp: 30 W

Treatment time: 1 h

Flow of CO: 250 ml/h

Flow of H_2: 125 ml/h

Flow or Ar: 3 standard ft^3/h (6 min, 3 min before reaction, and 3 min after)

*Cost of CO tank (V = 4.44 m^3) = $ 238.70 CAD

*Cost of H_2 tank (V = 5.41 m^3) = $ 178.38 CAD

*Cost of Ar tank (V = 9.33 m^3) = $ 41.80 CAD

**Cost of H_2O_2 (500 ml) = $ 167.33 CAD

*The costs of the gases were obtained from Air Liquide Canada.

**The cost of H_2O_2 (30%) was obtained from Fisher Scientific.

1.1.2 Calculations

Consumption of UVC lamp in PICVD treatment

$$Consumption = \frac{(30\ \text{W})(1\ \text{h})}{1000} = 0.03\ \text{kWh}$$

Rate D (6.159 ¢/kWh), obtained from Hydro Quebec on October 14, 2021.

$$Cost\ UV\ lamp = 0.03\ \text{kWh}\left(\frac{\$0.062\ \text{CAD}}{\text{kWh}}\right) = \$\mathbf{0.00186\ CAD}$$

Cost of gases

$$\$CO = \frac{250\ \text{ml}}{\text{h}}(1h)\left(\frac{1\ \text{m}^3}{10^6\text{cm}^3}\right)\left(\frac{\$238.70}{4.44\ \text{m}^3}\right) = \$\ 0.01344\ \text{CAD}$$

$$\$H2 = \frac{125\ \text{ml}}{\text{h}}(1\ \text{h})\left(\frac{1\ \text{m}^3}{10^6\ \text{cm}^3}\right)\left(\frac{\$178.38}{5.41\ \text{m}^3}\right) = \$\ 0.00412\ \text{CAD}$$

$$\$Ar = \frac{84{,}950.54\ \text{ml}}{h}(0.1\ \text{h})\left(\frac{1\ \text{m}^3}{10^6\text{cm}^3}\right)\left(\frac{\$41.80}{9.33\ \text{m}^3}\right) = \$\ 0.03806\ \text{CAD}$$

Total cost of gases: **$ 0.05562 CAD**

Cost of H_2O_2

$$\$H2O2 = \frac{1\ \text{ml}}{\text{h}}(1\ \text{h})\left(\frac{167.33}{500\ \text{ml}}\right) = \$\ \mathbf{0.3346\ CAD}$$

Total cost for 1 h PICVD treatment: **$0.3921 CAD**

Consumption of energy in Plasma treatments

Reference 25

Two doses of O_2-plasma treatment were employed: 10 and 20 min, operating in continuous wave (CW) mode at 100 W.

a) Considering t = 10 min

$$Consumption = \frac{(100\ \text{W})(\frac{10}{60}\ \text{h})}{1000} = 0.0166\ \text{kWh}$$

$$Plasma\ energy\ cost = 0.0166\ \text{kWh}\left(\frac{\$0.062\ \text{CAD}}{\text{kWh}}\right) = \$0.0010\ \text{CAD}$$

b) Considering t = 20 min

$$Consumption = \frac{(100\ \text{W})(\frac{20}{60}\text{h})}{1000} = 0.0333\ \text{kWh}$$

$$Plasma\ energy\ cost\ (20\ \text{min}) = 0.0333\ \text{kWh}\left(\frac{\$0.062\ \text{CAD}}{\text{kWh}}\right) = \$0.0021\ \text{CAD}$$

Reference 29

O_2-plasma treatment was employed considering a treatment time of 10 min operating at 400 W.

$$Consumption = \frac{(400\ \text{W})(\frac{10}{60}\text{h})}{1000} = 0.0666\ \text{kWh}$$

$$Plasma\ energy\ cost\ (10\ \text{min}) = 0.0666\ \text{kWh}\left(\frac{\$0.062\ \text{CAD}}{\text{kWh}}\right) = \$0.0041\ \text{CAD}$$

APPENDIX D ARTICLE 3 SUPPLEMENTARY INFORMATION

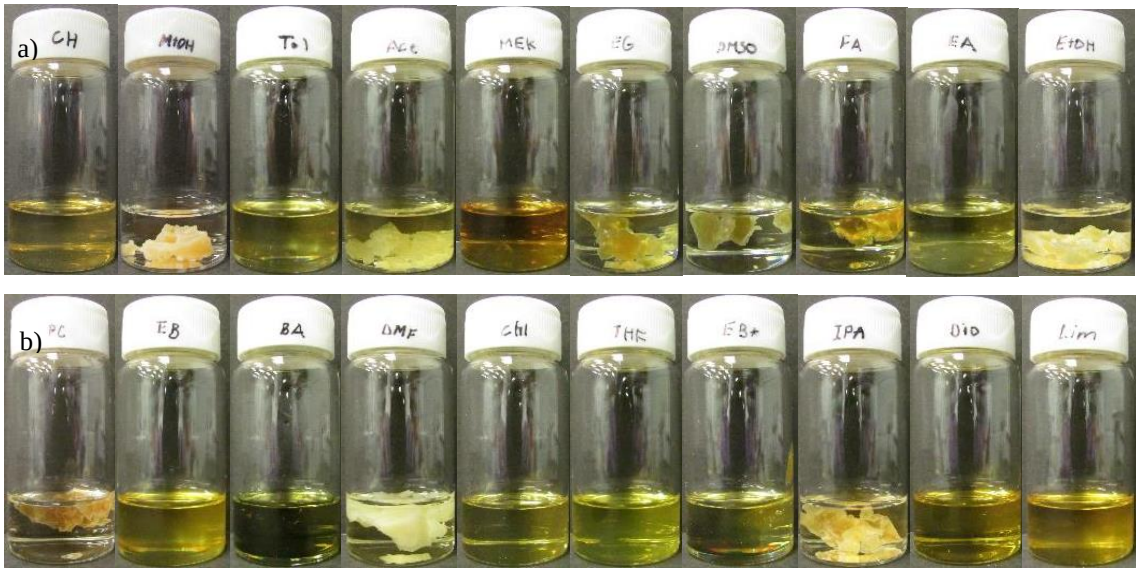

Figure D.1 Dissolution of SBR in organic solvents after having passed 24 h. Solvents from left to right a) cyclohexane, methanol, toluene, acetone, methyl ethyl ketone, ethylene glycol, dimethyl sulfoxide, formamide, ethyl acetate, ethanol, and b) propylene carbonate, ethyl benzene, benzyl alcohol, dimethyl formamide, chloroform, tetrahydrofuran, ethyl benzoate, 2-propanol, 1,4-dioxane and d-limonene.

APPENDIX E LIST OF CONTRIBUTIONS

a) Articles published in peer-review journals

[1] Torres-Castillo, C.S., Tavares, J.R., (2022), Thermally Conductive Styrene-Butadiene Rubber/Boron Nitride Nanotubes Composites, Published in Journal of Composites Science.

[2] Torres-Castillo, C.S., Tavares, J.R., (2022), Covalent functionalization of boron nitride nanotubes through photo-initiated chemical vapour deposition, Published in The Canadian Journal of Chemical Engineering.

[3] Torres-Castillo, C.S., Bruel, C., Tavares, J.R., (2020), Chemical affinity and dispersibility of boron nitride nanotubes, Published in Nanoscale Advances.

b) Presentations in conferences or symposiums

[4] Torres-Castillo, C.S., Tavares, J.R., Covalent functionalization of BNNT through Photo-initiated chemical vapor deposition, 72nd Canadian Chemical Engineering Conference (CCEC 2022), Vancouver, British Columbia, Canada, 23-26 October 2022, Oral presentation.

[5] Torres-Castillo, C.S., Bruel, C., Tavares, J.R., Cohesion parameters of Boron Nitride Nanotubes, 36th International Conference of the Polymer Processing Society (PPS 36), Montreal, Quebec, Canada, 26-29 September 2021, Oral presentation.

[6] Torres-Castillo, C.S., Bruel, C., Tavares, J.R., Cohesion parameters of Boron Nitride Nanotubes, Canadian Chemical Engineering Conference (CCEC 2020 Virtual), Virtual, 26-30 October 2020, Poster presentation.

[7] Torres-Castillo, C.S., Veerubhotla, A.V., Bruel, C., Tavares, J.R., Cohesion Parameters of Boron Nitride Nanotubes Obtained by Organic Dispersions, 14th CREPEC Annual Colloquium, Quebec City, Quebec, Canada, December 2019, Poster presentation.

[8] Torres-Castillo, C.S., Tavares, J.R., Thermodynamic assessment of Boron Nitride Nanotubes dispersion, 7th Edition of the Chemical Engineering Joint Research Day, Montreal, Quebec, Canada, 20-21 March 2019, Oral presentation.